LARGE DEFORMATIONS OF THIN PLATES SUBJECTED TO IMPULSIVE LOADING

by

G.N. NURICK

1987

Submitted to the University of Cape Town
for the degree of Doctor of Philosophy.

For Denise, Saul and Jessica

DECLARATION

I, Gerald Norman Nurick, declare that this thesis is essentially my own work and has not been submitted in this or in a similar form for a degree at any other University.

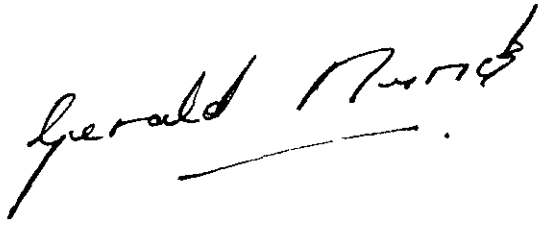

ABSTRACT

The dynamic response of structures subjected to blast and impact loading has been obtained relatively simply using rigid-plastic or rigid-viscoplastic material idealisations. It is essential, however, that the predictions of these idealised theories should be checked against experimental results, and over the past twenty years several experimental studies have been carried out. This thesis describes a series of experiments on fully clamped circular, square and rectangular steel plates. The final mid-point deflections measured were between 3 and 12 plate thicknesses; and the deflection time history was measured using a light interference technique. While the deflection-time history was being recorded, the impulse was simultaneously being measured by means of a ballistic pendulum upon which the plates were attached. The impulse was provided by sheet explosive which was arranged in such a way that the plate was subjected to a uniformly distributed impulse.

In addition an extension of a mode approximation method, based on the assumption that membrane stresses predominate, is presented. This method assumes that the material behaviour can be modelled as rigid-viscoplastic, and that at any instant the shapes of the displacement and the velocity field are the same. Points on the plate surface were first assumed to displace perpendicular to the initial surface: this assumption was then relaxed to permit points to move perpendicular to the current surface. In both cases, the predicted transverse displacements agreed well with the experimental data. The predicted radial strain distribution exhibited trends similar to the experimental data in the case where lateral displacements were modelled.

ACKNOWLEDGEMENTS

My sincere gratitude to the following:

Professor J.B. Martin: for his untiring guidance and encouragement.

Mr. R. Beverton: for preparing and detonating the explosive charges.

Mr. J. Mayer: for his ideas and assistance with the electronic equipment.

Messrs. L. Watkins, J. Gordon, A. Warburton, M. Batho and H. Tomlinson: for preparing the plate specimens and associated test equipment.

Dr. H.T. Pearce: for compiling and running the computer programme.

Professor S.R. Bodner: for his advice using explosive material.

Professor L.P. Adams and Miss A. Tregidga: for their assistance in measuring the deformed plates.

Mrs. I.E. von Bentheim for transforming a very untidy draft into a neat thesis.

AECI (Pty) Limited for providing the explosive material.

The Foundation for Research Development for their financial assistance.

TABLE OF CONTENTS

		Page
Declaration		(i)
Abstract		(ii)
Acknowledgements		(iii)
Table of Contents		(iv)
List of Figures		(vi)
List of Tables		(viii)
Nomenclature		(ix)
Chapter 1.	INTRODUCTION	1
Chapter 2.	EXPERIMENTAL DETAILS	4
2.1	INTRODUCTION	4
2.2	EXPERIMENTAL MEASUREMENTS	11
2.3	LIGHT INTERFERENCE EQUIPMENT FOR DEFLECTION MEASUREMENT	11
2.4	EXPERIMENTAL PROCEDURE	16
2.4.1	Introduction	16
2.4.2	Explosive Material	20
2.4.3	Ballistic Pendulum	22
2.4.4	Calibration of Photodiodes	26
2.4.5	Effect of Explosive Mass and Geometry	30
2.5	TEST RESULTS	32
2.5.1	Instrumentation Results	32
2.5.2	Comment on the Light Interference Equipment	35
2.5.3	Test Readings	35
2.5.3.1	Deflection-Time Recording	35
2.5.3.2	Impulse	35
2.5.3.3	Measured Deflection	36
2.5.3.4	Plate Thickness Measurement	36
2.5.3.5	Test Results of Uniaxial Yield Tests	36
2.5.3.6	Tables of Test Data	36
Chapter 3.	THEORETICAL CONSIDERATIONS	46
3.1	INTRODUCTION	46
3.2	MODE APPROXIMATION	53
3.3	MEMBRANE ANALYSIS	55
3.3.1	Plastic String Analysis	55
3.3.2	Application to Plates	62
Chapter 4.	RESULTS:	71
4.1	INTRODUCTION	71
4.2	COMPARISON OF PRESENT EXPERIMENTAL DATA WITH PREVIOUS RESEARCHERS	87

Page

Chapter 5. DISCUSSION AND CONCLUSION 103

5.1 OVERVIEW 103

5.2 THEORETICAL SOLUTION 103

5.3 EMPIRICAL SOLUTION 106

5.4 IN CLOSING 109

REFERENCES 110

FURTHER READING 118

PAPERS PUBLISHED 118

APPENDICES

A.1 - Resume of Approximate Methods for Predicting Deformation of Thin Plates Subjected to Uniform Impulsive Loading

A.2 Equations of Equilibrium in Detail

A.3 Program Listing

LIST OF FIGURES

		Page
Figure 2.1	Schematic Layout of Test Rig	13
Figure 2.2	Circuit Diagram of Light Interference Rig	13
Figure 2.3	Photograph of Test Rig	15
Figure 2.4	Uniaxial Stress Strain Tensile Test for Series I Material	17
Figure 2.5a	Uniaxial Stress Strain Tensile Test for Series II and IV Material	18
Figure 2.5b	Uniaxial Stress Strain Tensile Test for Series III Material	19
Figure 2.6	Arrangement of Explosive in Concentric Annuli of Plate Shape	21
Figure 2.7	Ballistic Pendulum Configuration	24
Figure 2.8	Pendulum Geometry	25
Figure 2.9	Static Calibration of Light Interference Equipment	27
Figure 2.10	Graph of Final Mid-Point Deflection vs Steady State Voltage Change for Series I Tests	29
Figure 2.11	Graph of Final Mid-Point Deflection vs Steady State Voltage Change for Series IV Tests ...	29
Figure 2.12	Graph of Final Mid-Point Deflection vs Steady State Voltage Change for Series III Tests ..	29
Figure 2.13	Graph of Impulse vs Mass of Explosive for Series I Tests	31
Figure 2.14	Graph of Impulse vs Mass of Explosive for Series IV Tests	33
Figure 2.15	Graph of Impulse vs Mass of Explosive for Series III Tests	33
Figure 2.16	Graph of Impulse vs Mass of Explosive for Series II Tests	33
Figure 2.17	Graph Showing Impulse as a Function of Plate Shape and Mass of Explosive	33
Figure 2.18	Deflection-Time Curve with Light Interference	34
Figure 2.19a	Typical Deflection-Time Curves	38
Figure 2.19b	Typical Deflection-Time Curves	39
Figure 2.19c	Typical Deflection-Time Curves	40
Figure 2.20a	Contour Plots of Deformed Plates	41
Figure 2.20b	Contour Plots of Deformed Plates	42
Figure 3.1	Model showing Transverse Displacements only	56
Figure 3.2a	Model showing Transverse and Lateral Forces	57
Figure 3.2b	Model showing Transverse and Lateral Displacements	57
Figure 3.3	Perpendicular Motion of the i^{th} Node	58
Figure 3.4	Discretisation of Circular Plates	67
Figure 3.5	Discretisation of Square Plates	67
Figure 3.6	Discretisation of Rectangular Plates	68
Figure 3.7	Forces Acting on the i^{th} Node	69
Figure 3.8	Flowchart of Problem Solver	70
Figure 4.1	Graph of Deflection-Thickness Ratio vs. Impulse for Circular Plates	74
Figure 4.2	Graph of Deflection-Thickness Ratio vs. Impulse for Square Plates	75
Figure 4.3	Graph of Deflection-Thickness Ratio vs. Impulse for Rectangular Plates	76
Figure 4.4	Graph of Deflection-Thickness Ratio vs. Dimensionless No. $\alpha^{\frac{1}{2}}$	77

		Page
Figure 4.5	Radial Strain Distribution for Circular Plates	78
Figure 4.6	Radial Strain Distribution for Square Plates	79
Figure 4.7	Radial Strain Distribution for Rectangular Plates	80
Figure 4.8	Final Mode Profile and Contour Plot - Circular Plates	81
Figure 4.9	Final Mode Profile and Contour Plot - Square Plates	82
Figure 4.10	Final Mode Profile and Contour Plot - Rectangular Plates	83
Figure 4.11	Graph of Time to Reach Initial Deflection vs Impulse for Circular Plates	84
Figure 4.12	Graph of Time to Reach Initial Deflection vs Impulse for Square Plates	85
Figure 4.13	Graph of Time to Reach Initial Deflection vs Impulse for Rectangular Plates	86
Figure 4.14	Graph of Deflection-Thickness Ratio vs. Johnson's Damage Number for Different Plate Geometries and Loading conditions	91
Figure 4.15a	Graph of Deflection-Thickness Ratio vs Dimensionless No. ϕ_c	92
Figure 4.15b	Graph of Deflection-Thickness Ratio vs Dimensionless No. ϕ_c Showing Least Squares Correlation	93
Figure 4.16a	Graph of Deflection-Thickness Ratio vs Dimensionless No. ϕ_q	94
Figure 4.16b	Graph of Deflection-Thickness Ratio vs Dimensionless No. ϕ_q Showing Least Squares Correlation	95
Figure 5.1	Graph of Deflection-Thickness Ratio vs $\phi_{c,q}$	107

LIST OF TABLES

		Page
Table 2.1	Resume and Results of Experimental Techniques of Impulsively Loaded Plates	9
Table 2.2	Characteristics of the Photovoltaic Cell ...	13
Table 2.3	Details of Ballistic Pendulum	26
Table 2.4	Test Data for Circular Plates	43
Table 2.5	Test Data for Square Plates	44
Table 2.6	Test Data for Rectangular Plates	45
Table 4.1	Regime of Damage	96
Table 4.2	Dimensionless Parameters	97
Table 4.3	Summary of Comparative Experimental Data	98
Table A.1	Resume of Approximate Methods for Predicting Deformation of Thin Plates Subjected to Uniform Impulsive Loading	

NOMENCLATURE

Upper Case Characters

A	Area of plate
A_o	Area of plate over which impulse is imparted
B	breadth of quadrangular plate
F	force
I	total impulse
L	length of quadrangular plate
L	distance between nodes of undeformed plate.
R	circular plate radius
Z	direction of motion perpendicular to plate shape.

Lower Case Characters

ℓ	physical distance between nodes after deformation
m	lumped mass
n	material constant
t	plate thickness
t	time
u	transverse displacement
$\dot{u}$	transverse velocity
$\ddot{u}$	transverse acceleration
v	impact velocity
v	lateral displacement
$\dot{v}$	lateral velocity
$\ddot{v}$	lateral acceleration

Greek Characters

α	Johnsons Damage Number
β	Geometry number
ϵ	strain
$\dot{\epsilon}$	strain rate
$\dot{\epsilon}_o$	strain rate material constant
λ	aspect ratio
λ	scaler multiplier
ρ	density
ϕ	Modified damage number
$\underline{\phi}$	Mode shape, contours
$\underline{\phi}_i$	Intermediate Contours
σ	stress
σ_o	static yield stress
σ_d	damage yield stress
θ	tangent to the horizontal
ζ	loading parameter

Subscripts

c	centre node
i	i^{th} node

CHAPTER 1 - INTRODUCTION

The deformation of thin plates subjected to large impulsive loads has interested researchers for several decades. There have been many theoretical models supported by some experimental studies. In almost all cases the models presented were for a single plate geometry with the associated experimental evidence provided by other researchers. This study presents an approach which can be used for several geometries.

In the first section of Chapter 2 of this thesis the previous experimental work is summarized. Measurements of the dynamic response of structures such as beams and plates have been reported using various testing techniques. These include situations where the structure is subjected to air pressure waves created by explosive devices, underwater explosive forming, direct impulsive loading using plastic sheet explosives and spring loaded arms. These investigations have primarily been concerned with the final deformed shape and the deflection-time history. Whereas it is simple to measure the deformed shape of a structure, the deflection-time history is more difficult to measure and methods used include high speed photography, stereophotogrammetric techniques, strain gauges and condenser microphones. Chapter 2 continues by describing the experiments of this study. Sheet explosive was used to simulate impulsive loading, the magnitude of the impulse being measured by a ballistic pendulum. The deflection-time history was recorded using a light-interference technique in which photo-voltaic diodes were used to measure the light interference patterns obtained during deformation. Deflections of up to 20 mm during a time period of 200 μs were observed in over 100 experiments on fully clamped circular, square and rectangular plates.

The tests were carried out on mild steel plates which was regarded as rigid-viscoplastic. The rigid-viscoplastic constitutive relation adopted was

$$\frac{\dot{\epsilon}}{\dot{\epsilon}_0} = \left[\frac{\sigma}{\sigma_0} - 1\right]^n$$

where σ, $\dot{\epsilon}$ are stress and strain rate respectively, σ_0 is

the static yield stress and $\dot{\epsilon}_o$, n are material constants.

Chapter 3 begins with a summary of the theoretical studies previously reported. The first studies predicted small deflections for circular plates. This was extended by adding membrane effects to the bending effects and further extended when only the membrane stretching action was considered while assuming a deformed shape. Several proposals using energy methods were also used, all with an assumed deformed shape profile. The approximate methods discussed rely on the mode concepts.

Predictions of deformations for quadrangular plates (very few compared to circular plate predictions), also considered the bending action of the plate, membrane effects and energy methods.

Chapter 3 continues with a description of the mode approximation presented in this study which is applicable to any geometry and is based on the assumption that membrane stresses predominate, and that at any instant the shapes of the displacement field and the velocity field are the same. Very simple kinematic and dynamic conditions are imposed, and an iterative forward integration scheme is used to advance the solution in time.

Two approaches were attempted: the first assumed, as did all previous predictions, that material points on the plate move perpendicular to the initial plane of the plate, while the second assumed a displacement field in which the trajectory of every point on the surface remains normal to the deforming plate surface.

In Chapter 4 both the experimental and theoretical results are presented and compared. These experimental results are also compared with experimental results obtained by other researchers. From an analysis of all the experimental results an empirical relationship between the deflection-thickness ratio and a function of impulse, plate geometry, plate dimensions and material properties is presented.

Chapter 5 concludes this thesis with a discussion and interpretation of the results. Experimental results and theoretical predictions are shown to compare favourably for all three plate geometries investigated.

CHAPTER 2 - EXPERIMENTAL DETAILS.

2.1. INTRODUCTION

There have been several experimental studies to measure large deformations of plates subjected to blast and impact loading. These investigations have primarily been concerned with the measurement of the final deformed shape, while only some measurements of the deflection-time history and impulse have been reported. The magnitude and shape of the deformed plate depend on the form of impulsive loading. Whereas it is simple to measure this final deformed shape of the structure, the deflection-time history and, to a lesser degree, the impulse are more difficult.

Earliest studies reported were mainly concerned with structures subjected to underwater explosive charges. Taylor [1] describes experiments of large steel plates, approximately 1,83 x 1,22 m, subjected to underwater explosive blasts fired at various distances from a position normal to the plate through its mid-point. The principal measurements made in cases where the plate did not burst were the volume contained between the dished plate and its original position, and the maximum displacement. Travis *et al* [2] and Johnson *et al* [3] studied the effect of underwater explosive forming on fully clamped circular discs of various thicknesses and different materials. Again the maximum displacement was measured. In Refs [1-3] the response time and the impulse were not measured. Johnson *et al* [4,5] in other investigations measured the displacement-time history using pin-contactors developed by Minshall[6]. The pins were positioned at known intervals apart and as the blank made contact with each pin a signal was generated and displayed on an oscilloscope. Finnie[7] investigated, on several plate materials and plate thicknesses, the experimental relationship between deformation and explosive parameters such as charge mass and stand off distance. Williams[8] used high speed photography (15000 frames per second) to

photograph, against a graticule, the growing bulge of a plate specimen. Boyd[9] reported on underwater explosive tests on circular plates, in which the total applied impulse was determined using empirical formulae reported by Cole[10]. Bednarski[11] presented results of a circular membrane subjected to an abrupt pressure rise by the underwater detonation of explosives. The deformation of the membrane was measured with a high speed camera kit equipped with a stereoscopic attachment. The filming speed was 6000 frames per second and the entire process was filmed with as few as ten frames. The deflection-time history was plotted for the entire plate.
The range of deformations of the above experiments are 10 - 120 deflection- thickness ratios [1,2,3,8,11], and the plate specimens are deformed in approximately 1500μs[11].

The second type of impulsive loading was reported by Witmer *et al* [12] in which work by Hoffman[13] was described. Pressure waves were created by an air-blast from detonations of spherical charges of pentolite of various masses placed on the central axis and normal to, and at various distances from, the test specimen. The magnitude of the permanent deformations measured were up to 16 plate thicknesses. No impulse or response time-history measurements were reported.

The third type of impulsive loading was first reported by Humphreys[14], which involved the use of sheet explosive and a ballistic pendulum. Layers of Dupont sheet explosive of thickness 0.4 mm each were applied to a clamped beam, separated from the beam by a layer of sponge rubber to prevent spallation. The test specimens were rigidly clamped to a ballistic pendulum. The burn rate of the explosive was 6700 ms^{-1}. This is higher than the speed of sound in the materials used. Johnson[15] reports the speed of sound in the following materials; carbon steel 5150 ms^{-1}, aluminium 5700 ms^{-1}, copper 3700 ms^{-1}, brass 3350 ms^{-1}. It was thus felt that a fair approximation to instantaneous uniform loading was obtained. The deform-

ation-time history was measured by means of using a high speed camera modified for split frame use capable of achieving effective speeds of 10000 to 12000 frames per second. The explosion was initiated at the centre of the test specimen by means of a pigtail of the same material leading back to a standard detonator inside a rigid container to shield the pendulum from the detonator blast. A Fastax camera was attached to the pendulum behind the test specimen and was shielded from the blast so that the light produced from the explosion was prevented from reaching the camera lens. No strain measurements were made owing to the difficulty encountered in keeping strain gauges from being spalled off by the initial explosively produced transverse stress waves. Humphreys reports that the two assumptions inherent in the successful use of this technique are verified in the first eight frames. The explosion starts to occur in the second frame and is completely over in the fourth frame (a time span of approximately 200 - 250 μs) before the beam had noticeably moved at all. Subsequent motion takes place under no load, purely as a result of the inertia. Thus the assumption of an initial velocity condition under impulsive loading is reasonable. The final plastic deformation was observed by the sixth frame - hence deformation taking place in approximately 150 - 200μs - which is extremely short compared to the natural period of the ballistic pendulum. (In Humphreys experiments this period was 4,43 sec.) Thus all plastic deformation is over well before the pendulum has moved at all. The recorded pendulum swing gives a direct indication of the maximum potential energy of the system after the dissipation of energy in plastic work. This potential energy is used to calculate the maximum velocity of the whole pendulum system and hence gives an accurate measure of the applied impulse.

The sheet explosive/ballistic pendulum method has been used by several researchers during investigations of different types of specimens. The deflection-time history was not always measured. Florence and Firth[16] conducted experiments on pinned and clamped beams separating the sheet explosive from the beam by a layer of Neoprene. The rig on which the beams were attached was fixed, and the impulse was measured by calibration of the sheet explosive. Several of these experiments were photographed using a Beckman and Whitley framing camera. Florence and Wierzbicki[17,18] performed similar experiments on full edge - clamped circular plates, in which only the final deflection of the plate profile was measured. Duffey and Key[19,20] also calibrated the sheet explosive for experiments on fully edge clamped circular plates. A high speed camera was used to measure the displacement-time history and strain gauges were used in some cases for strain measurements.

Jones *et al* [21] describes experiments on end-clamped wide beams and rectangular plates in which the impulse was measured directly using a ballistic pendulum.
Jones *et al* [22] subsequently describes experiments on fully clamped rectangular plates using the same techniques. A significant result of this work was that it appears that the type of attenuator, i.e. foam or neoprene, did not influence the outcome of the test, except that the impulsive velocity varied depending on the attenuator used. Further work by Jones and Baeder[23] investigated fully clamped rectangular plates of varying length to breadth ratios. Symonds and Jones[24] also reported on fully clamped beams attached to a ballistic pendulum. In the experiments described in Refs[21-24] only the final deformations were measured.

Bodner and Symonds[25], in investigating the dynamic plastic loading of frames using a ballistic pendulum, measured the time-history response of the frame by using wire resistance strain gauges placed at the top of the

columns on both sides. Bodner and Symonds[26] also investigated the response of fully clamped circular plates, but this time measured the deflection-time history by using a condenser microphone placed near the centre of the plate.

The range of deflection-thickness ratios for the plate experiments using sheet explosive is 0,4-9,0 [17-20,25] for circular plates and 0,2 - 10,0[21-23] for quadrangular plates which is significantly smaller than those due to underwater explosion tests. The deformed plates reach their maximum deflection in approximately 150 - 200 μs[20,26]; also significantly less than those due to underwater explosion tests.

Ghosh *et al* [27,28,29] used another method, described in detail by Ghosh and Travis [30], to subject a membrane to an impulsive load. This method made use of an inertial forming machine which is comprised of a spring loaded arm which carries a pair of clamping rings holding the membrane at its end. The arm is drawn back against the resistance of the springs by a winch arrangement. After release the arm accelerates the membrane and clamping ring assembly to a maximum speed of 55 ms^{-1}, and is brought to rest when the clamping ring strikes an anvil and separates from the arm following the failure of a set of shear pins. The arrest of the clamping ring is followed by the deformation of the membrane under its own inertia. Strain gauges were used to measure the strain-time histories, but at higher initial velocities these gauges spalled from the specimens. Deflection-thickness ratios of up to 45 were measured.

Table 2.1 summarizes the plate test results of all the methods described above.

TABLE 2.1- Resume and Results of Experimental Techniques of Impulsively Loaded Plates

A CIRCULAR PLATES

	Diameter mm	Specimen Type	Plate Thickness mm	Deflection Thickness Ratio	Response Time μs
Underwater Blast					
Travis & Johnson 1962 [2]	150	Stainless Steel	0.9	35 - 54	
		Mild Steel	0.9	20 - 45	
			1.2	16 - 36	
			1.6	17 - 24	
		Brass	0.9	31 - 48	
			2.0	15 - 23	
		Titanium	0.9	22 - 37	
		Aluminium	0.9	22 - 35	
			2.0	11 - 20	
		Copper	0.9	27 - 48	
			2.0	16 - 24	
Finnie 1962 [7]	140	Steel	1.2	47	
			1.6	36 - 38	
			2.7	18	
			3.3	17	
			6.4	8	
		Titanium and Alloys	1.3	38 - 48	
			3.2	9 - 18	
			6.2	4 - 9	
Boyd 1966 [9]	200	Aluminium	1.3	53	
Bednarski 1969 [11]	200	Mild Steel	0.83	60	1700
Air Blast					
Witmer, Balmer Leach, Plaan 1963 [12]	610	Aluminium Alloy	3.2	16	
			6.4		
			9.6	9	
Inertial Forming Machine					
Ghosh et al 1976 [27] 1979 [30] 1984 [29]	120	Lead	0.61	44	
		Aluminium	0.31	42	
Sheet Explosive Blast					
Florence & Werzbicki 1966 [17] 1970 [18]	100	Aluminium	6.3	1.6 - 7	
		Mild Steel	6.3	0.4 - 4	
Duffey & Key 1967 [19] 1968 [20]	150	Aluminium	1.6	4 - 9	
			3.2	1.5 - 1.7	
		Mild Steel	1.6	3 - 4	
Bodner & Symonds 1979 [26]	64	Titanium	2.3	0.9 - 6	
		Mild Steel	1.9	0.5 - 7	
Nurick	100	Mild Steel	1.6	4 - 12	140-190

Table 2.1 (continued)

B NON-CIRCULAR PLATES

	Dimensions mm	Specimen Type	Plate Thickness mm	Deflection Thickness Ratio	Response Time μs
Underwater Blast					
Taylor 1942 [1]	1830 x 1220	Steel	3.1	51	
			4.4	6 - 25	
			5.9 - 6.4	12 - 35	
			9.3	2 - 21	
Sheet Explosive Blast					
Jones, Uran & Tekin 1970 [22]	129 x 76	Mild Steel	1.6	3.5 - 7.0	
			2.5	1 - 4.5	
			4.4	0.3 - 1.7	
		Aluminium	3.1	1.8 - 3.5	
			4.8	0.8 - 2.4	
			6.2	0.2 - 1.4	
Jones & Baeder 1972 [23]	128 x 32	Mild Steel	2.7	0.3 - 1.2	
		Aluminium	2.7.	0.5 - 1.2	
	128 x 64	Mild Steel	2.7	0.8 - 4	
		Aluminium	2.7	1.2 - 3	
	128 x 96	Mild Steel	2.7	0.7 - 7.5	
		Aluminium	2.7	2.0 - 4.5	
	128 x 128	Mild Steel	2.7	1.6 - 9.5	
		Aluminium	2.7	3.0 - 6.0	
Nurick	113 x 70	Mild Steel	1.6	3 - 12	
	89 x 89	Mild Steel	1.6	6 - 12	90-180

2.2 EXPERIMENTAL MEASUREMENTS

Of prime importance when dealing with such complicated experiments is simplicity of the measuring device. Methods such as high speed photography require high precision coordination between the film speed and the explosion. At 12000 frames per sec. the event is completed in two to three frames. In addition there is the inherent danger of damaging expensive equipment. Strain gauges appear to be useful only for relatively low deflection-thickness ratios. The condenser microphone measured only average results over the central region of the plate.

In addition to measuring the deformation-time history, measurement of the impulse is required. These impulse measurements have been obtained in several ways - either by a separate series of explosive calibration tests [17-20], or from a knowledge of the explosive density of the sheet[21-23] or as in Bodner and Symonds[26] where direct impulse measurements were made for each test. The desirability of this option is worth emphasising. The impulse per unit mass of charge depends not only on the charge mass, but on the geometry of the charge and the configuration adjacent to the specimen. Duffey and Key[20] indicate that it may also depend on the specimen properties.

The experimental technique presented here makes use of a light interference method to measure the deflection-time history while simultaneously measuring the impulse directly by means of a ballistic pendulum. Also measured were the final mid-point deflection, the radial plate thickness variation and the uniaxial yield properties of the plate material. Each of these measurements is discussed in more detail hereafter.

2.3 LIGHT INTERFERENCE EQUIPMENT FOR DEFLECTION MEASUREMENT

The concept of light interference could be used in principle for measuring deflections of any magnitude and which take place over any time range, for example 20μs to several hours. However, the device to be described was developed specifically for measuring the deflection-time

history at the centre of an impulsively loaded plate. From the previous discussion, specifications for the design of the device require that it should have the ability to;

i) record the deflection of a localised region of the plate as opposed to the average deflection over a larger area,
ii) record deflections up to 20 mm, being some 13 plate thicknesses in this case.
iii) to record the peak deflections, occurring some 100-200μs after detonation, and the final deflections after a few ms.
iv) operate on a ballistic pendulum behind the specimen.

The basis of the instrument is a light sensitive cell, in this case a silicon photovoltaic diode, which produces an electrical output dependent on the light intensity over the cell. The characteristics of the diode are given in Table 2.2

In Fig. 2.1 a side view schematic of the general layout of the rig is shown. The specimen plate is clamped between two holding plates. A torque wrench was used to ensure that equal torque on all nuts was maintained. The light rays travel parallel and adjacent to the bottom face of the specimen plate at the one extreme, and parallel to the plate at the other extreme. Hence movement of the plate through any part of this distance will interfere with the light rays.

Slots are cut into the bottom holding plate into which the prisms are secured. The prisms are 3 mm wide and are designed in such a way that the depth of the parallel rays of light is slightly greater than the anticipated maximum deflection of the plate. The slot in the plate must be kept as narrow as possible in order to

TABLE 2.2 - Characteristics of the Photovoltaic Cell

Storage Temperature	-50 to +100	°C
Reverse Voltage	1	V
Rise Time	4	μs
Temperature Coefficient of V_t	-2	mV/°C
Temperature Coefficient of I_k	0,1	%/°C
Photo Sensitive Area	7 (3,4 mm x 2,1 mm)	mm²

V_t = open-circuit voltage

I_k = short-circuit current

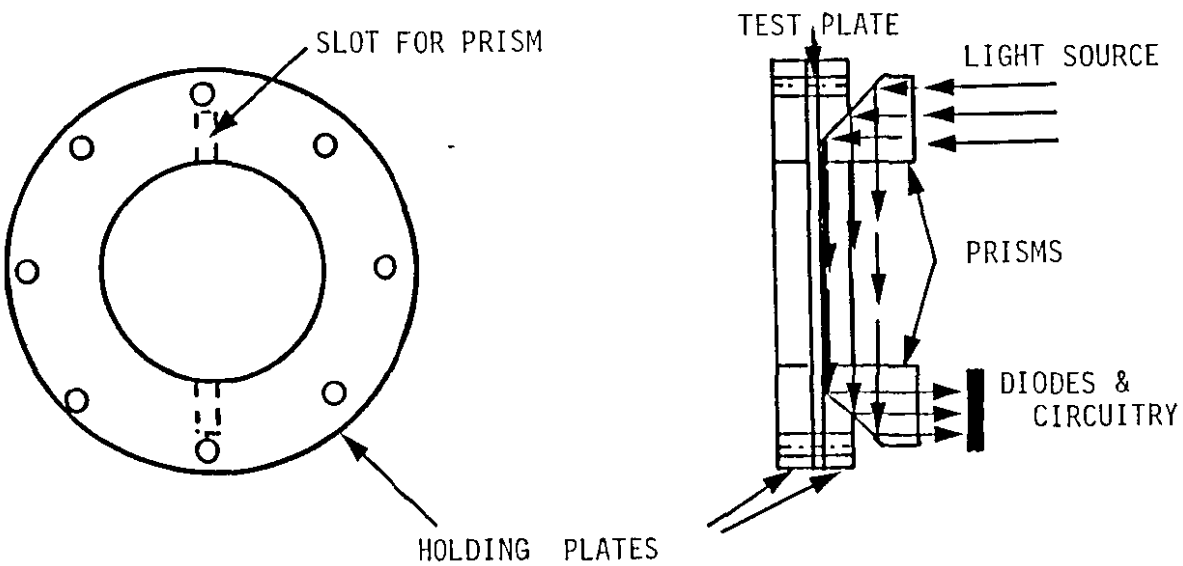

FIGURE 2.1 SCHEMATIC LAYOUT OF TEST RIG

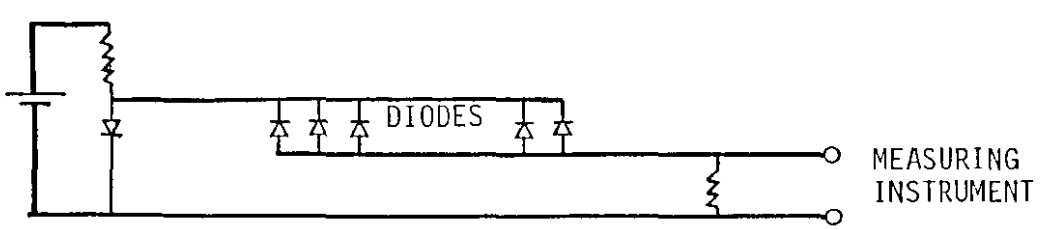

FIGURE 2.2 CIRCUIT DIAGRAM

i) minimise the discontinuity created on the supporting perimeter of the plate and

ii) measure the deflection at the centre of the plate.

Since the photosensitive area of the diode is small compared with the maximum deflection, many diodes are arranged side by side. This is achieved by glueing them to a perspex bar which is mounted on a vibration resistant rubber strip fixed to the frame.

The circuit diagram for the photovoltaic cells is shown in Fig. 2.2. The light source is a 24 volt d.c. 250 watt light bulb powered remotely by a regulated power supply. Since this bulb is heat generating, the light source is cooled by means of a small fan. This is only necessary for experiments of longer than several minutes duration where drift due to heat was measured at no more than 0,05% per minute (or 3% per hour).

The holding plates stand on several steel legs which are fixed to a base plate, as shown in Fig.2.3. The complete apparatus is then fixed to one end of the ballistic pendulum and counter masses are secured to the other end. A black hood, of heavy rubber and dark material, is secured around the apparatus in order that no external light, such as the flash of the detonation will interfere with the reading.

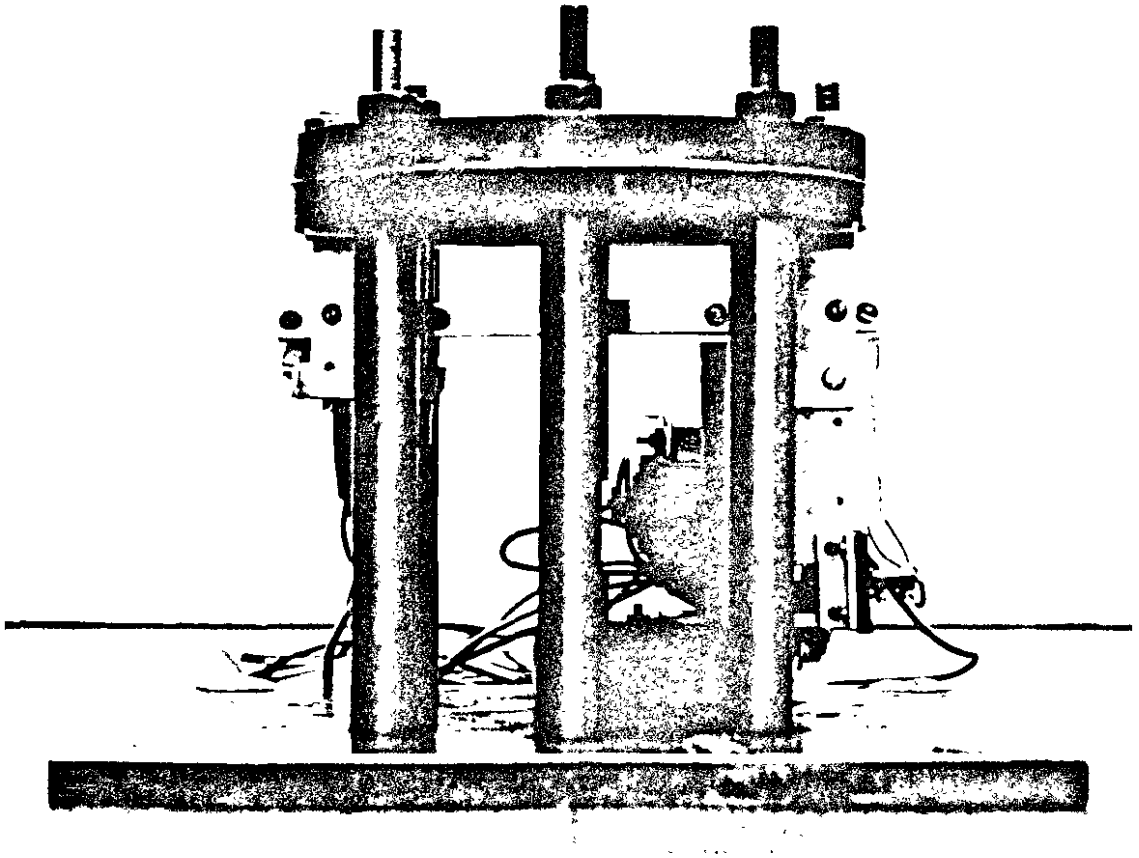

FIGURE 2.3 Photograph of Test Rig

2.4. EXPERIMENTAL PROCEDURE

2.4.1 Introduction

Several series of experiments were performed classified as

Series I - initial tests on circular plates to reproduce and extend previous work in order that a working knowledge of the experimental systems are understood. This involved 36 tests.
Series II - 46 tests on rectangular plates
Series III - 38 tests on square plates
Series IV - 20 tests on circular plates

The Series I experiments were performed in order that a thorough understanding of the experimental method was obtained. The plate specimens were cut from in-stock cold rolled steel and were not annealed. Typical stress-strain curves for this material are shown in Fig. 2.4. No distinct yield stress can be identified.

Subsequently Series II - IV experiments were performed, again using cold rolled structural steel plate. In these cases yield stresses were noted in the typical uniaxial stress-strain curves, as seen in Figs. 2.5a and 2.5b. The static yield stress was computed using the results of the tests and substituting into the rigid viscoplastic constitutive equation.

$$\frac{\sigma}{\sigma_*} = 1 + \left[\frac{\dot{\epsilon}}{\dot{\epsilon}_*}\right]^{1/n}$$

The average static yield stresses for the two plates were 282 MPa and 296 MPa respectively.

In all cases the steel was 1,6mm thick and after clamping the dimensions of the plates were: circular 100 mm diameter, square 89 mm x 89 mm and rectangular 113 mm x 70 mm.

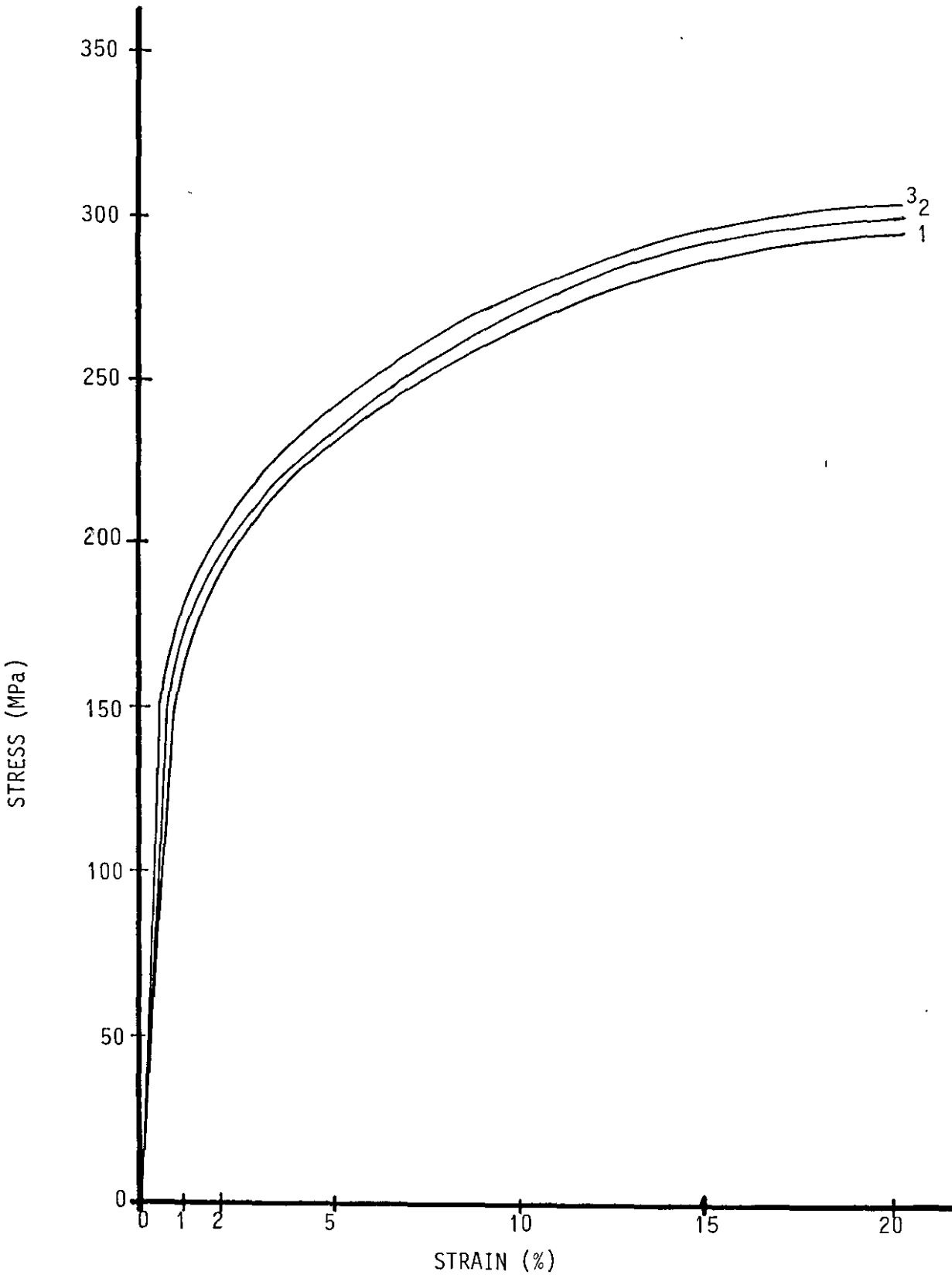

FIGURE 2.4 UNIAXIAL STRESS STRAIN TENSILE TEST FOR SERIES I MATERIAL

STRAIN RATES 1. $1{,}3 \times 10^{-4}\ s^{-1}$

2. $6{,}6 \times 10^{-4}\ s^{-1}$

3. $1{,}3 \times 10^{-3}\ s^{-1}$

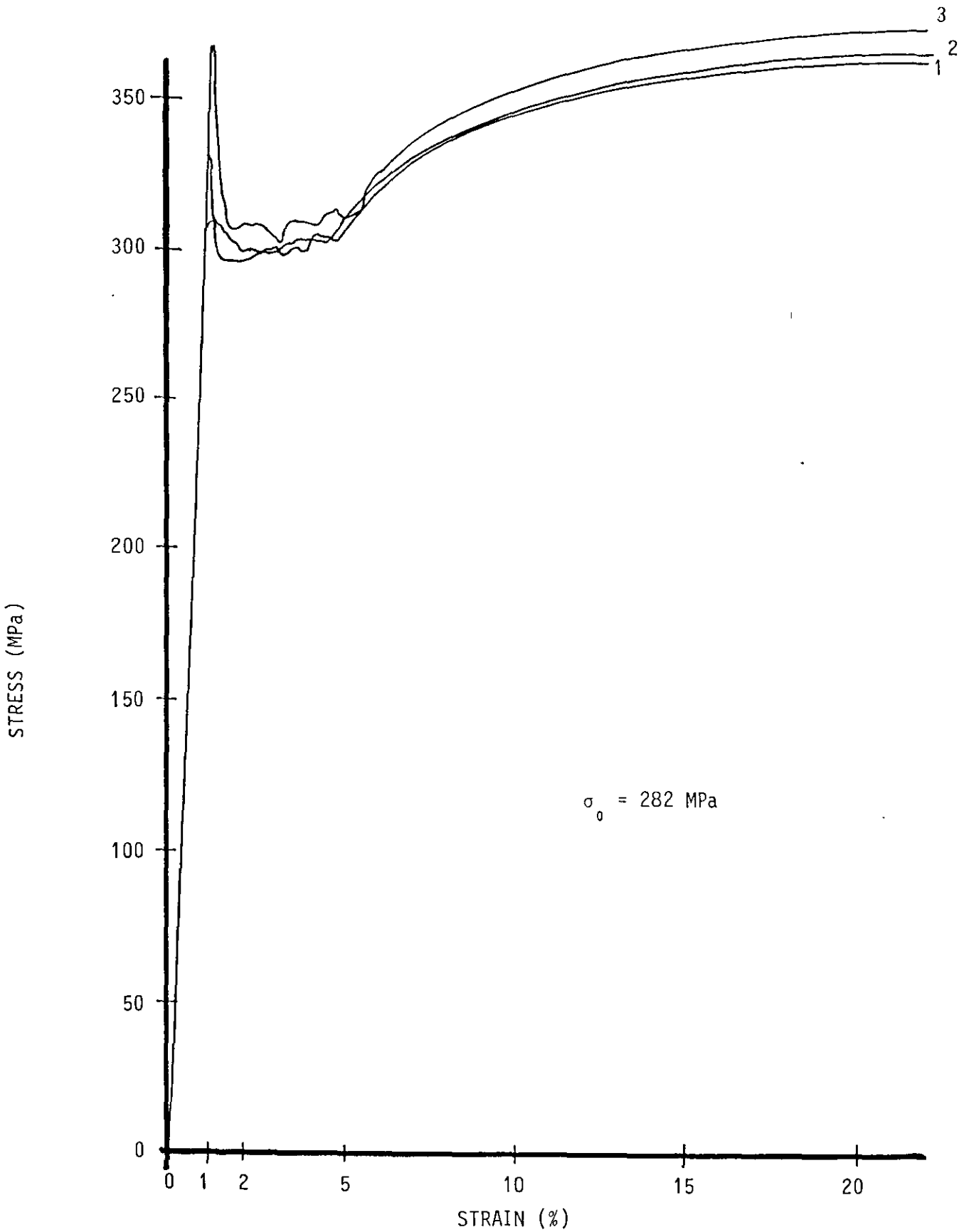

FIGURE 2.5a UNIAXIAL STRESS STRAIN TENSILE TEST FOR SERIES II and IV MATERIAL

Strain Rates 1. $3{,}3 \times 10^{-4}\ s^{-1}$
2. $1{,}3 \times 10^{-3}\ s^{-1}$
3. $6{,}7 \times 10^{-3}\ s^{-1}$

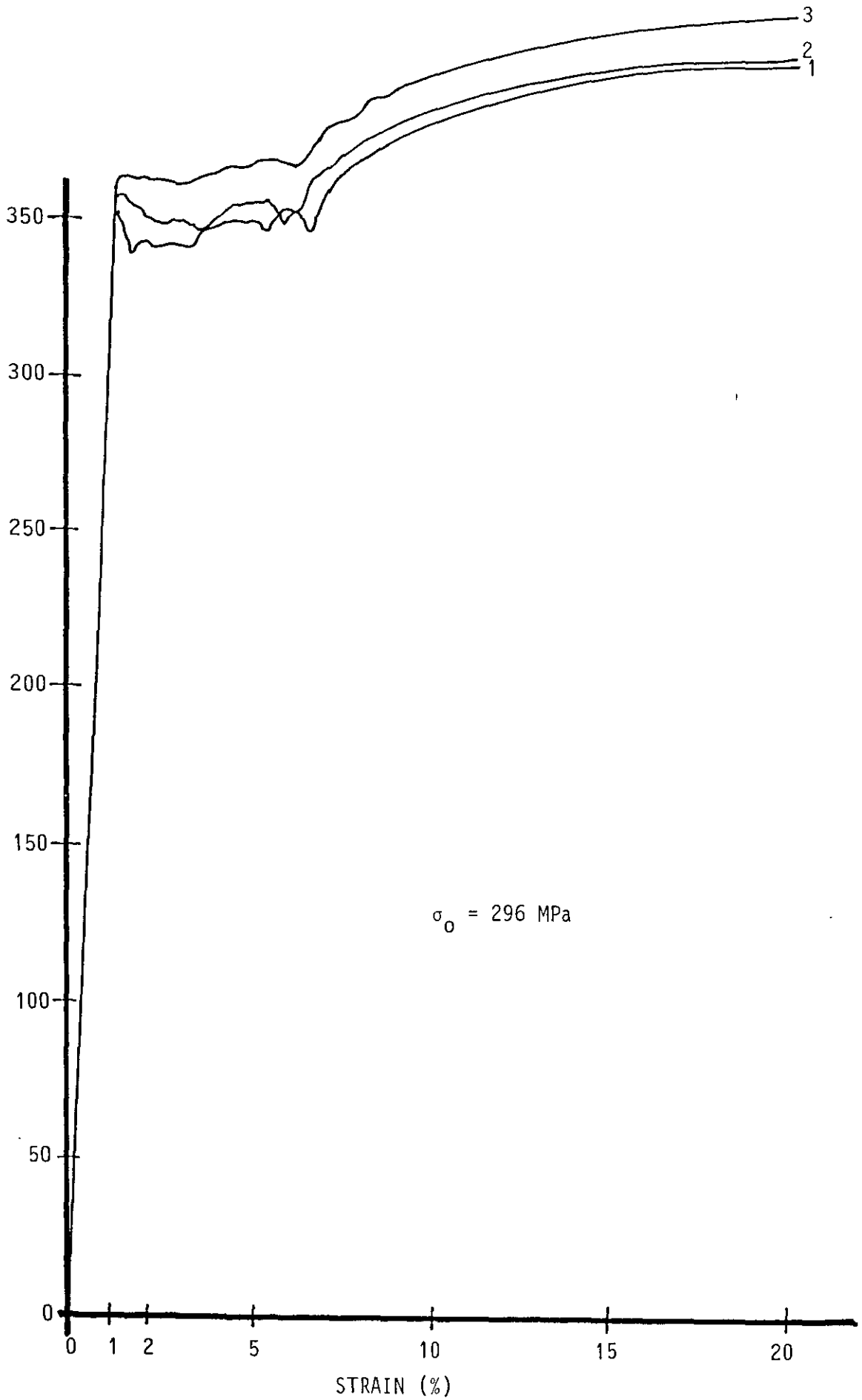

FIGURE 2.5b UNIAXIAL STRESS STRAIN TENSILE TEST FOR SERIES III MATERIAL

Strain Rates 1. $1{,}3 \times 10^{-3}$ s^{-1}
2. $6{,}7 \times 10^{-3}$ s^{-1}
3. $3{,}3 \times 10^{-2}$ s^{-1}

The choice of length/breadth(L/B) ratio of the rectangular plate was based on the golden rectangle rule[31] which requires that L/B = (L+B)/L.
Hence in this case L = 1,618B, where L, B are the length and breadth respectively.

2.4.2 Explosive Material.

The sheet explosive used in the experiments was Metabel with an average thickness of 3,2 mm, a density of 1,47 $g.cm^{-3}$ and a detonation velocity of 6500-7500 ms^{-1}.

The explosive in its manufactured state was too thick to allow a uniform layer to be placed on the full area of the plate. Further if the explosive was rolled to a thickness of less than 3mm it would not detonate. Hence Bodner[31] suggested that three concentric rings be made, as shown in Fig. 2.6a, arranged in such a way that there was on average a uniform distribution of explosive mass over the specimen. Two concentric rings were also used, as shown in Fig. 2.6b. This configuration was primarily used to obtain smaller deflection thickness ratios than the initial configuration. Deflection-thickness ratios of 6,6 to 12,4 were obtained using three concentric rings, while deflection thickness ratios of 3,9 to 12,1 were obtained using two concentric rings.

Hence in Series II - IV experiments the Metabel was arranged in two concentric annuli of the shape of the plate, as shown in Figs. 2.6b, 2.6c, 2.6d. The rings were interconnected by cross leaders, which were in turn connected by a main leader at the plate centre to a shielded detonator.

In all cases the sheet explosive was placed on a 16 mm polystyrene pad, of the dimensions of the exposed plate, to attenuate the shock transmitted to the plate, provide a uniform impulse and prevent spallation of the specimen.

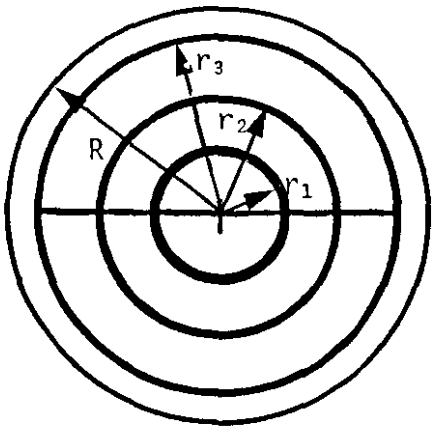

FIGURE 2.6a CIRCULAR 3-RING CONFIGURATION

r_1 = 0,29R
r_2 = 0,57R
r_3 = 0,86R

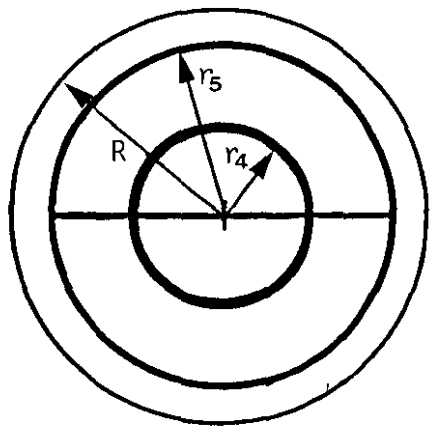

FIGURE 2.6b CIRCULAR 2-RING CONFIGURATION

r_4 = 0,41R
r_5 = 0,82R

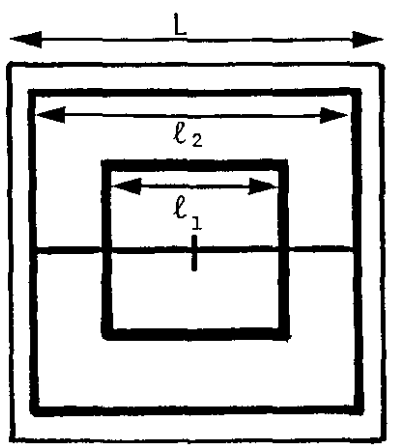

FIGURE 2.6c SQUARE

ℓ_1 = 0,49L
ℓ_2 = 0,84L

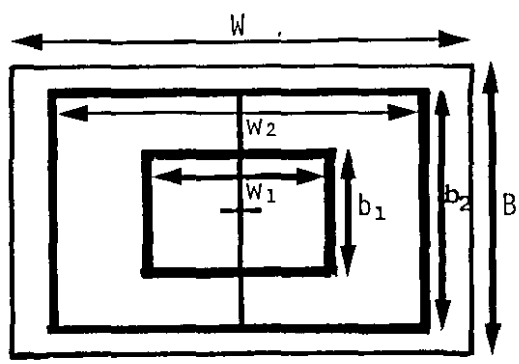

FIGURE 2.6d RECTANGULAR

w_1 = 0,50W
w_2 = 0,87W
b_1 = 0,50B
b_2 = 0,87B

FIGURE 2.6 ARRANGEMENT OF EXPLOSIVE IN CONCENTRIC ANNULI OF PLATE SHAPE

2.4.3 Ballistic Pendulum

The ballistic pendulum used to measure the impulse consisted of a length of I-beam suspended by four strands of spring steel wire from the concrete slab ceiling in the blasting room. This room was approximately 2,5 m x 3,5 m in floor area. The pendulum was levelled by means of adjustable screws fitted at the attachment of the wires to the pendulum. At the front end of the pendulum the experimental rig was attached, while at the other end a fixture was available on which balance masses could be sited. This ensured that wires carry approximately equal loads and assists the application of the impulse through the centroid of the pendulum. Also at the back end of the pendulum was a pen to record the pendulum oscillation.

A general layout of the pendulum is shown in Fig. 2.7, while Fig. 2.8 shows the pendulum motion.

The linearised equation of motion of the pendulum, assuming viscous damping, is

$$\ddot{x} + 2\beta\dot{x} + w_n^2\, x = 0 \qquad (2.1)$$

where

$$\beta = \frac{C}{2M},\ w_n = \frac{2\pi}{T} \text{ and } \omega_d = (\omega_n^2 - \beta^2)^{1/2}$$

and C is the damping coefficient, M is the total mass of the pendulum, experimental rig, balance masses and explosive, and T is the natural period of the pendulum motion. The solution of eqn. (2.1) is given by

$$x = \frac{(e^{-\beta t})\dot{x}_o \sin w_d t}{w_d} \qquad (2.2)$$

where $\dot{x}_o$ is the initial velocity of the pendulum.

Let x_1 be the horizontal displacement at $t = \frac{T}{4}$

and $-x_2$ be the horizontal displacement at $t = \frac{3T}{4}$

and substituting into equation (2.2) gives

$$x_1 = \frac{\dot{x}_0 T}{2\pi} \; e^{-\frac{1}{2}\beta T},$$

$$x_2 = \frac{\dot{x}_0 T}{2\pi} \; e^{-3/4\beta T}.$$

Hence $$\frac{x_1}{x_2} = e^{\frac{1}{2}\beta T},$$

to give $$\beta = \frac{2}{T} \; \ell n \frac{x_1}{x_2}, \qquad (2.3)$$

and $$\dot{x}_0 = \frac{2\pi}{T} x_1 \; e^{-\frac{1}{2}\beta T}. \qquad (2.4)$$

The impulse can now be calculated as

$$I = M\dot{x}_0 \qquad (2.5)$$

The period T is simply determined by measuring a number of pendulum oscillations. The damping constant is calculated from equation (2.3) where x_1, x_2 are found from pendulum oscillations in which the pendulum is held away from the vertical and released. Table 2.3 gives the constants for the pendulum used in these experiments.

The distance moved by the pendulum and that measured by the pen are not the same and this must be accounted for. Consider Fig. 2.8, in which the horizontal distance from the end of the pendulum to the recording pen is given by

$$d_1 = (Z^2 - a^2)^{\frac{1}{2}}$$

while at peak oscillations the distance d_2 is

$$d_2 = (Z^2 - (a + y)^2)^{\frac{1}{2}}$$

For small angles

$$x_1 \approx R\theta \text{ and } y \approx \frac{R\theta^2}{2}$$

Hence $$y = \frac{x_1^2}{2R} \qquad (2.6)$$

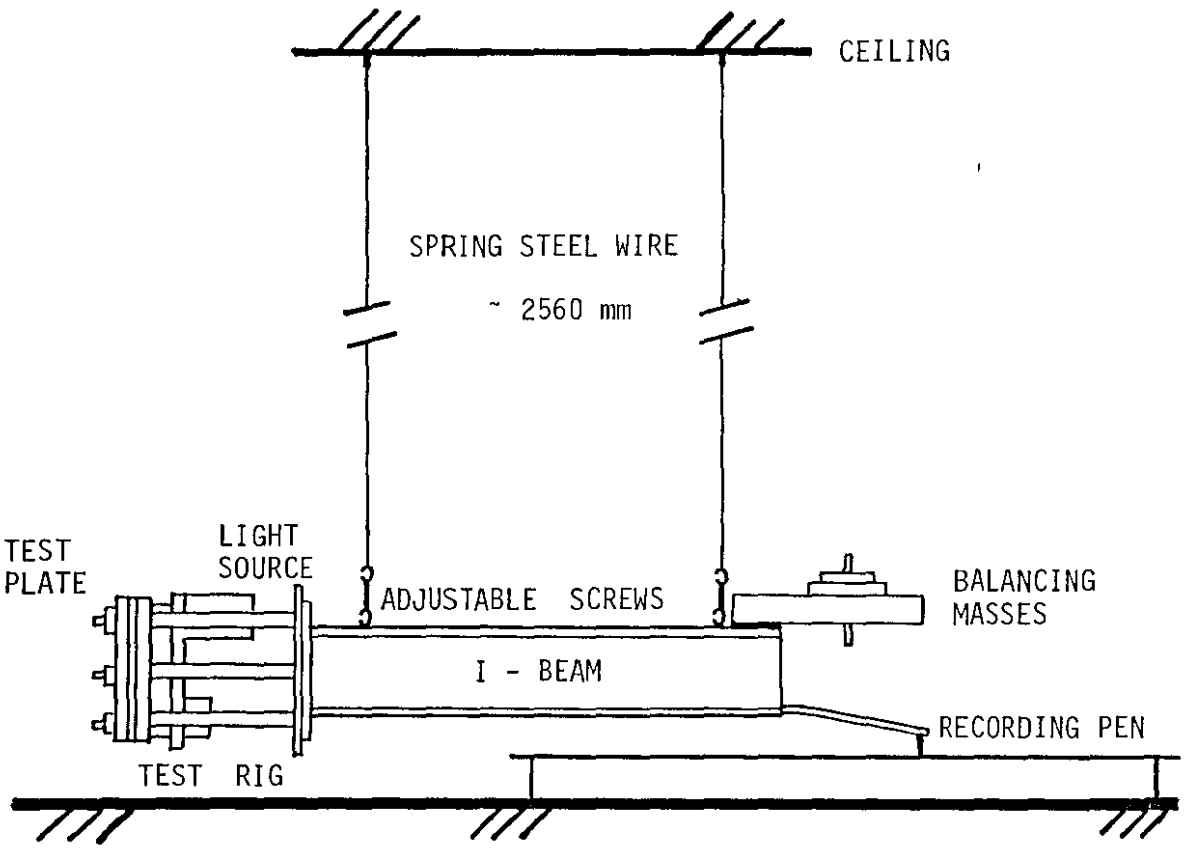

FIGURE 2.7 BALLISTIC PENDULUM CONFIGURATION

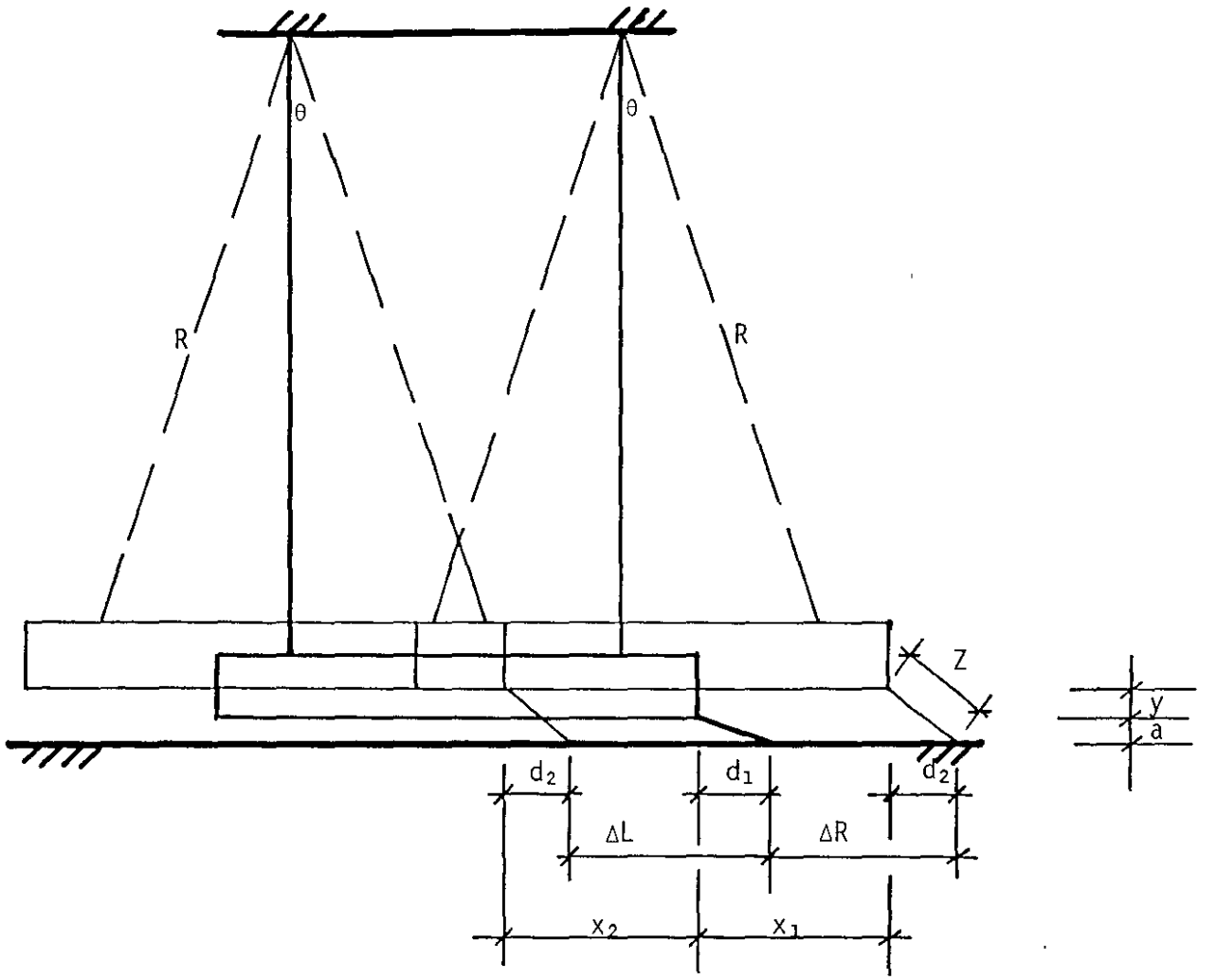

FIGURE 2.8 PENDULUM GEOMETRY

From Fig. 2.8

$$x_1 = \Delta R + d_1 - d_2$$

which becomes

$$x_1 = \Delta R + (Z^2 - a^2)^{1/2} - \left[Z^2 - \left[a + \frac{x_1^2}{2R}\right]^2\right]^{1/2} \qquad (2.7)$$

and similarly

$$x_2 = \Delta L - d_1 + d_2$$

$$= \Delta L + (Z^2 - a^2)^{1/2} - \left[Z^2 - \left[a + \frac{x_1^2}{2R}\right]^2\right]^{1/2} \qquad (2.8)$$

where ΔL, ΔR, Z, a and R are measured and hence x_1, x_2 can be calculated

Table 2.3 - Details of Ballistic Pendulum

R	2563	mm	Mass of I-beam	22,0 kg
Z	180,4	mm	Mass of test rig	20,4 kg
a	139	mm	Mass of Counter balance	24,15 kg
T	3,20	sec		
β	0,0129	per sec.	Typical pen stroke	40 - 135 mm

2.4.4 Calibration of Photo-diodes

During Series I the photodiodes were statically calibrated at three light intensity settings for zero deflections of 75 mV, 85mV, 100mV respectively. The calibration curves which are shown in Fig. 2.9, exhibit similar trends. All experiments in Series I were performed with the light intensity set at the 85mV zero deflection setting. This was chosen as it presented the best deflection range with minimal drift within the capabilities of the voltage regulator and the data acquisition instrumentation.

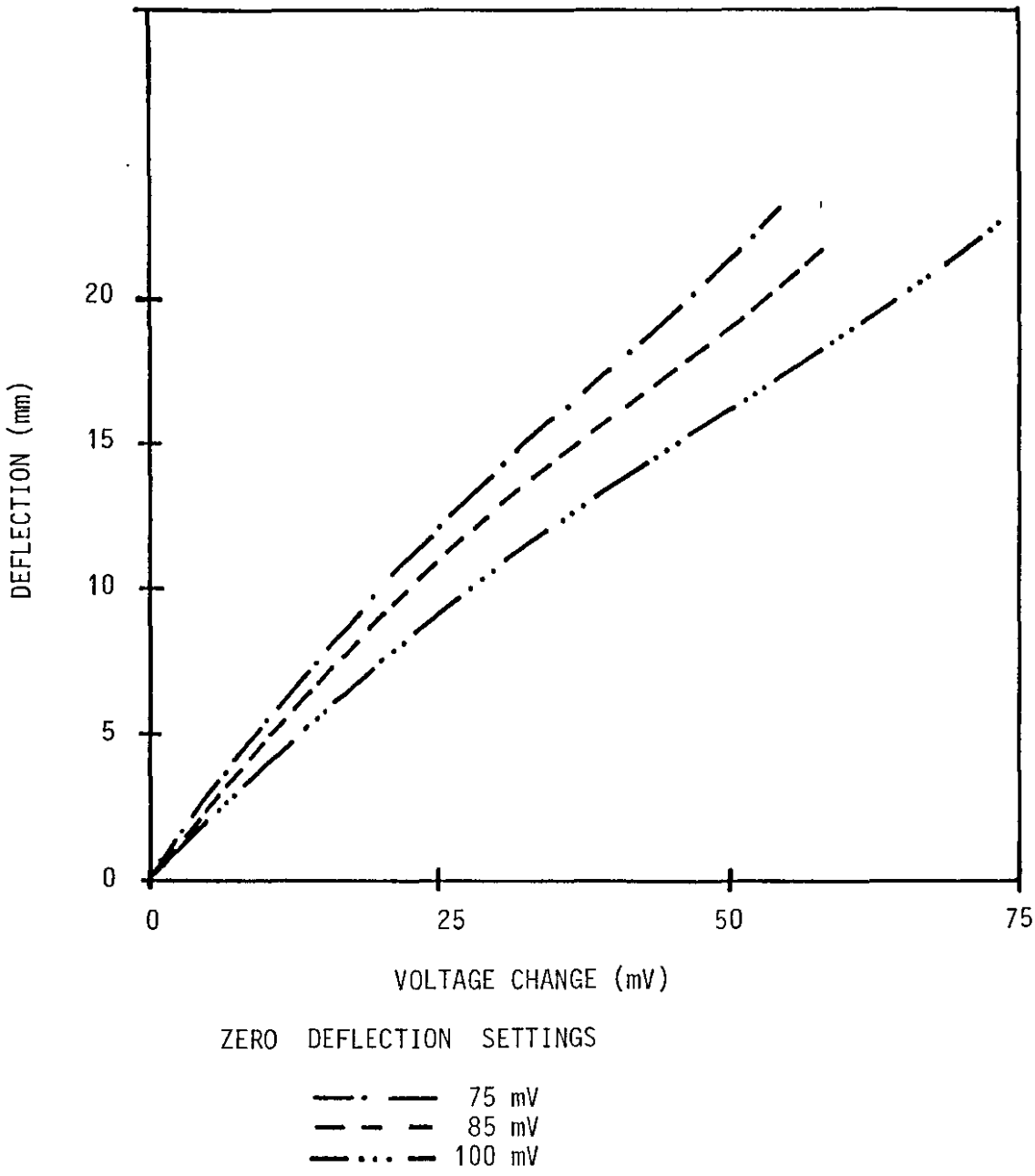

FIGURE 2.9 STATIC CALIBRATION OF LIGHT INTERFERENCE EQUIPMENT

A comparison of the predicted static calibration deflection and measured deflection by mechanical means indicated a reasonably close correlation for small deflections, but for larger deflections the results show large errors. However, a plot of measured deflection versus steady state voltage change, as shown in Fig. 2.10, exhibits a good linear least squares fit ($r = 0,949$). The band width shown in Fig. 2.10 indicates an oscilloscope variation of $\pm$ 1,6 mV, due to the chosen oscilloscope voltage setting which gives a variation of $\pm$ 0,8 mV for both the initial and final readings. This bandwidth envelopes most of the data points, and hence Fig. 2.10 was used as a dynamic calibration analysis. This indicated that although the rise time of the photodiodes was rated at 4μs, these diodes are sensitive to rate of change, and hence no further static calibration was attempted for Series II to IV experiments.

Figs. 2.11 and 2.12 show Series III and IV results of measured deflection versus steady state voltage change. Again good least squares fits are exhibited with correlations of $r = 0,946$ and $r = 0,962$ respectively, and again most data points are within the $\pm$ 1,6 mV bandwidth. In these two sets of experiments the same prisms were used, which accounts for the gradients of the least squares line being similar. The variation in the y-intercept of these two lines is probably due to the fact that the prisms were set at different distances from one another for the two sets of experiments.

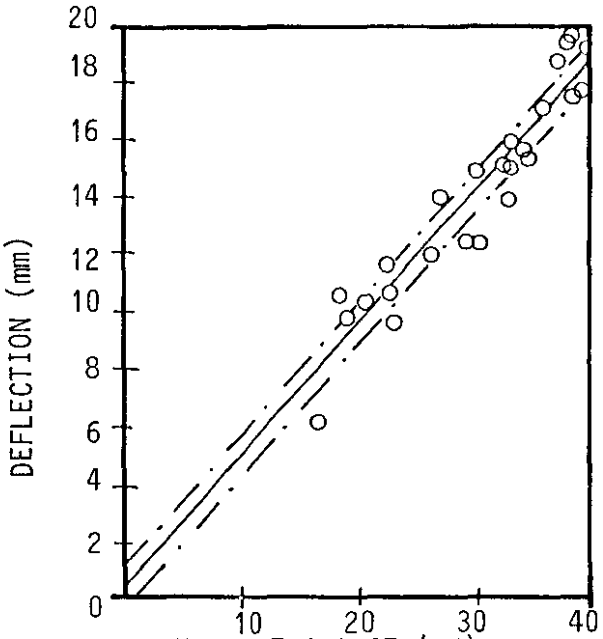

FIGURE 2.10 GRAPH OF MEASURED FINAL MID-POINT DEFLECTION vs STRAIN STATE VOLTAGE CHANGE FOR SERIES I TESTS

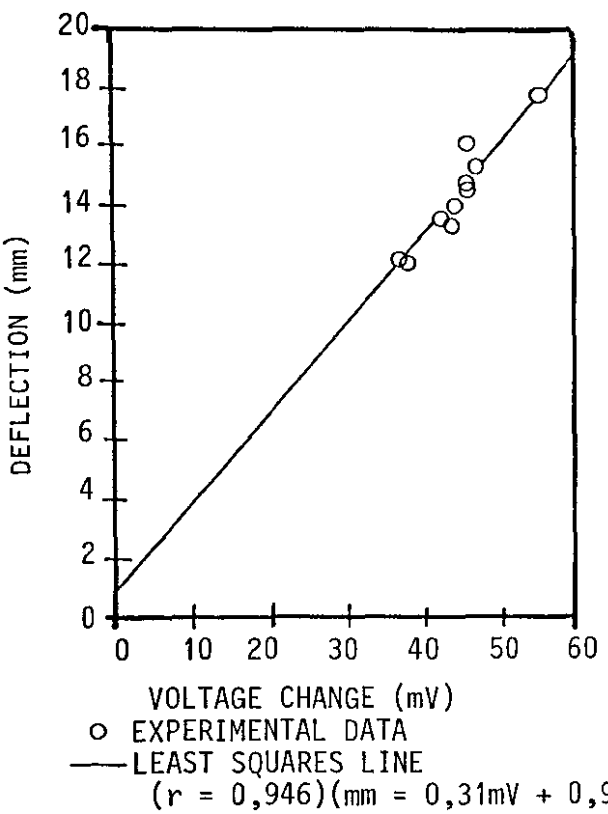

FIGURE 2.11 GRAPH OF MEASURED FINAL MID-POINT DEFLECTION VS STEADY STATE VOLTAGE CHANGE FOR SERIES IV TESTS

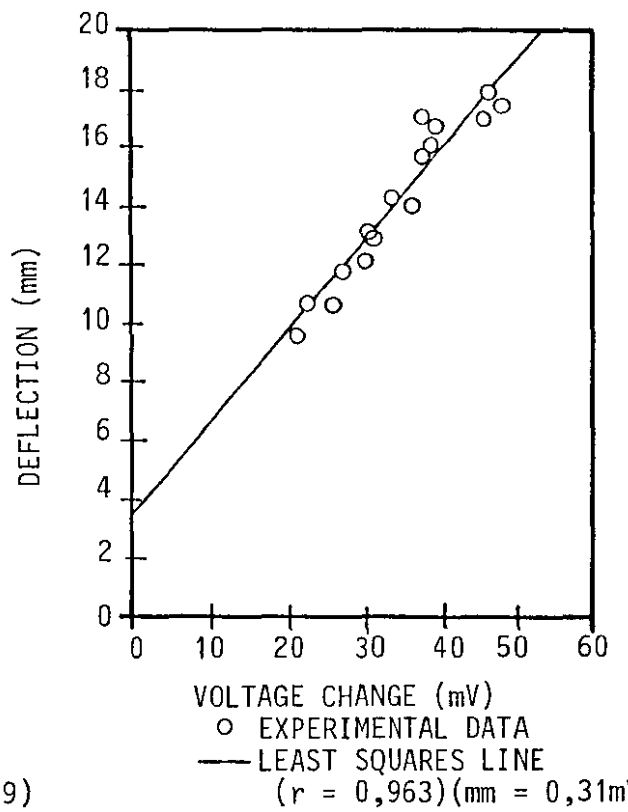

FIGURE 2.12 GRAPH OF MEASURED FINAL MID-POINT DEFLECTION VS STEADY STATE VOLTAGE CHANGE FOR SERIES III TESTS

2.4.5 Effect of Explosive Mass and Geometry

One of the reasons for developing the light interference measuring device was to be able to measure the deflection-time history while simultaneously measuring the impulse. The advantages of such a system avoid the necessity of

i) a separate series of calibration tests
ii) the possible variation in the specified specific impulse of the explosive.
iii) the variation that might occur because of factors such as variable plate material, geometry and boundary conditions.

All the above have been previously encountered, see for example Florence [17], Duffey [19] and Bodner and Symonds [26], in which Dupont Datasheet explosive was used, even though this type of explosive appeared to be of uniform thickness and constant specific impulse. In the experiments described in this thesis it is evidentally more important to overcome these factors because of the nature of the Metabel explosive used and the fact that variable plate geometries were investigated.

The next two paragraphs describe how the layout of the explosive is related to the resulting impulse and hence the need to undertake experiments in this way.

Series I experiments were performed with the explosive cut into strips and laid out in concentric rings as shown in Figs. 2.6a, 2.6b. The impulse for different explosive masses and configurations are shown in Fig. 2.13. For equal masses of the same configuration, the results show large variations of impulse, e.g. for 7g of explosive laid out in the two ring configuration, the resulting impulse ranges from 9 Ns to 12 Ns. For similar masses but different configurations the resulting impulse varies significantly, e.g. 8,6g of explosive results in impulses ranging from 8,5 Ns to 10,4 Ns for the 3 ring configuration and ranging from 14,3 Ns to 15,4 Ns for the 2 ring configuration.

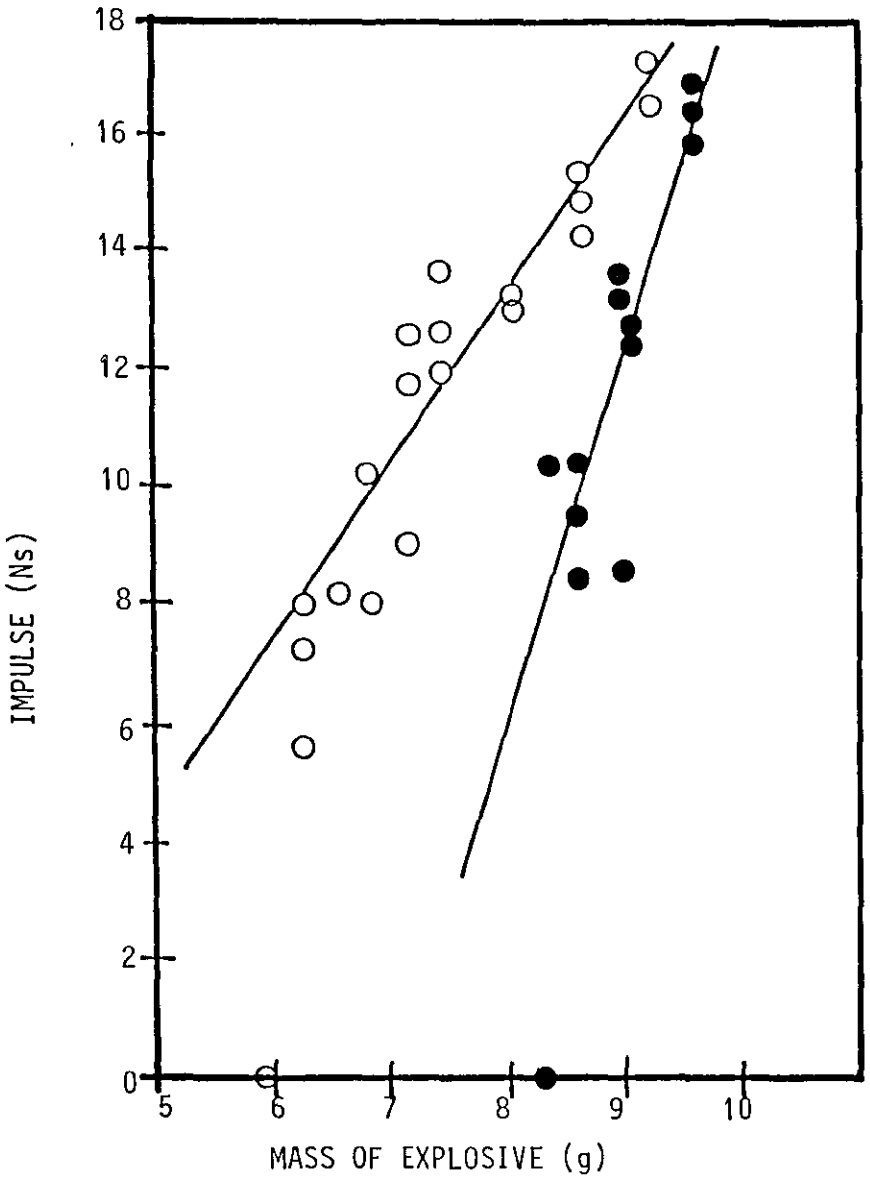

○ 2-RING CONFIGURATION - LEAST SQUARES LINE, r = 0,933:Ns = 3,0g - 10,7
● 3-RING CONFIGURATION - LEAST SQUARES LINE, r = 0,857:Ns = 6,4g - 44,9

FIGURE 2.13 GRAPH OF IMPULSE VS MASS OF EXPLOSIVE FOR SERIES I TESTS

These variations are further illustrated in Series II to IV experiments, as shown in Figs. 2.14, 2.15, 2.16, 2.17. Although the correlations between impulse and mass of explosive according to the least squares lines are good, it is noted that variations, in some cases, are significantly large. Further there may be some statistical evidence that Figs. 2.14, 2.15, and 2.16 are similar but Fig. 2.17 shows the variations as a function of plate geometry.

In all cases it was observed that the explosive would not fire for a total mass of less than 5,5 g. This is simply because the Metabel would not detonate if rolled too thinly.

2.5. TEST RESULTS

2.5.1 Instrumentation Results

In the Series I experiments 36 tests were conducted over a period of 6 consecutive work days, of which 22 tests were complete in the following respects,

i) the explosive detonated correctly,
ii) the peak time was recorded
iii) the peak voltage was recorded
iv) the full time history was recorded.

Of the remaining fourteen tests, the following problems occurred:

i) in one test, the oscilloscope triggered before the explosion.
ii) in four tests the explosive did not detonate
iii) in five tests light from the explosion penetrated the black hood and interfered with the readings.
iv) in one test the bulb sheared at its base
v) the reason for three unsuccessful tests could not be determined.

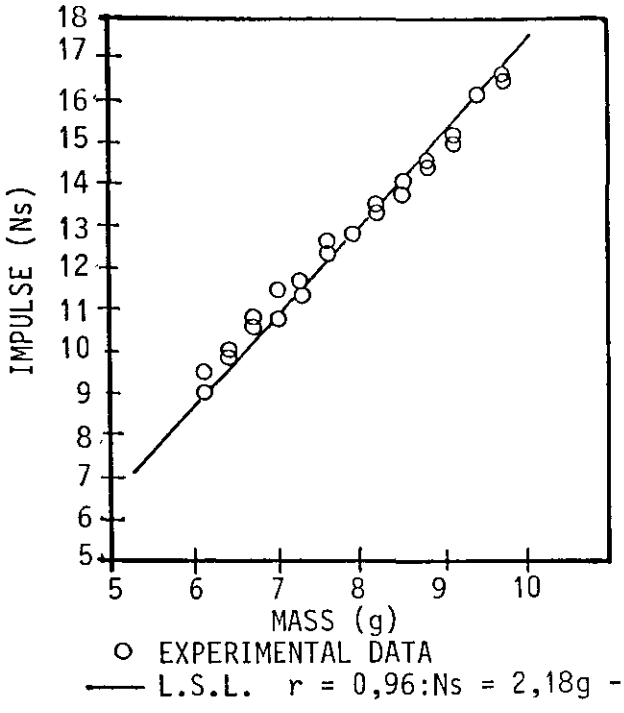

FIGURE 2.14 GRAPH OF IMPULSE VS MASS OF EXPLOSIVE FOR SERIES IV TESTS

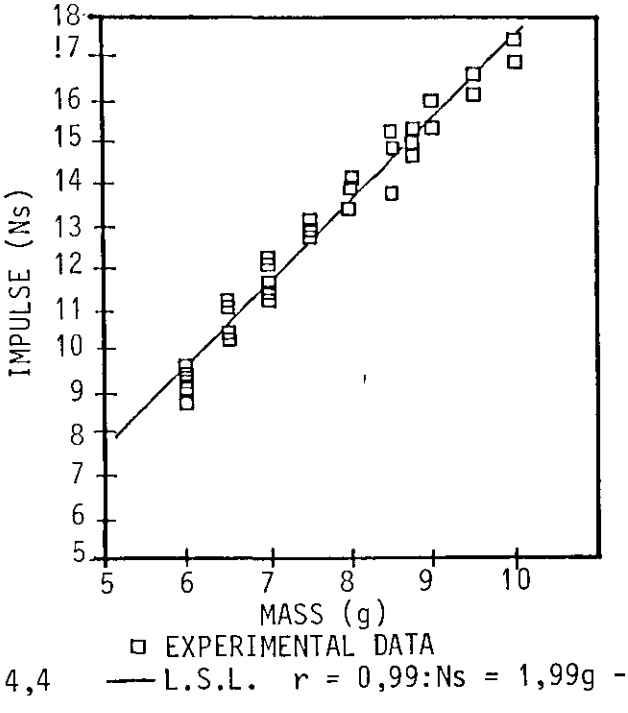

FIGURE 2.15 GRAPH OF IMPULSE VS MASS EXPLOSIVE FOR SERIES III TESTS

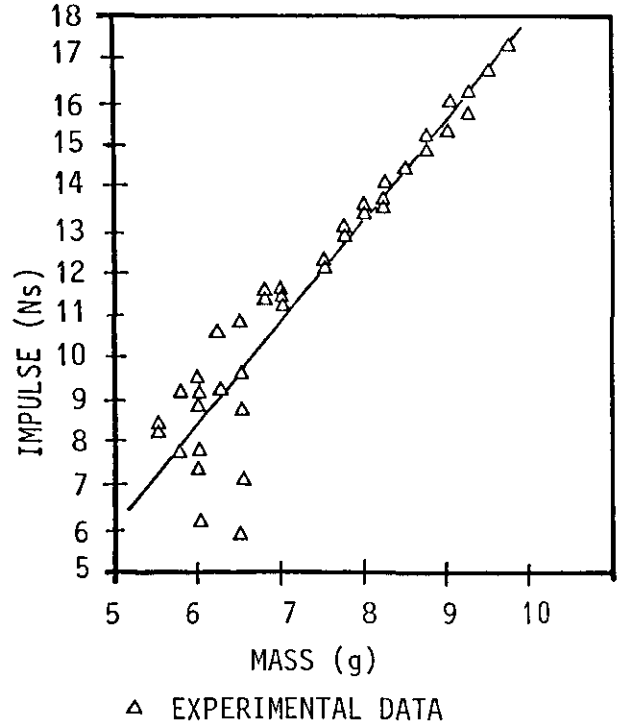

FIGURE 2.16 GRAPH OF IMPULSE VS MASS OF EXPLOSIVE FOR SERIES II TESTS

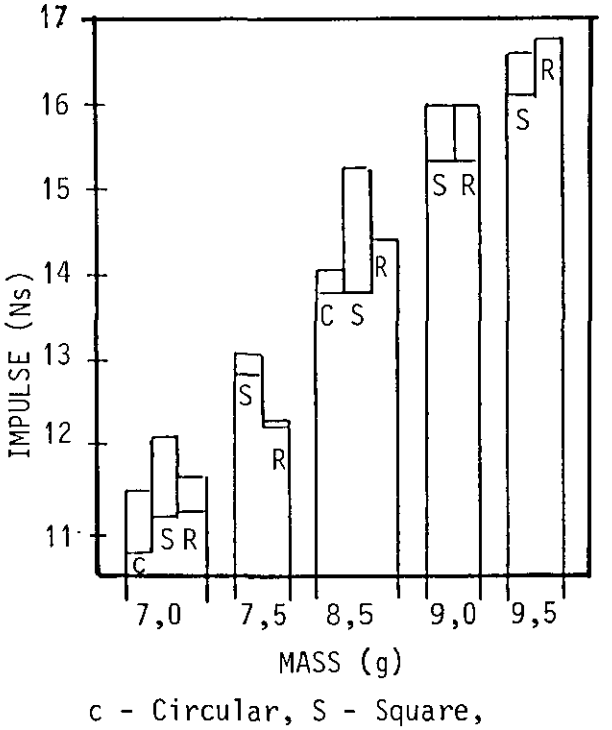

c - Circular, S - Square,
R - Rectangular

FIGURE 2.17 GRAPH SHOWING IMPULSE AS A FUNCTION OF PLATE SHAPE AND MASS OF EXPLOSIVE

(Note: L.S.L. is least squares line)

Problem cases (i) to (iv) are understood and easily rectified, and the light interference technique still recorded a reading. It was thus considered that the measuring device exhibited good reliability and hence could be used for further experiments.

During Series II to IV experiments, a further 105 tests were performed with similar reliability. The major problems encountered were:

i) light interference due to holes in the black hood. This did not always nullify the result as the initial part of the reading was complete and only the steady state part destroyed, as shown in Fig. 2.18.

ii) on several occasions the light bulb sheared at its base, which also did not appear to affect the results. This destruction was particularly noticeable at the higher impulse values.

iii) the prism material was subjected to "clouding", due to the impulse. This reduced the transparent characteristics of the prisms, but this does not appear to have affected the results - the deflection time histories are all consistently similar.

2.5.2 Comment on the Light Interference Equipment

The light interference equipment developed for these experiments exhibits characteristics indicating the usefulness, reliability and cost-effectiveness of the device.

i) The deflection-time history at a defined sector of a structure can be measured. The shape of these curves are in agreement with other measurements, Bodner[26], Duffey[19], as are the times to reach the initial peak deflections.

ii) The device shows a high degree of repeatability as illustrated in Figs. 2.11 and 2.12.

iii) The cost effectiveness of the device is illustrated by

(a) The small capital cost. Material costs are less than US $100 and manufacturing time is estimated at about 40 man hours.

(b) The advantage of avoiding the necessity of a separate series of calibration tests.

2.5.3 Test Readings

2.5.3.1 Deflection-Time Recording

Figs. 2.19 shows typical deflection-time history responses for the central deflection of the plates of different geometries. The response was recorded for a period of 14 ms, and the first 2 ms of each reading is shown expanded in order that the initial response can be more closely investigated. The information extracted from such a recording is the time to reach the initial peak, the change in voltage for the initial peak and the change in voltage for the final deflection. The latter two readings are converted to deflection measurements.

2.5.3.2 Impulse

The movement of the pendulum was measured and the impulse determined as described in section 2.3.3

2.5.3.3 Measured Deflection

The final mid-point deflection was measured using two methods, firstly by means of a vernier and secondly by means of a reflex metrograph. The latter technique allows full field displacement measurements and results in contour plots of the deformed plates as shown in Fig. 2.20 Four hundred points on each plate were digitised, interpolated and hence plotted.

2.5.3.4 Plate Thickness Measurement

The thickness of the deformed plate was measured by means of a vernier. These measurements took place approximately along specified contours, and the average along one contour was determined.

2.5.3.5 Test Results of Uniaxial Yield Tests

These are shown in Figs. 2.4 and 2.5

2.5.3.6 Tables of Test Data

Tables 2.4, 2.5, 2.6 present the test readings.

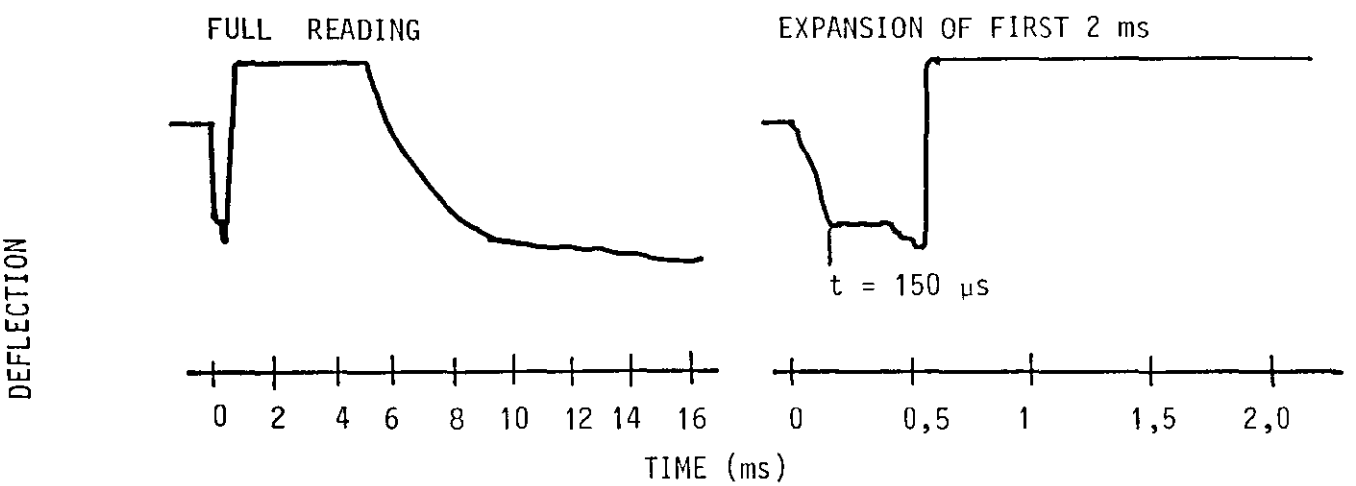

FIGURE 2.18 DEFLECTION - TIME CURVE WITH LIGHT INTEREFERENCE
TEST NO. 0805851

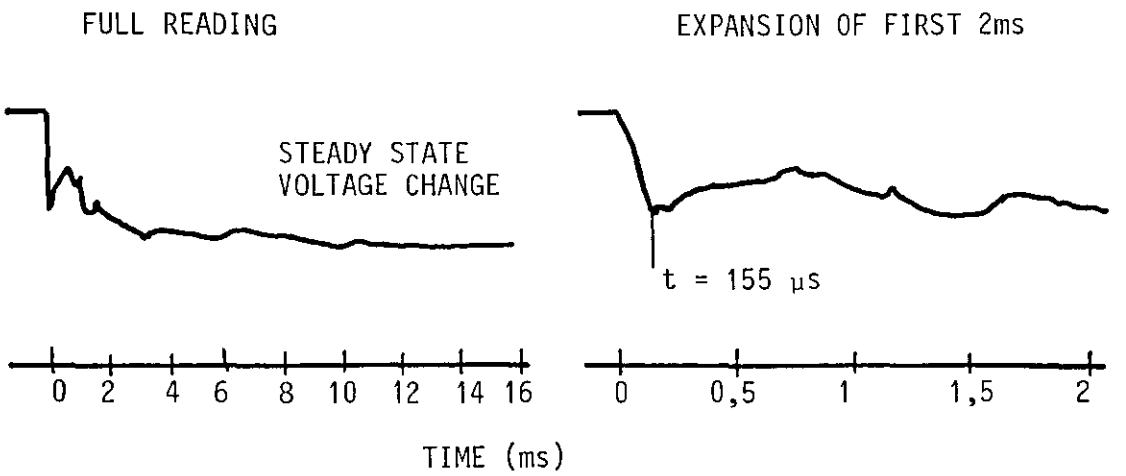

FIGURE 2.19a-1 CIRCULAR PLATE: TEST NO. 1106854

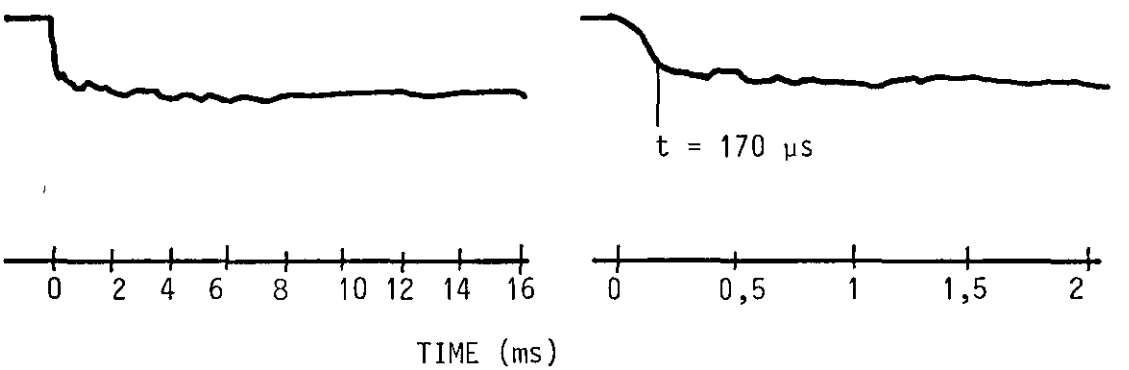

FIGURE 2·19a-2 SQUARE PLATE: TEST NO. 2504852

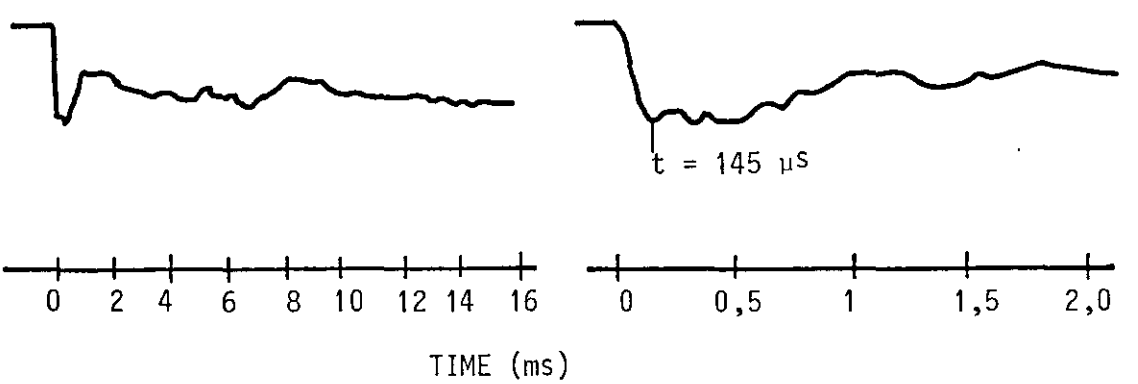

FIGURE 2.19a-3 RECTANGULAR PLATE: TEST NO. 2801851

FIGURE 2.19a TYPICAL DEFLECTION - TIME CURVES

VOLTAGE CHANGE (mV) = DEFLECTION

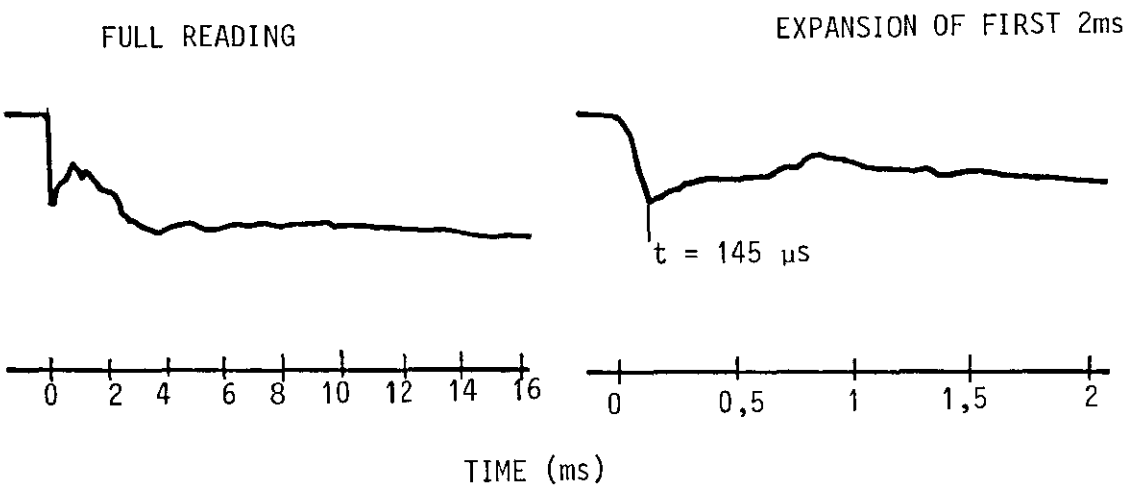

FIGURE 2.19b-1 CIRCULAR PLATE: TEST NO. 1106852

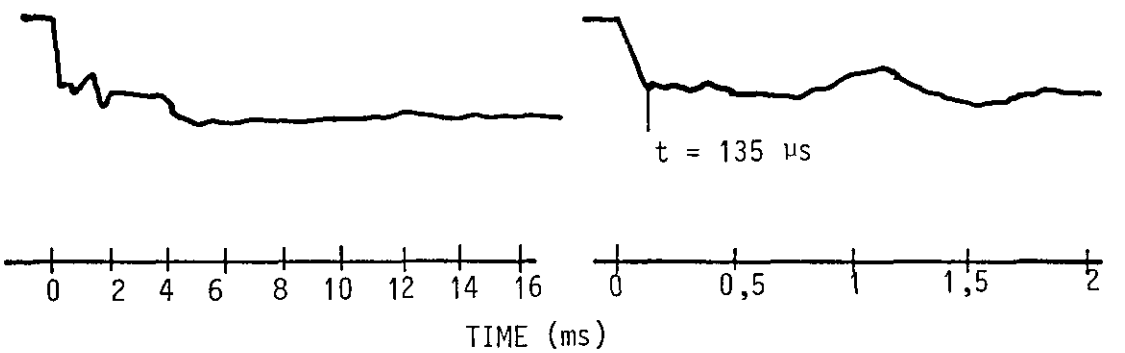

FIGURE 2.19b-2 SQUARE PLATE: TEST NO. 0605855

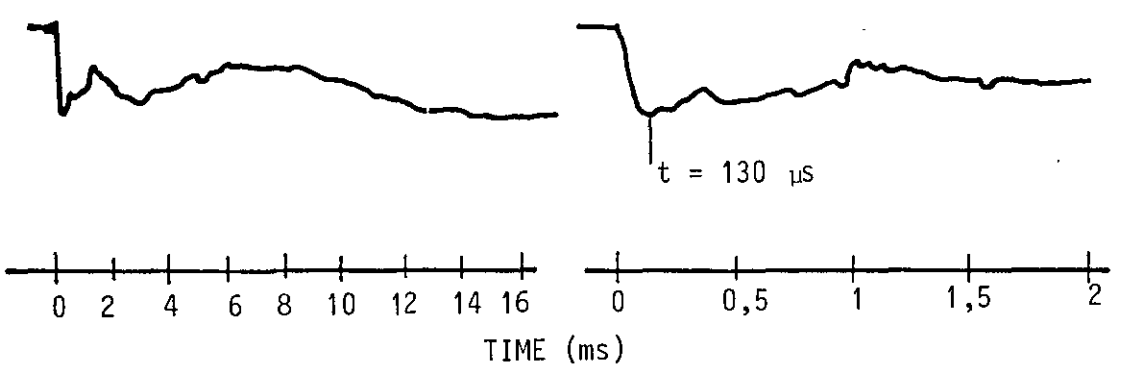

FIGURE 2.19b-3 RECTANGULAR PLATE: TEST NO. 2501851

FIGURE 2.19b TYPICAL DEFLECTION - TIME CURVE

VOLTAGE CHANGE (mV) = DEFLECTION

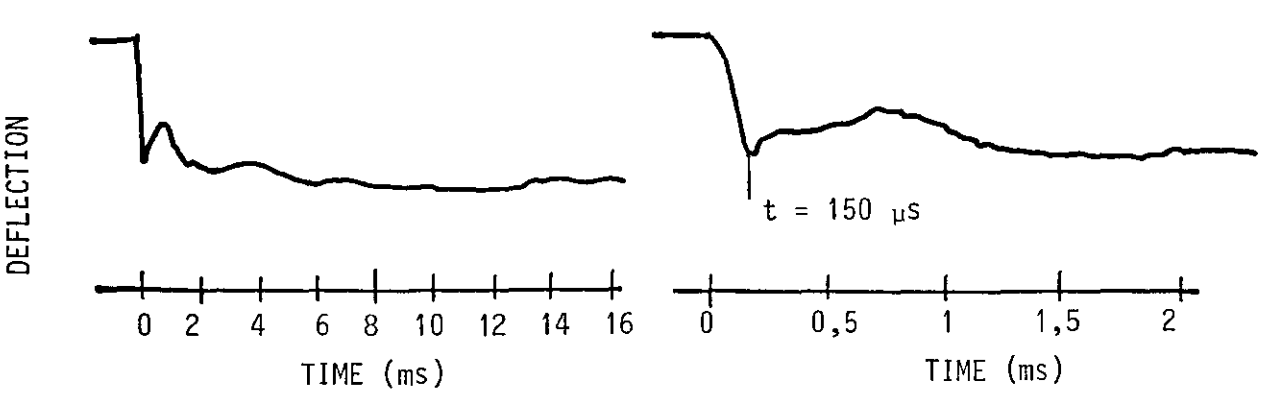

FIGURE 2.19c-1 CIRCULAR PLATE: TEST NO. 1306854

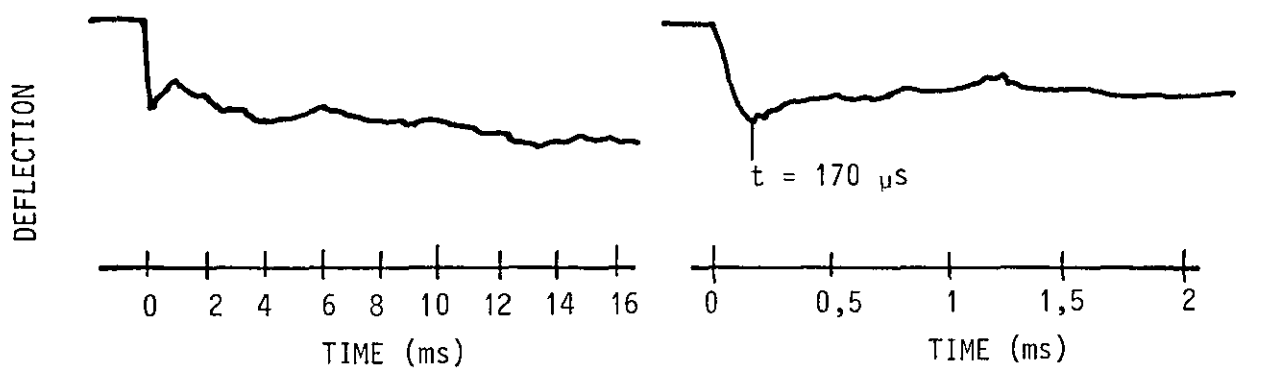

FIGURE 2.19c-2 SQUARE PLATE: TEST NO. 2204854

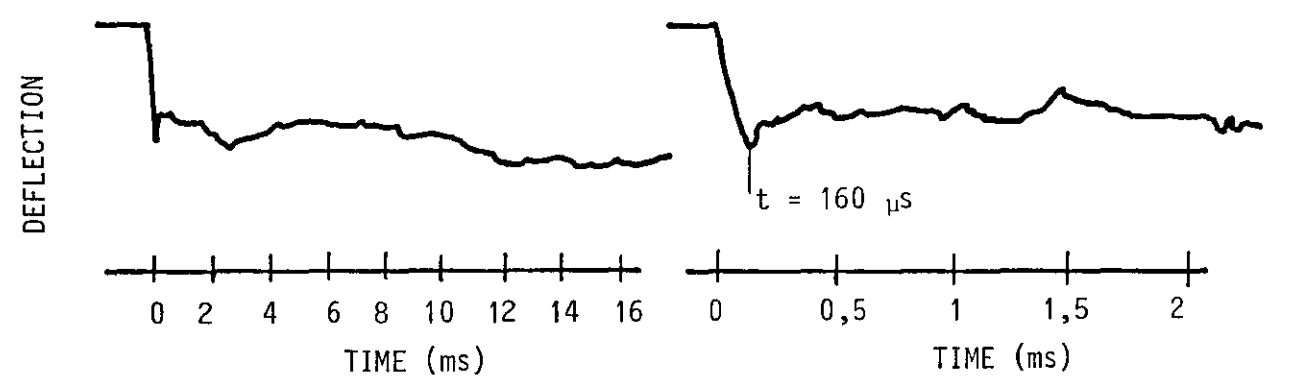

FIGURE 2.19c-3 RECTANGULAR PLATE: TEST NO. 2101853

FIGURE 2.19c TYPCIAL DEFLECTION - TIME CURVES

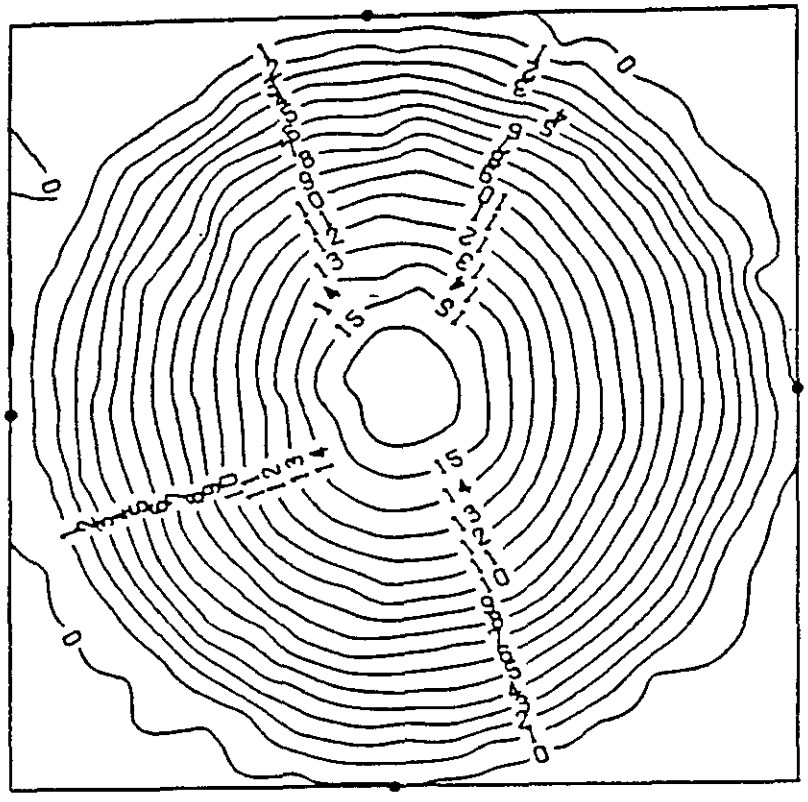

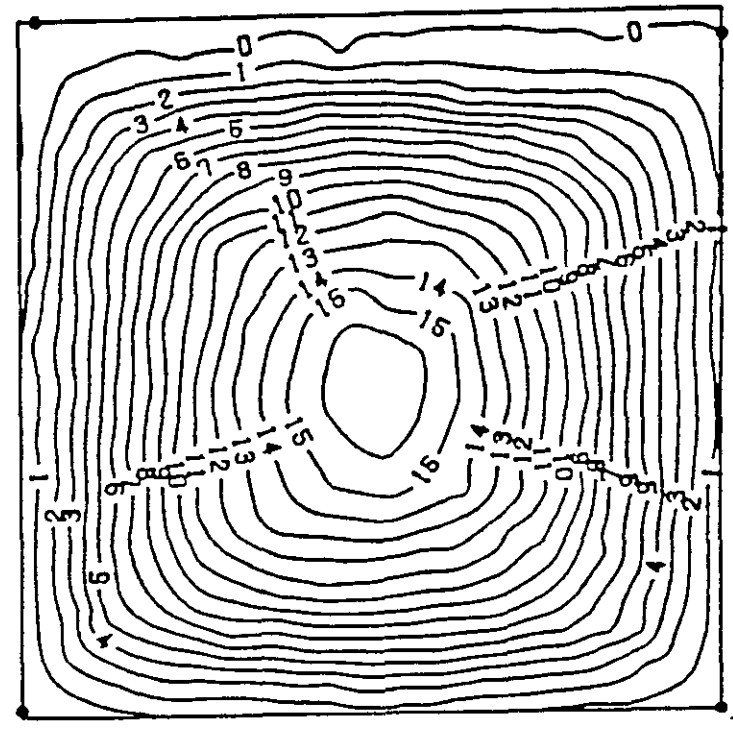

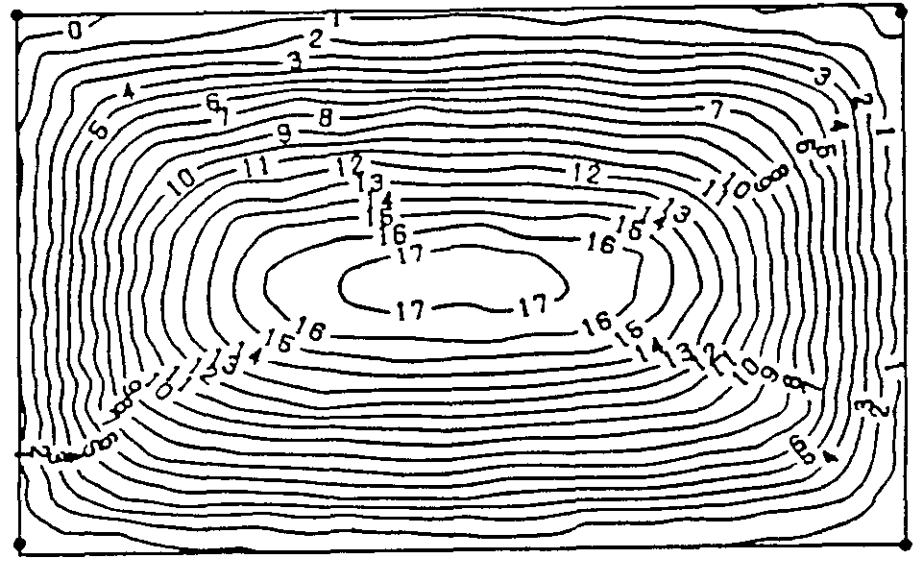

FIGURE 2.20a CONTOUR PLOTS OF DEFORMED PLATES

	Test No.
Circular Plate	1706852
Square Plate	0605857
Rectangular Plate	2901854

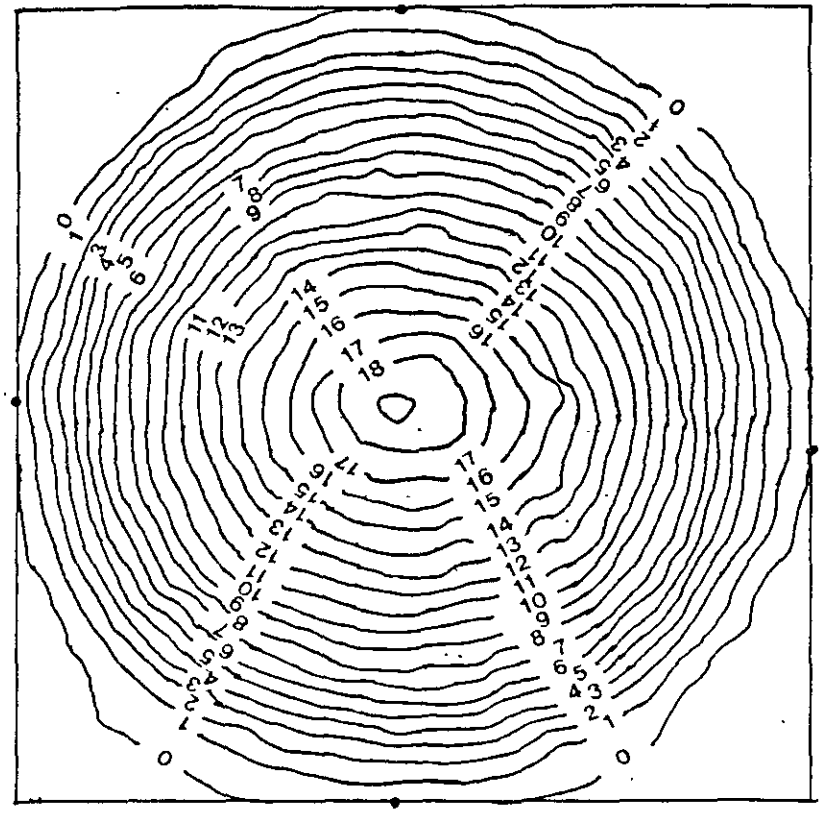

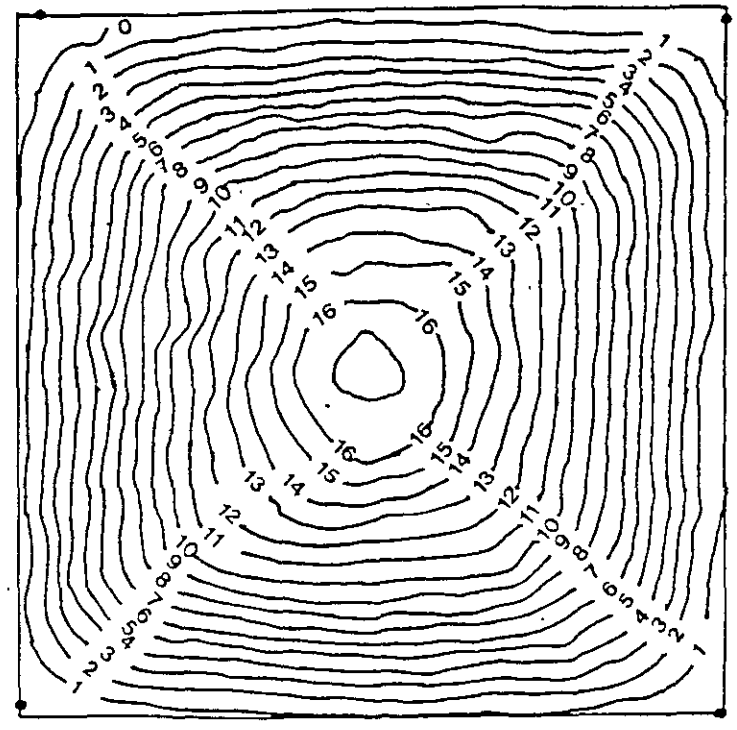

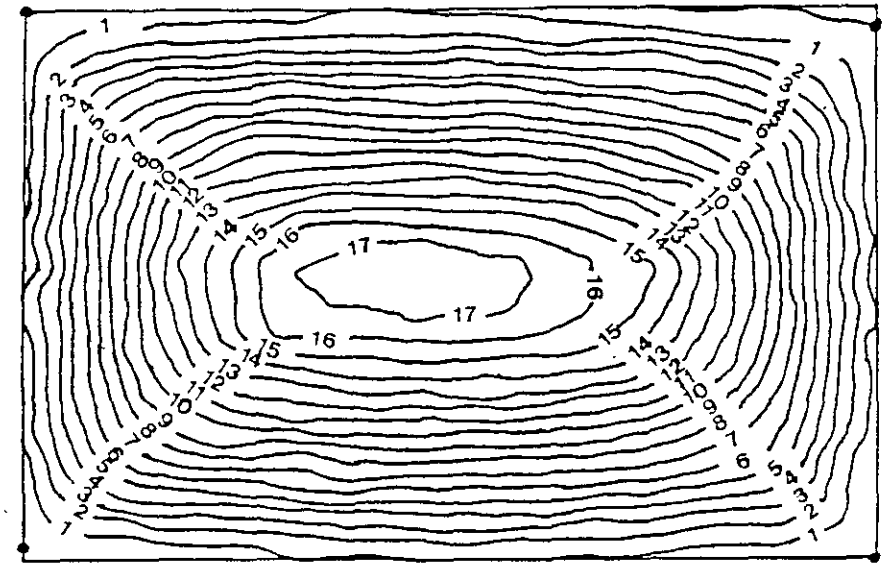

FIGURE 2.20b CONTOUR PLOTS OF DEFORMED PLATES

	Test No.
Circular Plate	1906854
Square Plate	0705853
Rectangular Plate	0102851

TABLE 2.4 Test Data for Circular Plates

Test No.	Explosive Mass (g)	Impulse (Ns)	Measured Mid-Point Deflection (mm)	Deflection Thickness Ratio	Peak Time (μs)
1006851	6.1	9.0	10.62	6.64	-
2	6.1	9.5	10.90	6.81	145
3	6.1	5.6	6.14	3.84	140
4	6.4	10.0	11.96	7.48	155
5	6.4	9.9	12.08	7.55	165
1106851	6.7	10.8	12.26	7.66	150
2	6.7	10.6	12.20	7.63	145
3	7.0	10.8	12.80	8.00	140
4	7.0	11.5	13.62	8.51	155
5	7.3	11.7	13.22	8.26	180
6	7.3	11.4	14.00	8.75	185
1306851	7.6	12.6	14.90	9.31	165
2	7.6	12.4	14.60	9.31	150
3	7.9	12.9	15.28	9.55	155
4	7.9	12.8	16.08	10.05	150
5	8.2	13.6	16.30	10.19	185
6	8.2	13.4	16.38	10.24	150
1706851	8.5	14.1	17.70	11.06	170
2	8.5	13.8	17.06	10.66	160
1906851	8.8	14.7	18.56	11.60	150
1906852	9.0	15.6	19.60	12.40	Tearing Occurred

TABLE 2.5 Test Data for Square Plates

Test No.	Explosive Mass (g)	Impulse (Ns)	Measured Mid-Point Deflection (mm)	Deflection Thickness Ratio	Peak Time (μs)
1704851	6.0	9.5	10.46	6.54	145
2	6.5	11.2	11.58	7.24	160
3	7.0	12.1	12.54	7.84	160
4	6.0	8.7	9.44	5.90	140
2204851	6.5	11.2	12.78	7.99	160
2	7.0	11.4	12.78	7.99	160
3	7.0	11.4	13.10	8.19	170
4	7.5	12.8	13.98	8.74	170
5	8.0	13.4	14.44	9.03	160
6	8.5	13.8	15.66	9.79	175
2304851	9.0	15.3	17.78	11.11	165
2	9.5	16.6	19.14	11.96	-
3	9.0	16.0	17.96	11.23	175
4	10.0	17.5	19.86	12.41	155
2404951	8.5	15.3	17.40	10.88	150
2504851	8.0	14.0	15.18	9.49	-
2	7.5	12.9	14.10	8.81	-
3	7.0	12.2	12.76	7.98	150
4	8.0	13.9	15.50	9.69	155
5	6.5	10.5	11.14	6.96	105
2904851	6.0	9.6	9.62	6.01	150
2	6.0	9.4	9.84	6.15	100
3	6.5	10.3	11.72	7.33	135
4	6.0	9.3	9.92	6.20	-
5	7.0	11.2	13.10	8.19	155
6	6.0	9.1	10.40	6.50	-
0605851	6.0	9.5	10.62	6.64	145
2	6.0	9.7	10.62	6.64	150
3	6.5	10.4	12.12	7.58	150
4	7.0	11.7	13.00	8.13	145
5	7.5	13.1	14.32	8.95	135
6	8.0	14.1	15.70	9.81	160
7	8.5	14.9	16.94	10.59	165
0705851	8.75	15.3	16.72	10.45	145
2	8.75	14.7	16.36	10.23	160
3	8.75	15.0	17.09	10.68	-
4	9.0	15.3	17.34	10.84	150
5	9.5	16.1	17.86	11.16	150
0805851	10.0	16.9	20.00	12.50	150
2404852	10.5	19.0	21.30	13.3	Tearing Occurred

TABLE 2.6 Test Data for Rectangular Plates

Test No.	Explosive Mass (g)	Impulse (Ns)	Measured Mid-Point Deflection (mm)	Deflection Thickness Ratio	Peak Time (μs)
0801851	5.5	5.2	4.68	2.93	-
2	6.0	9.1	7.58	4.74	-
0901851	6.5	7.1	6.38	3.99	-
2	6.5	5.8	5.30	3.31	175
1501851	6.0	7.4	7.56	4.73	-
2	6.0	6.1	7.26	4.54	-
1601851	6.5	8.8	9.04	5.65	-
2	6.5	9.6	9.86	6.16	205
1701851	7.0	11.6	12.02	7.51	155
2201851	7.0	11.2	11.88	7.43	-
2	7.5	12.2	13.40	8.38	-
3	7.5	12.2	12.68	7.93	-
2301851	6.0	8.8	9.12	5.70	-
2	6.0	9.5	9.98	6.24	-
3	6.0	7.8	9.48	5.93	-
4	7.75	13.1	13.88	8.68	155
2501851	7.75	12.8	13.62	8.51	130
2	8.0	13.6	14.50	9.06	145
3	8.0	13.4	14.60	9.13	160
4	8.25	14.1	14.88	9.30	-
5	8.25	13.7	14.82	9.26	-
2801851	8.25	13.8	14.26	8.91	145
2	8.25	13.6	14.52	9.08	145
2901851	8.50	14.5	14.86	9.29	150
2	8.50	14.5	15.30	9.56	150
3	8.75	14.9	15.84	9.90	175
4	9.00	15.3	16.72	10.45	-
0102851	9.25	15.7	16.72	10.45	160
2	9.50	16.7	17.88	11.16	145
3	9.75	17.4	18.24	11.40	115
0402851	8.75	15.2	16.58	10.36	-
2	5.5	8.3	8.40	5.25	120
3	5.5	8.4	8.82	5.51	-
4	5.75	9.1	9.84	6.15	-
5	5.75	7.8	9.42	5.89	-
0502851	6.25	10.5	10.76	6.73	-
2	6.25	9.2	10.36	6.48	-
3	6.75	11.6	11.98	7.49	145
4	6.75	11.3	12.00	7.50	-
5	7.00	11.6	12.58	7.86	-
0702851	7.50	11.4	12.12	7.58	-
2	6.50	10.8	11.02	6.89	-
3	6.50	-	10.98	6.86	-
4	9.0	16.0	16.60	10.88	-
5	16.3	17.86	11.16	-	
0102854	10	17.7	20.34	12.71	Tearing Occurred

CHAPTER 3 - THEORETICAL CONSIDERATIONS

3.1 INTRODUCTION

Jones[32] reports that it was during World War II that Taylor[1], Hudson[33], Richardson and Kirkwood[34] were the first to conduct theoretical studies into the influence of dynamic loads on the behaviour of thin disks or circular plates. These authors based their proposals on bending action only. Frederick[35], a few years later, also proposed a mechanism of behaviour somewhat similar to that of Hudson[33], while Griffith and Vanzant[36] recorded dynamic load carrying capacities significantly greater than the corresponding static values. These results, at higher loading rates, illustrated that elements of the plates tended to move in a transverse sense resulting in smaller circumferential strains than those from static tests. Hopkins and Prager[37] studied in particular the dynamic behaviour of simply supported circular plate subjected to a rectangular pulse. The plate was idealised as a rigid, perfectly plastic material, which is assumed to obey the Tresca yield condition and associated flow rate. Membrane forces were disregarded. Making the same assumptions and using a similar but more complicated mechanism of behaviour, Florence[38] solved the problem of a circular clamped plate loaded with a central rectangular pulse. Wang and Hopkins[39] studied the behaviour of a circular plate with a transverse velocity imparted instantaneously to the entire plate. Wang[40] found that the analysis simplifies considerably when the plate is simply supported around its outer edge. Florence[17] subjected some simply supported circular plates to uniformly distributed impulses and found, particularly for large impulses, that the theoretical analysis of Wang[40] overestimated considerably the final deformed shapes. This discrepancy arises because of the nature of the assumptions involved in the development of Wang's analysis which limits application of the results to plates with small

final deformations.

Perzyna[41] examined the influence of pulses of arbitrary shape by developing further the theory of Hopkins and Prager[37] to show that for a given impulse, the character of the pressure-time function has little influence on the final shape of the plate. However, Jones[32] reports that work by Sankaranarayanan[42] showed that the pulse shape influenced considerably the final deformation of plastic spherical caps to impact pressure loads, and work by Symonds[43] found somewhat less sensitivity to the pulse shape in beams.

Hopkins[44] developed a more general theory for plates loaded transversely with nonsymmetrical loads but disregarded any membrane forces and solved no particular problems.

Shapiro[45], who was the first to examine the dynamic behaviour of annular plates, studied the problem of a circular plate supported rigidly around an inner radius and loaded with a circular ring of impulsive velocity around its outer edge. Florence[46] reviewed this problem in order to assess the relative contributions of membrane forces and bending moments to the formation of the final deformed shape. It was found that a solution which considered interaction between the circumferential membrane force and circumferential bending moment was closer to the experimental values than the solutions for bending moment only and membrane force only, both of which overestimated considerably the final deformations. Witmer *et al*[12] developed a numerical method, the predictions of which compared favourably with experimental values recorded for large dynamic deformations of beams, rings, plates and shells.

Boyd[47] reconsidered the problem of dynamic deformation of a circular membrane and solved the governing

equations numerically for a general form of symmetrical pressure loading. Although any contributions arising from bending moments were neglected, this method predicted results similar to the corresponding values of Witmer *et al* [12]. Boyd[47], and Frederick[35] investigated the deformations of membranes made from a strain hardening material and discovered that a simplified rigid perfectly plastic analysis provides a remarkably accurate approximation to the true behaviour. Mundy and Newitt[48] examined carefully the dynamic behaviour of clamped copper membranes, and also presented some photographs taken from a high-speed cine film recorded during the passage of a hinge which formed around the outer edge of a plate at the first instant of impact and travelled inward toward the centre, where it remained until the plate came to rest. For an impulsive loading, Mundy and Newitt observed that the final deformed shapes are almost identical for all plates irrespective of thickness, diameter and load.

The method of Martin and Symonds[49], used to predict maximum deflections and time bounds for rigid-plastic plates loaded impulsively, compares well with the time bounds of Wang and Hopkins[39,40], but the deflections are overestimated by one third for the simply supported case and somewhat less for the plate with clamped edges. These results are obtained from a few lines of arithmetic, whereas the solution of Wang and Hopkins[39] in particular is time consuming.

Cooper and Shifrin[50] and Haythornthwaite and Onat[51] measured the static load-carrying capacity of initially flat circular plates, and observed that the bending only solution of Hopkins and Prager[52] underestimates considerably the load which could be supported if deflections of the order of the plate thickness or larger are permitted. In order to explain the strengthening effect under static loads Onat and Haythornthwaite[53] considered both bending moments and membrane forces in an analysis which reduces to the bending only theory of Hopkins and Prager[52] at very small deflections and to the behaviour as a membrane at large deflections.

It is clear from the foregoing that much effort had been concentrated on the dynamic deformation of plates in which either membrane forces [1, 33-35, 47] or bending moments [37-41, 44,45] alone were believed to be important. Moreover, with the exception of the numerical work of Witmer *et al* [12] and the analysis by Florence[46] for an annular plate, investigations had not been conducted into the interaction effects between membrane forces and bending moments, while for static loading the behaviour during all stages was fairly well understood[53].

Jones[32] therefore attempted to link the two distinct stages of plastic strain and describe the behaviour of plates dynamically loaded with deflections in the range where both bending moments and membrane forces are important. The analysis presented by Jones[32] predicts with reasonable accuracy the final deformations recorded by Florence[17] on a simply supported circular plate subjected to a uniform impulse.

Noble and Oxley [54] and Batra and Dubey[55] also extended the bending effects only concepts by adding membrane effects to the bending effects. Lippman[56] and Ghosh and Weber[27] then considered the membrane stretching action while assuming a deformed shape which has a radial thickness variation.

Guedes Soares[57] showed that the solution of problems of dynamic response of structures to intense loading is rather complicated when parts of it enter the plastic range. In the cases where the plastic strains associated with the response are large, the elastic strains can be neglected without significant loss in accuracy. This rigid-plastic idealisation of material behaviour is a useful simplification that has allowed some of these problems to become tractable.

Within this theory several exact solutions have been obtained, for example Lee and Symonds[58] and Hopkins and Prager[52]. However, even with this idealization problems were often difficult to solve and consequently some approximate methods were developed. These were initiated by the bounding theorems of Martin[59] and the mode approximation solutions introduced by Martin and Symonds[49].

The approximation methods were developed for the case of small deflections, but when considering the effects of intense loading, the non-linearities due to large deflections need be taken into account. In these cases an exact solution is often out of the question and even approximate ones are sometimes difficult. Symonds and Chon[60-62] proposed an extension of the original mode approximation solutions so as to account for finite deflections, but in doing so they had to resort to a series of instantaneous mode shapes throughout the response, which implied the use of numerical methods. As a consequence, the simplicity and the analytical character of the mode solutions was lost. When applying the same procedure to the case of a beam Guedes Soares [57] noticed that the shape of the modes was not changing significantly during the response. The same could be observed in the results of Chon and Symonds[62] on a circular plate. Guedes Soares[57] then indicated that the use of a permanent mode shape might be a

reasonable approximation with an unquestionable simplification of the analysis. Guedes Soares[57] believes that when exact solutions cannot be obtained, the approximate methods which are developed should be a compromise between the difficulty of treatment and the accuracy of results. Therefore Guedes Soares[57] proposed a procedure to study the behaviour of a circular rigid-plastic plate under impulsive loading, and showed how the mode approximation technique is extended to the case of finite deflections, retaining its original simplicity. The solution is obtained using the methodology developed by Jones[63] which had already been applied to beams, non-axisymmetric plates and shells of revolution.

The approach by Guedes Soares[57] consists in maintaining the basic procedure used in the small deflection range as proposed by Martin and Symonds[49]. Therefore the permanent mode shape appropriate for the infinitesimal deflection case is maintained on the large deflection range. This is very similar to what was done by Jones[63], Wierzbicki[64], and Kaliszky[65] who adopted one collapse mechanism for the whole structure response While the method of Jones[63] includes both bending and membrane effects, Symonds and Wierzbicki[66] consider only the membrane behaviour. They followed the same idea of estimating the response with a permanent mode shape. However, instead of choosing the shape of the initial phases of motion they chose the shape appropriate to the stage where only membrane effects exist. Therefore they obtained a mode shape in terms of Bessel functions as did Jones[32] for the second phase of his solution.

Florence[46] also used a membrane solution which gave worse results than his limited interaction approximation. In this case he used an approximate linear profile as the velocity field.

As Symonds and Wierzbicki[66] do not account for bending, their predictions underestimate the final deflection for small deflections, but improve for larger deflections when the energy dissipated in membrane effects becomes more important. Symonds & Wierzbicki predicted results for various types of loads supported by the experimental results of Bodner and Symonds[26].

Guedes Soares[57] used his predictions for both simply supported and fully clamped circular plates in which the choice of the mode shape resulted in different final predictions.

Perrone and Bhadra[67] presented a simplified method to account for plastic rate sensitivity with large deformations in which they considered a one dimensional string type problem. Building on this result they further presented [68] the procedure as applied to impulsively loaded, viscoplastic circular membranes. The procedure required a knowledge of the initial impulse velocity from which an energy balance between the initial kinetic energy and work done by plastic stretching of the system could be effected to give the final deformation. Circumferential strains were considered negligible and membrane effects were presumed to dominate over bending; in effect bending was ignored. These predictions were compared with the experiments of Bodner and Symonds [26] and exhibited good correlations. These predicted results were comparable to those of Symonds and Wierzbicki[66] who used a different simplifying procedure. Perrone and Bhadra[68] further state that essentially the same procedure should be applicable for any shape, for example a rectangular plate with the shape function being a product of sinusoidal functions in each of the coordinate directions multiplied by the amplitude parameter.

Westine and Baker[69] and later Baker[70] proposed

approximate methods using energy solutions in which they equated the strain energy stored in a plastically deformed member, with an assumed deformed shape, to the kinetic energy imparted to the structure. This is an extension of the work of Greenspan who Westine and Baker report equated the strain energy to the energy flux in the explosive blast wave. This procedure of Westine and Baker[69, 70] is shown to be applicable to circular and rectangular plates and is compared with experimental results of Florence[17] and Jones *et al*[22] for deflection thickness ratios of up to 7. The assumed deformed shape is sinusoidal in both coordinate directions.

Duffey[19] used a simplified energy method for rigid-plastic material behaviour and equated the strain energy to the initial kinetic energy imparted to the circular plate. Several deformed shape profiles were assumed, including sinusoidal and various polynomial forms to find the best fit to the experimental results.

Calladine[71] and Johnson[72] also considered simple energy concepts with an assumed deformed shape profile.

In Table A.1 a resume of the approximate methods is given

3.2 MODE APPROXIMATION

Mode approximations have been applied to impulsively loaded thin plates in which bending is ignored by several authors (see previous section), all who assumed a fixed mode shape. The model adopted here differs primarily in that the mode shape is computed at each time step, and a further difference occurs in that in addition to considering transverse displacements only, lateral displacements have also been included in the analysis.

Major assumptions in the analysis include

i) Membrane stresses predominate.

ii) Bending effects are ignored.

iii) Material behaviour is rigid viscoplastic, described by the relation between dynamic yield stress σ and strain rate $\dot{\epsilon}$ in the form

$$\sigma/\sigma_0 = 1 + (\dot{\epsilon}/\dot{\epsilon}_0)^{1/n}. \qquad (3.1)$$

iv) The shapes of the displacement field and the velocity field are the same.

v) Whereas previous predictions have assumed that material points on a plate move perpendicular to the initial plane of the plate, here we follow the hypothesis of Gamby and Lampi[73] who selected a displacement field in which the trajectory of every point on the surface remains normal to the plate surface.

Previous predictions for a circular plate give

$$u = u(r,t) \qquad \dot{u} = \dot{u}(r,t) \qquad (3.2a)$$
$$v = v(r,t) = 0 \qquad \dot{v} = \dot{v}(r,t) = 0 \qquad (3.2b)$$

where u,v are transverse and lateral displacement and u,v are transverse and lateral velocity respectively.

vi) The impulse is at time t=0 and external loads are zero for t>0.

$$I = I \text{ at } t = 0$$
$$= 0 \text{ at } t > 0$$

The analysis described in the following section is similar in concept but different in application to that of Perrone and Bhadra[68]. Whereas these authors assumed a fixed mode shape, the analysis presented here updates the mode shape at each time step.

3.3 MEMBRANE ANALYSIS

In structural elements, such as beams and plates, bending resistance will develop along with membrane forces when the deflection is much less than the thickness of the element. However, as the deflection increases, stresses due to stretching of the middle plane will dominate over bending stresses, and at this stage the behaviour of, for example, a beam is comparable to that of a plastic string. Perrone and Bhadra[68] presented this concept with a simple lumped mass at the midpoint. In their analysis the acceleration is the second differential of displacement resulting in a first-order nonlinear differential equation which is solved by numerical integration.

In this study the string concept forms the basis of the proposed model, as described in the next section (3.3.1). This concept is extended and applied to plates as described in section 3.3.2.

3.3.1 Plastic String Analysis

The string is sub-divided into several sections with associated lumped masses as shown in Fig. 3.1, and the acceleration is assumed to be a linear function of the velocity.

The model proposed included both transverse and lateral deflections adopted from the hypothesis of Gamby and Lampi[73] who, in considering a bulge test, selected a displacement field in which the trajectory of every point on the surface remains normal to the plate surface. This is shown in Figs. 3.2 and 3.3.

Fig. 3.2 shows the transverse and radial displacements of the nodes and the associated forces.

From Fig. 3.2.b, it is evident that

$$\ell_i = \left[L_i^2 + (u_i - u_{i+1})^2\right]^{1/2}$$

$$= \left[(u_i - u_{i+1})^2 + (L + v_{i+1} - v_i)^2\right]^{1/2}$$

Defining the strain in the ith element as

$$\epsilon = \frac{\ell^2 - L^2}{2L^2}$$

which becomes

$$\epsilon_i = \frac{(u_i - u_{i+1})^2 + (L + v_{i+1} - v_i)^2 - L^2}{2L^2} \qquad (3.3)$$

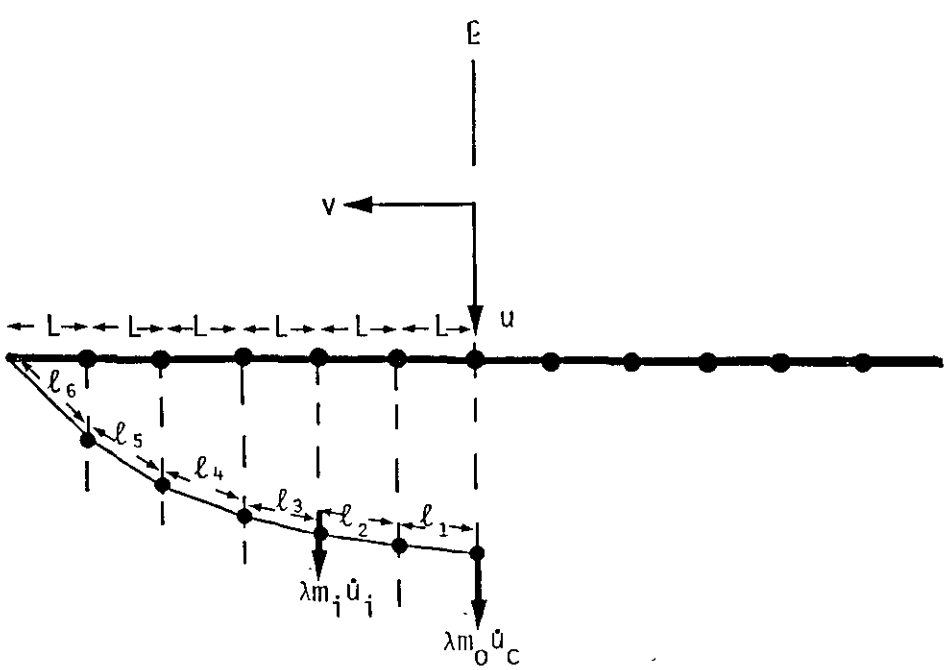

FIGURE 3.1 MODEL SHOWING TRANSVERSE DISPLACEMENTS ONLY

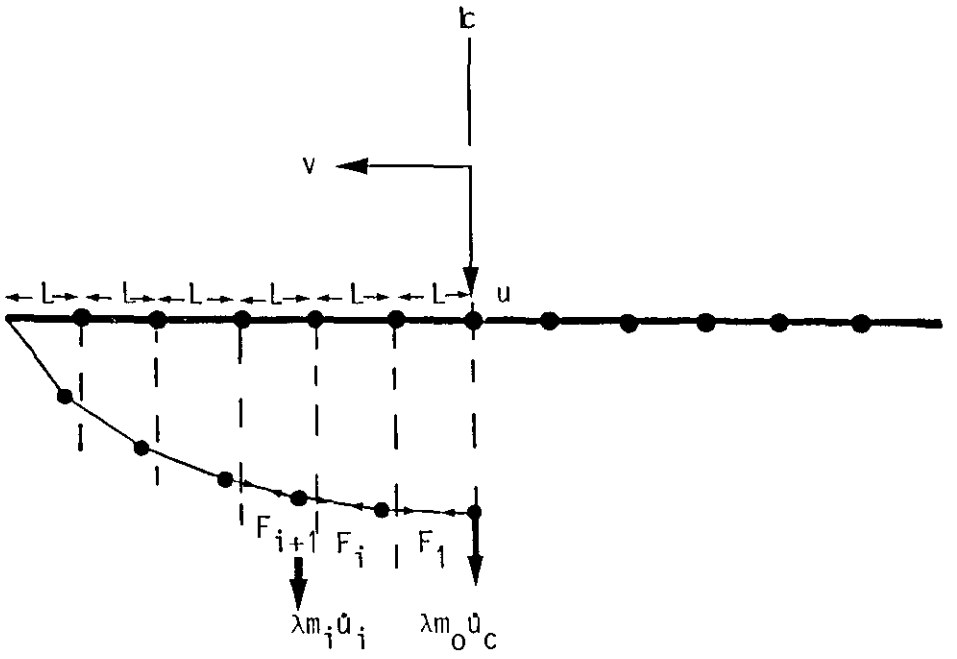

FIGURE 3.2a MODEL SHOWING TRANSVERSE AND LATERAL FORCES

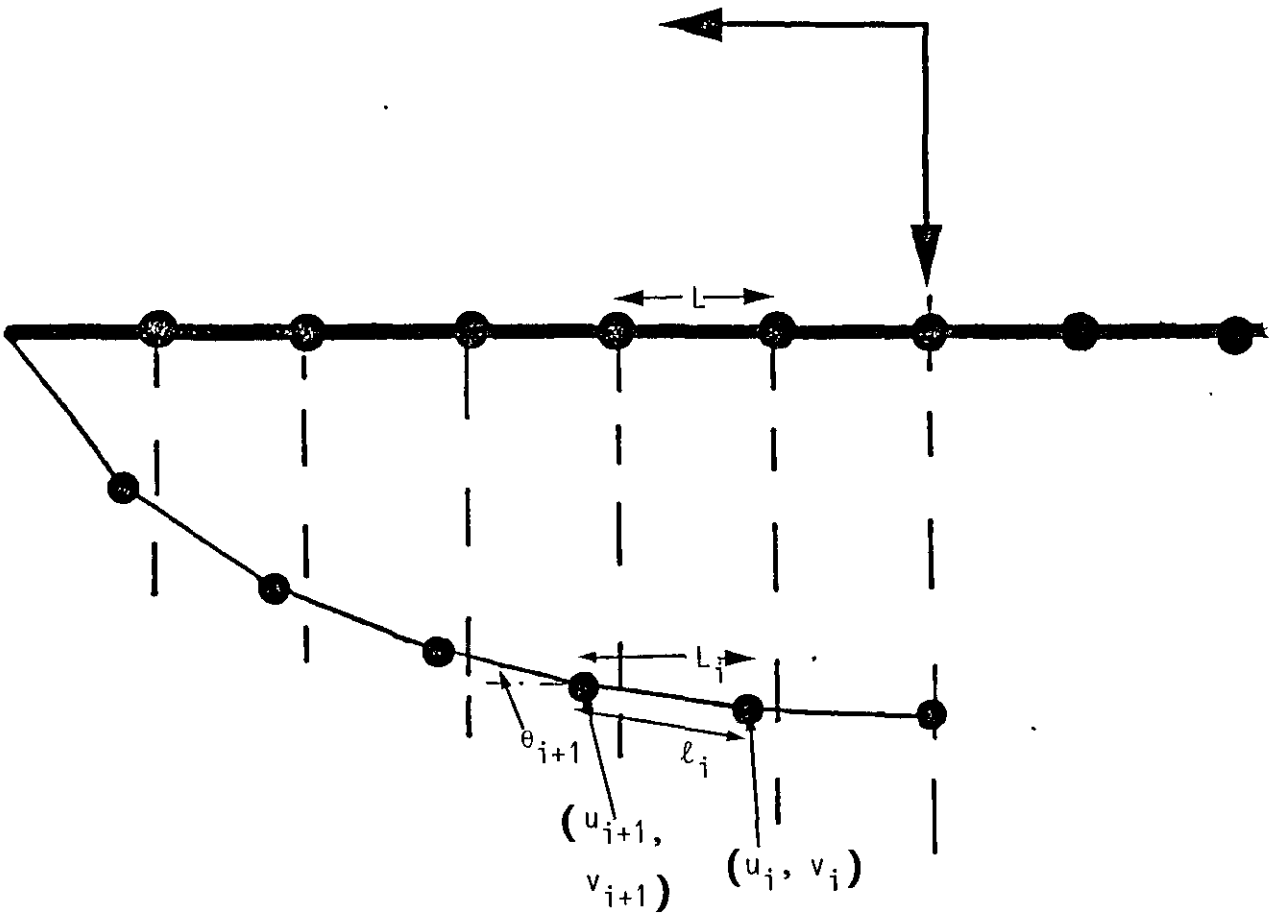

and hence the strain rate is

$$\dot{\epsilon}_i = \frac{(u_i - u_{i+1})(\dot{u}_i - \dot{u}_{i+1}) + (L + v_{i+1} - v_i)(\dot{v}_{i+1} - \dot{v}_i)}{L^2} \qquad (3.4)$$

Fig 3.3 shows the motion of the i^{th} node, where z bisects the angle between the tangents to the deformed shape on either side of the node, giving

$$\alpha = \tfrac{1}{2}(\theta_{i+1} - \theta_i)$$

where θ_i, θ_{i+1} are the tangents to the horizontal on either side of the node.

Hence the vertical component of z is $u = z \cos(\alpha + \theta_i)$

$$= z \cos\left[\frac{\theta_i + \theta_{i+1}}{2}\right]$$

and the horizontal component of z is $v = z \sin(\alpha + \theta_i)$

$$= z \sin\left[\frac{\theta_i + \theta_{i+1}}{2}\right]$$

where $z = (u^2 + v^2)^{\frac{1}{2}}$

and $v_{i+1} = u_{i+1} \operatorname{Tan}\left[\frac{\theta_i + \theta_{i+1}}{2}\right]$ (3.5

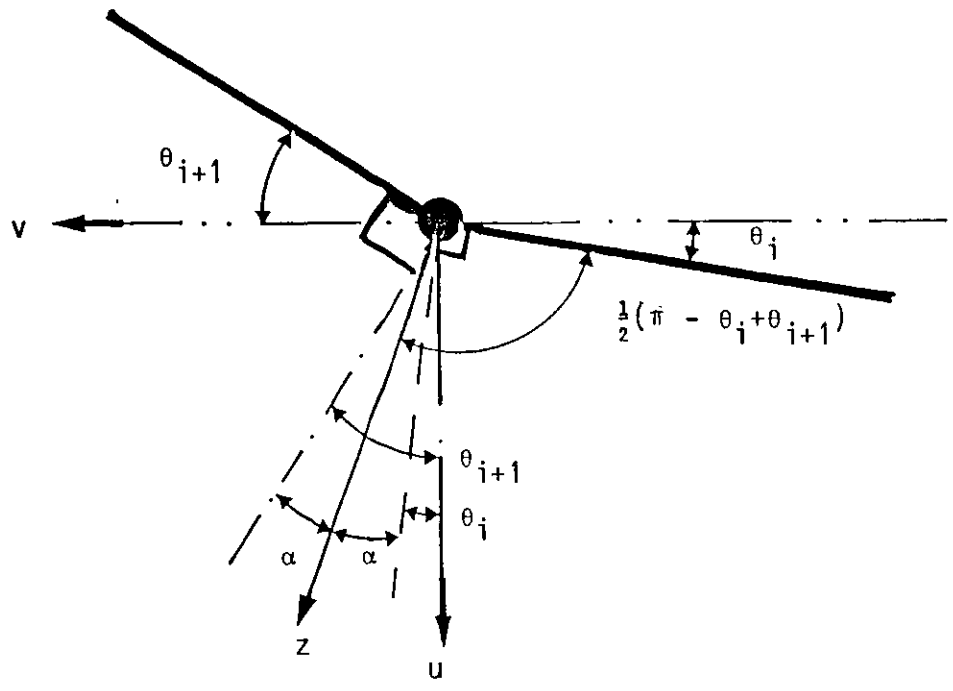

FIGURE 3.3 PERPENDICULAR MOTION OF i^{th} NODE

Writing

$$\sin\theta_i = \frac{u_i - u_{i+1}}{\ell_i} = \frac{u_i - u_{i+1}}{[(u_i - u_{i+1})^2 + (L + v_{i+1} - v_i)^2]^{1/2}} \quad (3.6a)$$

and

$$\cos\theta_i = \frac{L + v_{i+1} - v_i}{[(u_i - u_{i+1})^2 + (L + v_{i+1} - v_i)^2]^{1/2}} \quad (3.6b)$$

and using the identities

$$\sin\frac{A}{2} = \left[\frac{1 - \cos A}{2}\right]^{1/2} \qquad \cos\frac{A}{2} = \left[\frac{1 + \cos A}{2}\right]^{1/2}$$

$$\tan\frac{A}{2} = \left[\frac{1 - \cos A}{1 + \cos A}\right]^{1/2} = \frac{\sin A}{1 + \cos A} = \frac{1 - \cos A}{\sin A}$$

$$\tan(A+B) = \frac{\tan A + \tan B}{1 - \tan A \tan B}$$

Then

$$\tan\left[\frac{\theta_i}{2} + \frac{\theta_{i+1}}{2}\right] = \frac{\sin\frac{\theta_i}{2}(1 + \cos\frac{\theta_{i+1}}{2}) + \sin\frac{\theta_{i+1}}{2}(1 + \cos\frac{\theta_i}{2})}{(1 + \cos\frac{\theta_i}{2})(1 + \cos\frac{\theta_{i+1}}{2}) - \sin\frac{\theta_i}{2}\sin\frac{\theta_{i+1}}{2}} \quad (3.7)$$

The deformed geometry of the string is now defined by a mode shape ϕ, which varies with space and time. The transverse displacement is written as

$$u_i(r,t) = \phi_i(r,t)\, u_o(t) \quad (3.8)$$

where (r,t) are the coordinates of space and time and $u_o(t)$ is the central displacement, depending only on time. It is then further assumed that the transverse velocity and acceleration fields at time t can be written as

$$\dot{u}_i = \phi_i\, \dot{u}_o \;:\; \ddot{u}_i = \phi_i\, \ddot{u}_o \quad (3.9)$$

where $\dot{u}_o$ and $\ddot{u}_o$ are the transverse velocity and acceleration at the mid-point. This assumption implies that equation (3.8) can be differentiated at time t without taking into account the variation of the mode shape of ϕ

with time - this is referred to as an instantaneous or stationary mode assumption. From equation (3.9) it is evident therefore that at time t

$$\dot{u}_i = -\lambda \dot{u}_i \; ; \; \dot{u}_c = -\lambda \dot{u}_c \tag{3.10}$$

where λ is a scalar multiplier.

Extending the assumption that at any time t the shapes of the displacement field, the velocity field and the acceleration field are the same, then

$$\dot{v}_i = -\lambda v_i \tag{3.11}$$

where $\dot{v}_i$ is the radial acceleration, and thus

$$\dot{z}_i = -\lambda z_i \tag{3.12}$$

where $\dot{z}_i = (\dot{v}_i^2 + \dot{u}_i^2)^{1/2}$ and acts perpendicular to material surface.

To obtain a solution to the problem, it is assumed that, at any time t, $u_c(t)$ and $\dot{u}_c(t)$ are known and ϕ must be determined. The slope θ is determined by ϕ, and $\dot{v}$ depends on $\dot{u}_c$ and ϕ.

Where ϕ at the i^{th} node is defined as

$$\phi_i = \frac{u_i}{u_c} \tag{3.13}$$

and from the above assumptions, also defined as

$$\phi_i = \frac{\dot{u}_i}{\dot{u}_c} \tag{3.14}$$

The problem is solved by writing dynamic equations. At the centre,

$$2F_1 \sin \theta_1 = \lambda m_0 \dot{u}_0 \qquad (3.15)$$

and at any other node

$$F_{i+1} \sin \theta_{i+1} - F_i \sin \theta_i = \lambda m_i \dot{u}_i \qquad (3.16)$$

where F is the force and can be written as

$$F = \sigma \times \text{cross-sectional area of the string} \qquad (3.17)$$

where

σ is the stress,
θ is the inclination of the force to the horizontal,
λ is the scalar multiplier,
m_0, m_i are the lumped masses at the centre and nodes respectively,

and for unit width of a rectangular string

$$F = \sigma \times h \qquad (3.18)$$

where h is the thickness.

The stress σ is obtained from the rigid-viscoplastic constitutive equation

$$\sigma/\sigma_0 = 1 + (\dot{\varepsilon}/\dot{\varepsilon}_0)^{1/n}.$$

The right hand terms of eqns (3.15),(3.16) represent the inertia force of the lumped masses at the nodes.

The dynamic equations are then written as

$$2\,\sigma_0\left[1+\left[\frac{\dot{\epsilon}_1}{\dot{\epsilon}_0}\right]^{1/n}\right]h.\sin\theta_1 = \lambda m_0 u_0 \qquad (3.19)$$

$$\sigma_0\left[1+\left[\frac{\dot{\epsilon}_{1+1}}{\dot{\epsilon}_0}\right]^{1/n}\right]h.\sin\theta_{1+1}-\sigma_0\left[1+\left[\frac{\dot{\epsilon}_1}{\dot{\epsilon}_0}\right]^{1/n}\right]h.\sin\theta_1=\lambda m_1 u_1 \qquad (3.20)$$

Substituting eqns. (3.4),(3.5),(3.6),(3.7) and (3.14) into eqns (3.19) and (3.20), provides (k+1) equations for the multiplier λ and the model coefficients ϕ_1, ϕ_2, ... ϕ_k.

3.3.2 Application to Plates

In order to apply this procedure to plates, the plates were discretised by assuming contours along which ϕ is constant, as shown diagrammatically in Figures 3.4, 3.5 and 3.6. At the centre of the plate $\phi_0=1$, and the contour levels are labelled from the centre as ϕ_1, ϕ_2, ... ϕ_1. For the circular plate the contours are circular, as is dictated by axial symmetry. Similarly for the square plates, symmetry dictates square contours. For the rectangular plates, the contours have been formed by drawing lines at 45° to the clamped edges from the corners. These contours are approximately in accord with the contours found experimentally as shown in Figure 2.20.

The mode shape ϕ is assumed to vary linearly with distance between contour levels, so that between contour ϕ_1 and ϕ_{1+1} the mode shape is that of a frustum of a cone for the circular plate and the frustum of a pyramid for the quadrangular plates. Intermediate contours are also drawn equidistant between ϕ_1, ϕ_2...ϕ_1 which are labelled ϕ_1, ϕ_2...ϕ_1 as shown dotted in Figure 3.4, 3.5 and 3.6.

The mass m_i of the plate lying between contours $\bar{\phi}_i$ and $\bar{\phi}_{i+1}$ is lumped at contour ϕ_i, with the lumped mass m_o at the centre of the plate being the mass contained within the contour ϕ_1. It is now possible to write (i+1) dynamic equations for the lumped masses; the i^{th} contour or node is shown diagrammatically in Figure 3.7. The force $\lambda m_i \phi_i u_o$ is the intertia force arising from the deceleration of the node and it must be in equilibrium with the forces $\bar{F}_i$ and $\bar{F}_{i+1}$, where $\bar{F}_i$, $\bar{F}_{i+1}$ are the vertical components of the membrane stress integrated along the contour $\bar{\phi}_i$, $\bar{\phi}_{i+1}$.

Along the contour $\bar{\phi}_{i+1}$, the membrane stresses are assumed to be perpendicular to the contour. The strain component perpendicular to the contour is

$$\epsilon_{i+1} = \frac{u_o^2 (\phi_i - \phi_{i+1})^2 + (L + v_{i+1} - v_i)^2 - L^2}{2L^2} \quad (3.21)$$

and the strain rate is then taken as

$$\dot{\epsilon}_{i+1} = \frac{u_o \dot{u}_o (\phi_i - \phi_{i+1})^2 + (L + v_{i+1} - v_i)(\dot{v}_{i+1} - \dot{v}_i)}{L^2} \quad (3.22)$$

with the assumption that ϕ_{i+1} and ϕ_i are fixed at time t in the differentiation of eqn. (3.21). The stress component in the plate normal to the contour line ϕ_{i+1} is then computed from the relation between dynamic yield stress and strain rate (see eqn. (3.1)), in the following form

$$\sigma_{i+1} = \sigma_o \left[1 + \left[\frac{\dot{\epsilon}_{i+1}}{\dot{\epsilon}_o} \right]^{1/n} \right] \quad (3.23)$$

where σ_o is the static yield stress, and $\dot{\epsilon}_o$ and n are material parameters with the values of $40s^{-1}$ and 5 respectively. (Manjoine [74]).

The in-plane force per unit length is $h\sigma_{i+1}$, where h is the plate thickness, and the inclination of the force to the horizontal is θ_{i+1} where

$$\text{Tan } \theta_{i+1} = \frac{u_c(\phi_{i+1} - \phi_i)}{L_i + v_{i+1} - v_i} \tag{3.24}$$

It then follows that

$$\bar{F}_{i+1} = \int_{\bar{P}_{i+1}} h\sigma_{i+1} \sin \theta_{i+1} \, dP \tag{3.25}$$

where P_{i+1} is the length (or perimeter) of the contour $\bar{\phi}_{i+1}$.

The dynamic equations again take the form of equations (3.15, 3.16), where

$$\lambda m_o \dot{u}_c = \bar{F}_1 \tag{3.26}$$

and

$$\lambda m_i \phi_i \dot{u}_c = -\bar{F}_i + \bar{F}_{i+1}, \quad i = 1, 2 \ldots n \tag{3.27}$$

These equations are shown in enlarged form in Appendix A.2.

The initial conditions as a whole are $u_c(o)=0$ and $\dot{u}_c(o)=\dot{u}_{co}$. The initial central velocity is computed from the initial total impulse I, which is assumed to impart a uniform velocity to the plate given by

$$\dot{u}_o = I \Big/ \sum_{i=o}^{n} m_i \tag{3.28}$$

The initial mode velocity $\dot{u}_{c_0}$ is then obtained from a generalised momentum balance.

$$\dot{u}_{c_0} = \dot{u}_0 \left[\left[m_0 + \sum_{i=1}^{n} m_i \phi_i \right] \Big/ \left[m_0 + \sum_{i=1}^{n} m_i \phi_i^2 \right] \right] \quad (3.29)$$

where ϕ_i is the initial mode shape. This initial mode shape cannot in fact be computed since eqns. (3.24, 3.25) are singular for $u_c=0$. For this reason ϕ_i was taken to vary linearly, implying a conical or pyramidal initial mode shape. Further for the first time step t_1, the stiffness of the plate was assumed to be zero: hence

$$\dot{u}_c(t_1) = \dot{u}_c(0) = \dot{u}_{c_0}$$
$$u_c(t_1) = \dot{u}_{c_0} t_1 \quad (3.30)$$

The iterative solution then began on the second time step. At any time t it is then assumed that u_c and $\dot{u}_c$ are known and eqns. (3.26, 3.27) provide n+1 equations for the multiplier λ and the modal coefficients ϕ_1, ϕ_2 $\ldots\ldots\phi_n$. The equations are highly non-linear and are solved using a Newton -Raphson technique. The motion is integrated forward in time using an implicit constant average acceleration algorithm, written as

$$\dot{u}_c^{t+\Delta t} = \dot{u}_c^{t} + \frac{\Delta t}{2} [\ddot{u}_c^{t} + \ddot{u}_c^{t+\Delta t}]$$
$$u_c^{t+\Delta t} = u_c^{t} + \frac{\Delta t}{2} [\dot{u}_c^{t} + \dot{u}_c^{t+\Delta t}] \quad (3.31)$$

and

$$\ddot{u}_c^{t+\Delta t} = - \lambda \dot{u}_c^{t+\Delta t} \quad (3.32)$$

A second outer iteration is used to solve these equations as shown in the flow chart Fig.3.8. At the beginning of a time step, $u_c^{t+\Delta t} = u_c^{t}$ and the value of λ is taken from the last iteration of the previous time step. Equations (3.31) are used to obtain corrected values of $u_c^{t+\Delta t}$ and then λ is recomputed from the Newton-Raphson solution of (3.26, 3.27). This iterative procedure continues until a prespecified tolerance is met in order to continue to the next time step. The forward integration is terminated

at time t_f where $u_c(t_f)=0$. If in a particular time step the predicted velocity at the end of the step was negative, this step was taken as the final step and the u_c was assumed to vary linearly with time over this final step.

Solutions were found for a range of impulses for each of the plate geometries, using n=4, (ie ϕ_4). Using an initial time step of 5μs and subsequent time steps of 5μs the final time was approximately 100μs, so that in all about 20 time steps were used. Convergance of the algorithm was rapid, and an increase in the number of nodes or the number of time steps did not significantly change the solution.

Computationally the algorithm is considered efficient. The computations were executed in about 10-20 seconds on the Sperry 1100/80 mainframe computer at the University of Cape Town.

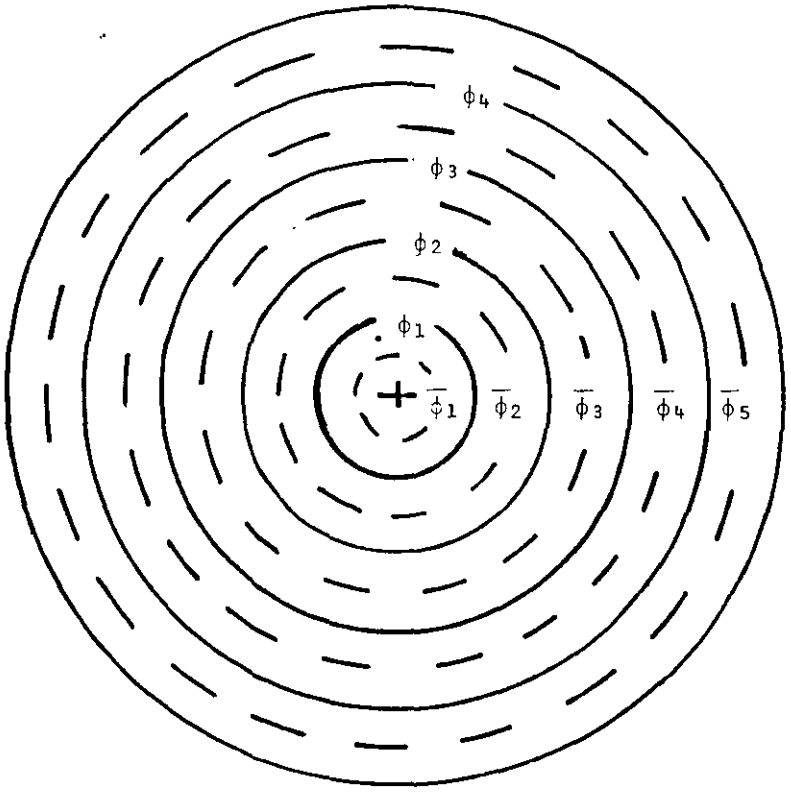

FIGURE 3.4 DISCRETISATION OF CIRCULAR PLATES
(ϕ_0 is the centre of the plate).

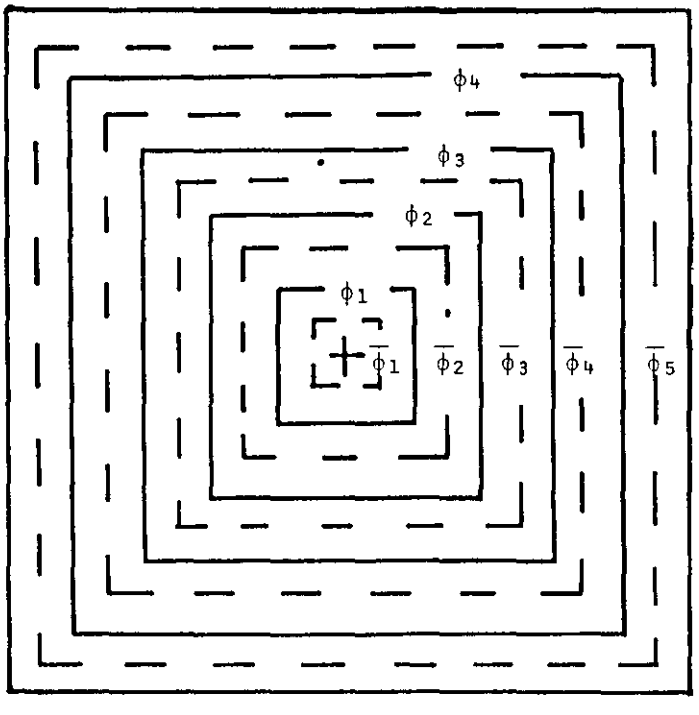

FIGURE 3.5 DISCRETISATION OF SQUARE PLATES
(ϕ_0 is the centre of the plate)

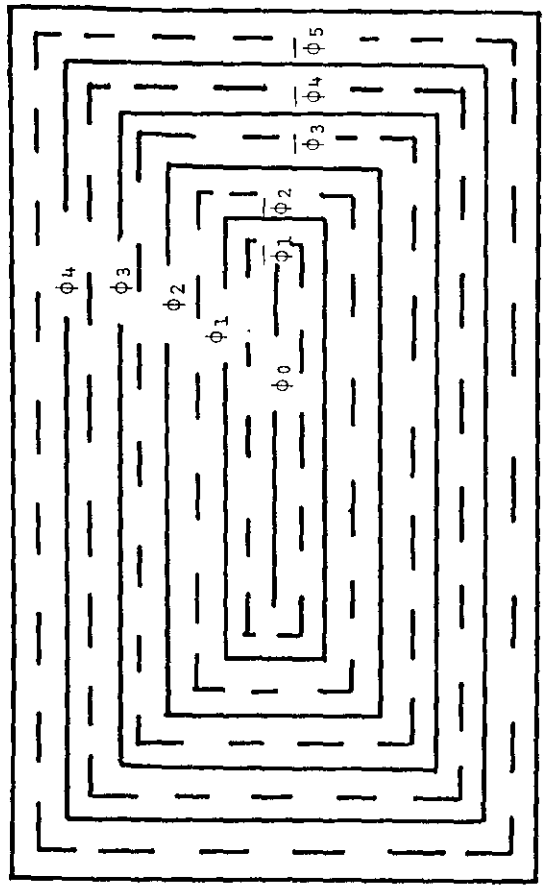

FIGURE 3.6 DISCRETISATION OF RECTANGULAR PLATES

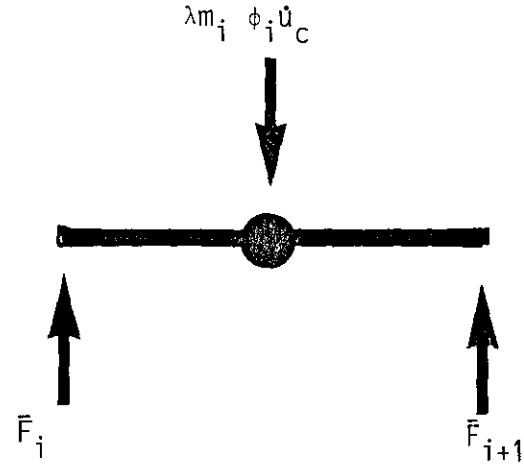

FIGURE 3.7 FORCES ACTING ON THE i^{th} NODE

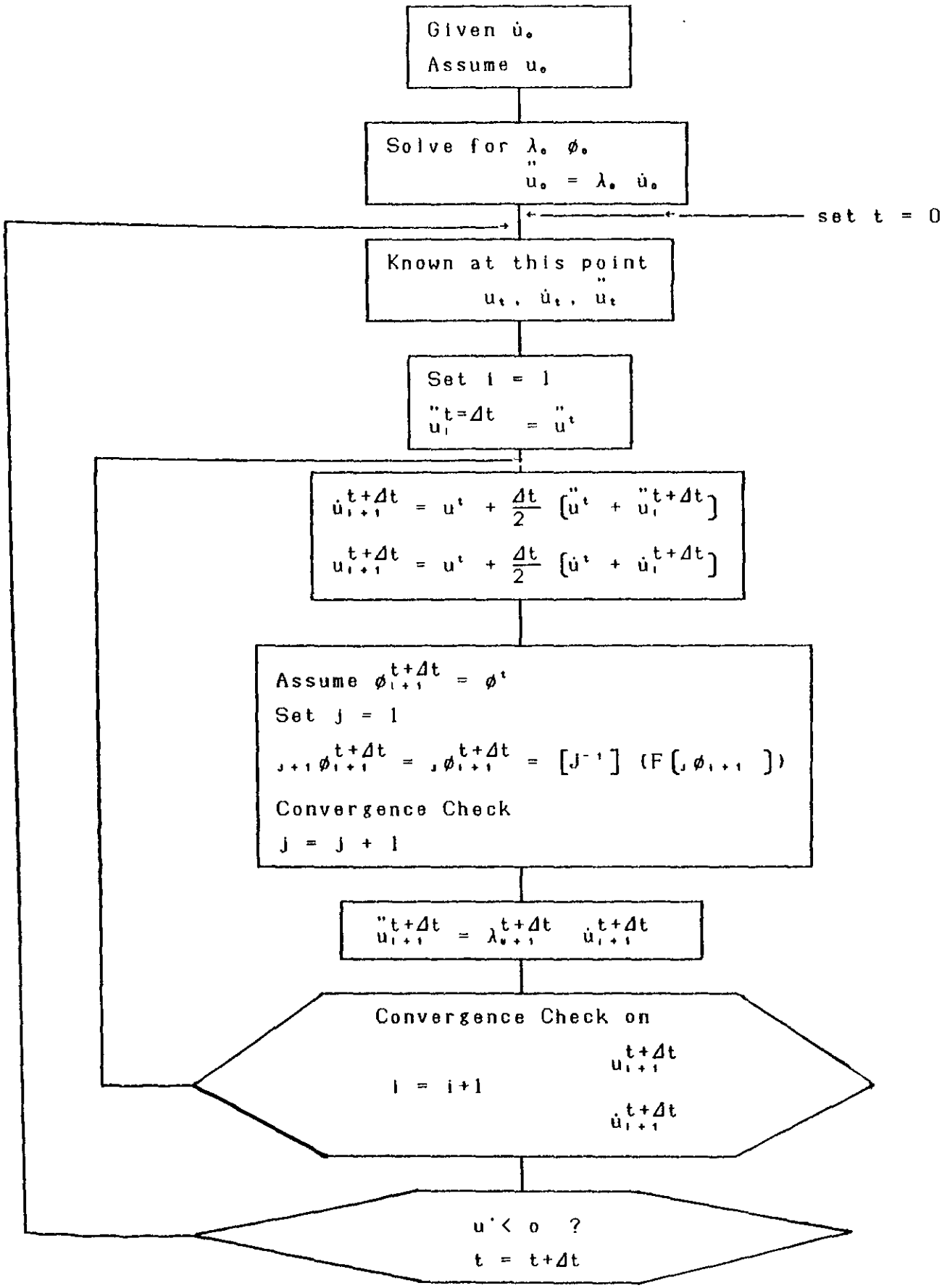

FIGURE 3.8 Flowchart of Problem Solver

CHAPTER 4 - RESULTS

4.1 INTRODUCTION

To assess the accuracy of the mode method presented in the previous chapter, the predictions are compared with the experimental results presented in Chapter 2. This is shown in Figures 4.1, 4.2 and 4.3, where the deflection-thickness ratio is plotted against impulse for circular, square and rectangular plates respectively. Also shown on these graphs are the predictions presented by other authors.

The range of experimental readings presented here is significantly larger than previously presented. The maximum deflection-thickness ratio is greater by a factor of almost two. Most previous predictions were compared with previous experiments and these results were in the range of up to approximately six to seven plate thicknesses for circular plates and eight to nine plate thicknesses for quadrangular plates. Most of these predictions compared favourably with the experiments. (see for example Guedes Soares[57], Symonds and Bodner[26], Duffey[20]. However, at larger deflection- thickness ratios, these predictions show tendencies to highly over estimate or under estimate the deflections. Several reasons could be attributed to this variance - the most likely being that the assumed deformed shape was constant throughout the motion, and that transverse deflections only were considered.

However, it is observed in Figures 4.1, 4.2 and 4.3 that by including lateral displacements into the model described in Chapter 3, the predicted transverse central displacement is marginally larger than the prediction without the lateral displacements. This may be attributed to the fact that by introducing the assumption that the displacement, velocity and acceleration fields act at all times perpendicular to the plate surface, the model assumes that the element between nodes is also rotated.

However, predicted results from both models proposed in this thesis compare favourably with the experimental results.

A dimensionless plot shown in Fig. 4.4 shows quite clearly that for plates of equal area and thickness subjected to equal total impulses the midpoint deflection of the circular plate exceeds that of the square plate, which in turn exceeds that of the rectangular plate.

The model as proposed in this thesis can also be used to predict the lateral strain distribution. This has hitherto not been possible. Previous attempts to predict these strain distributions, have shown a distribution which is inverted, ie the strain is small at the centre and large at the outer sections which is in disagreement with the experimental evidence. Figs. 4.5, 4.6 and 4.7 show the trend of the strain distribution compared with the measured strain distribution. These trends compare favourably. Also shown in Figs. 4.5 - 4.7 is the predicted strain distribution using the model in which lateral displacements were ignored

In Figs. 4.8 - 4.10 the predicted final mode shape profiles are shown plotted against the measured profiles. For both the circular and the square plates the predictions show good correlations with the measured profiles. In the case of the rectangular plates, both models tend to underestimate the deflection. This variation is attributed to the fact that the choice of the shape of the rectangular plate contours assumes uniform deflection along a central line. This is obviously not the case. However, the predictions do compare favourably with the experiments.

Figs. 4.11 - 4.13 show plots of time to reach initial deflections versus impulse. These plots, although showing very little correlation between the predicted and measured readings, show similar trends. These trends are similar to those reported by Bodner and Symonds[26].

Figs. 2.19a-c show a series of typical deflection-time histories at the centre of each plate. These measurements were recorded over a period of approximately 14 ms, as shown on the left side of the page, while the first 2 ms of deformation has been shown enlarged on the right side of the page.

The final mid-point deflections were measured mechanically by means of a vernier, while the full plate deformation was measured using a Reflex Metrograph, resulting in contour plots of the deformed plate. These are shown in Fig. 2.20

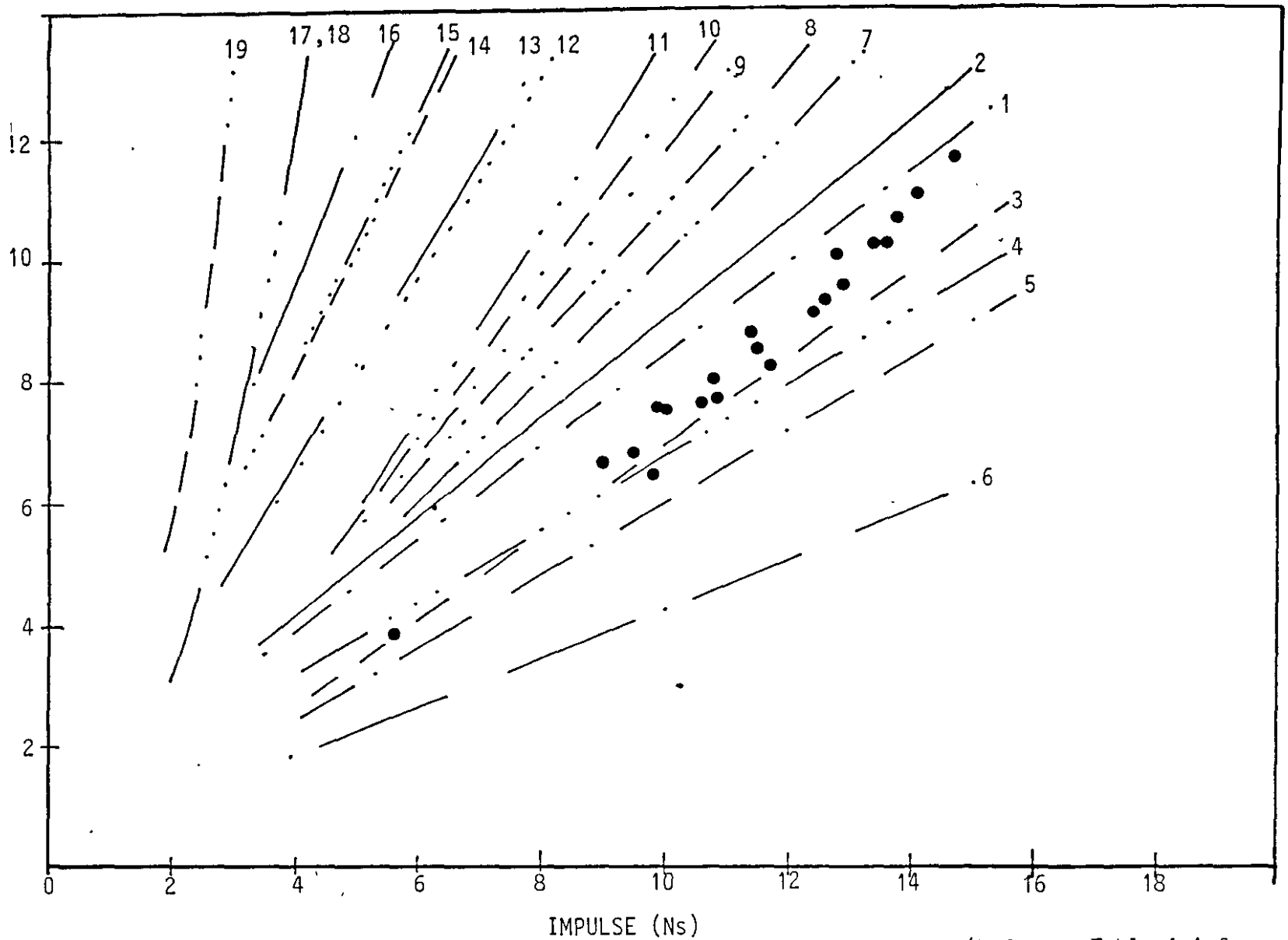

FIGURE 4.1 GRAPH OF DEFLECTION - THICKNESS RATIO vs IMPULSE FOR CIRCULAR PLATES. (Refer to Table A.1 for equations).
● Experimental Data; 1 - Model excluding Lateral Displacements; 2 - Model including Lateral Displacements; 3 - Lippman(56); 4 - Symonds & Wierzbicki(66); 5 - Perrone & Bhadra(68); 6,16 - Noble & Oxley - different mode shapes(54); 7,8 - Duffey - different mode shapes(19); 9 - Calladine(71); 10 - Guedes Soares(57); 11 - Westine & Baker(69); 12,17 - Wierzbicki & Florence - different mode shapes(18); 13 - Hudson(33); 14 - Batra & Dubey(55); 15 - Ghosh & Weber(27); 18 - Wang & Hopkins(39); 19 - Wang(40)

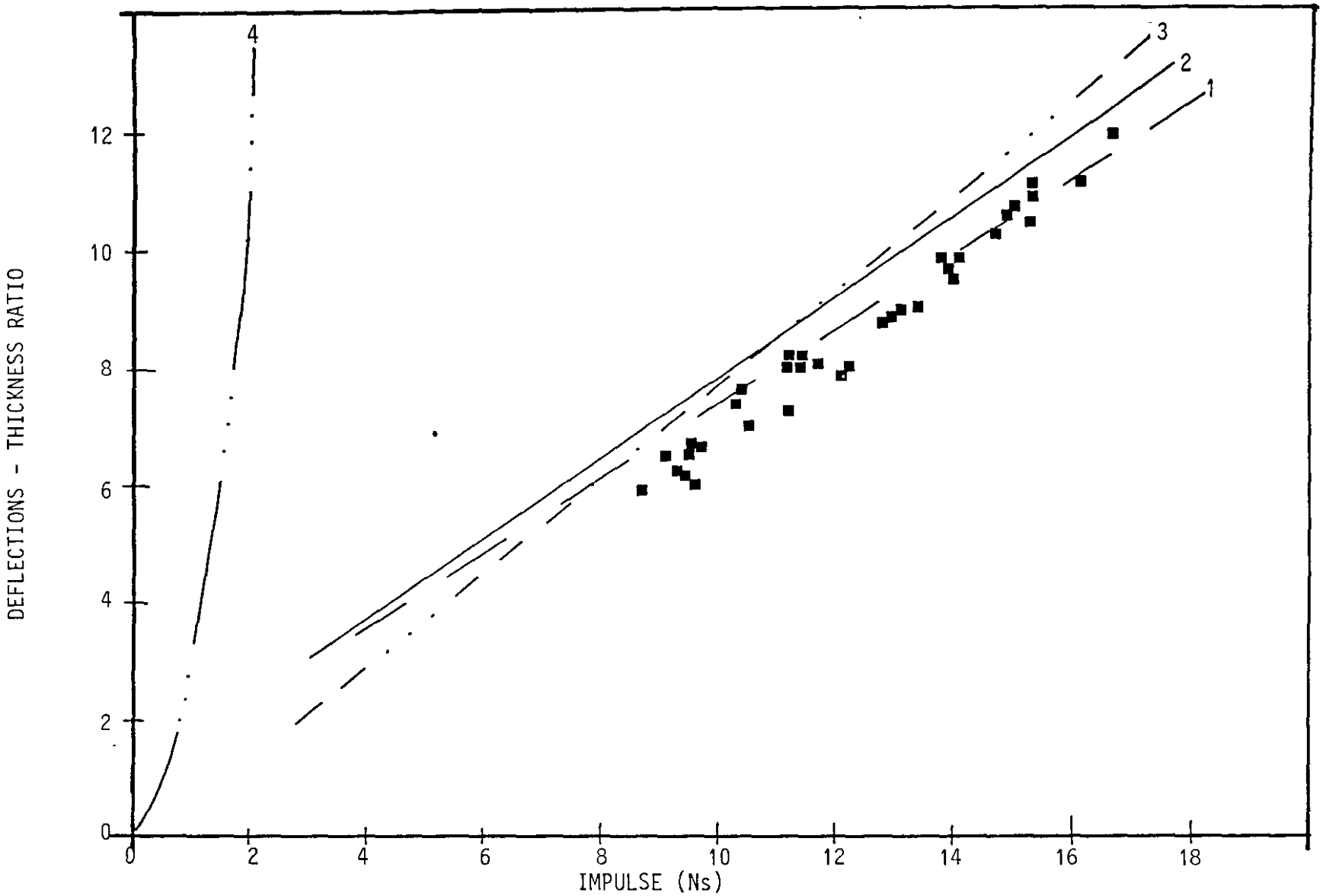

FIGURE 4.2 GRAPH OF DEFLECTION - THICKNESS RATIO vs IMPULSE FOR SQUARE PLATES.
(Refer to TableA.1for equations)
■ Experimental Data; 1 - Model including Lateral Displacements; 2 - Model excluding Lateral Displacements
3 - Baker(70); 4 - Jones et al(22,23)

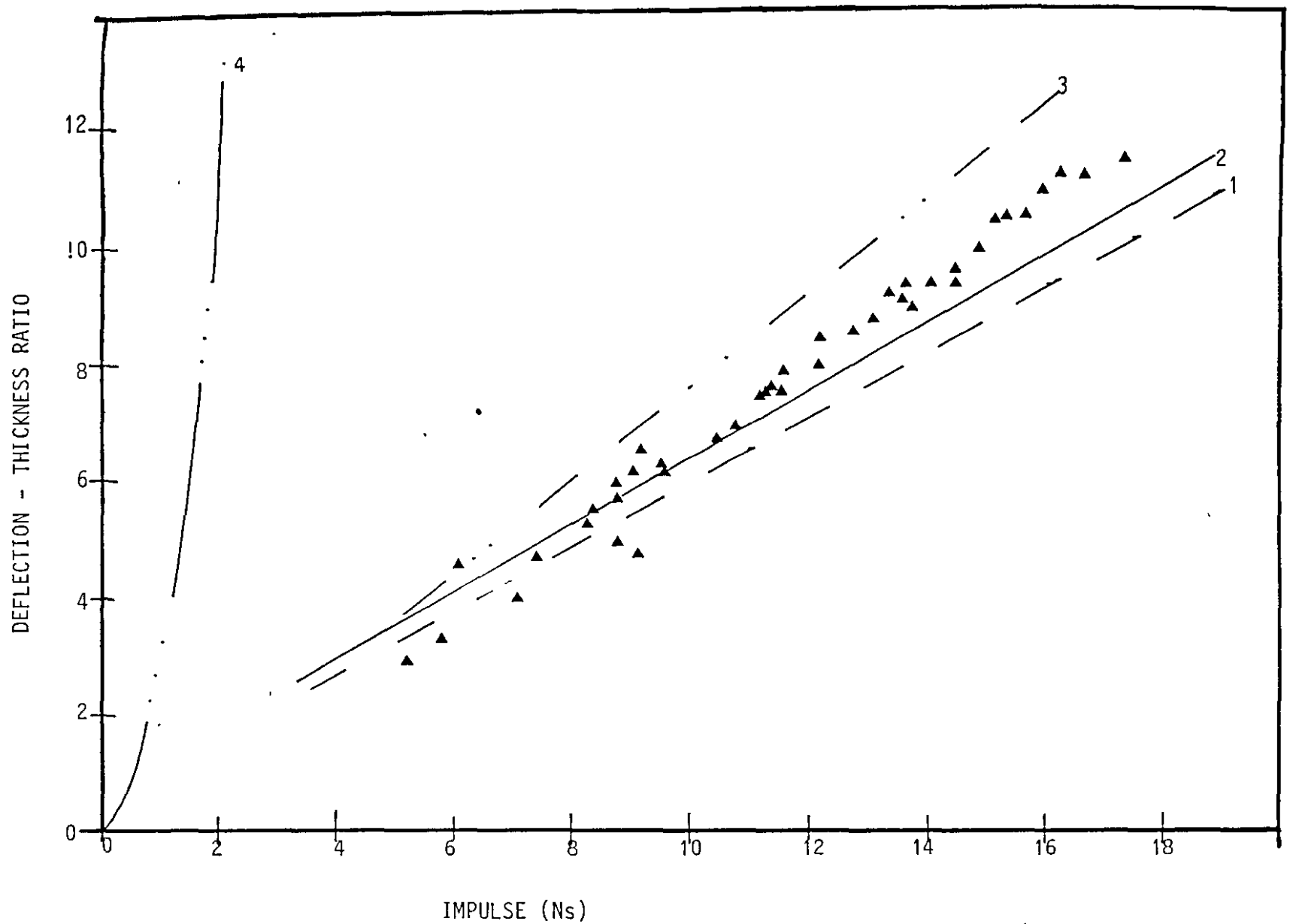

FIGURE 4.3 GRAPH OF DEFLECTION - THICKNESS RATIO vs IMPULSE FOR RECTANGULAR PLATES. (Refer to Table A.1 for equations)
▲ Experimental Data; 1 - Model including Lateral Displacements; 2 - Model excluding Lateral Displacements; 3 - Baker(70); 4 - Jones et al(22,23)

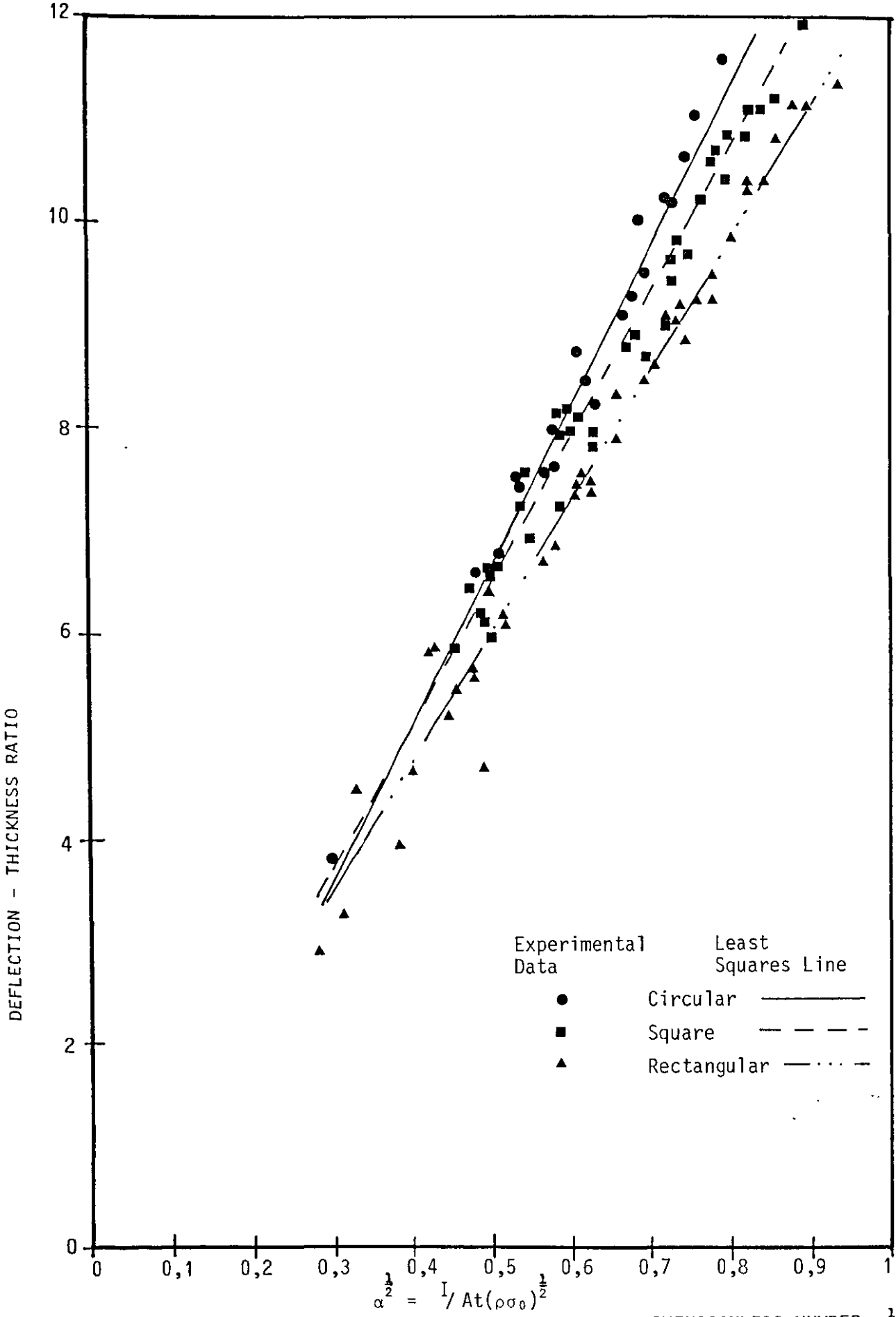

FIGURE 4.4 GRAPH OF DEFLECTION - THICKNESS RATIO vs DIMENSIONLESS NUMBER $\alpha^{\frac{1}{2}}$

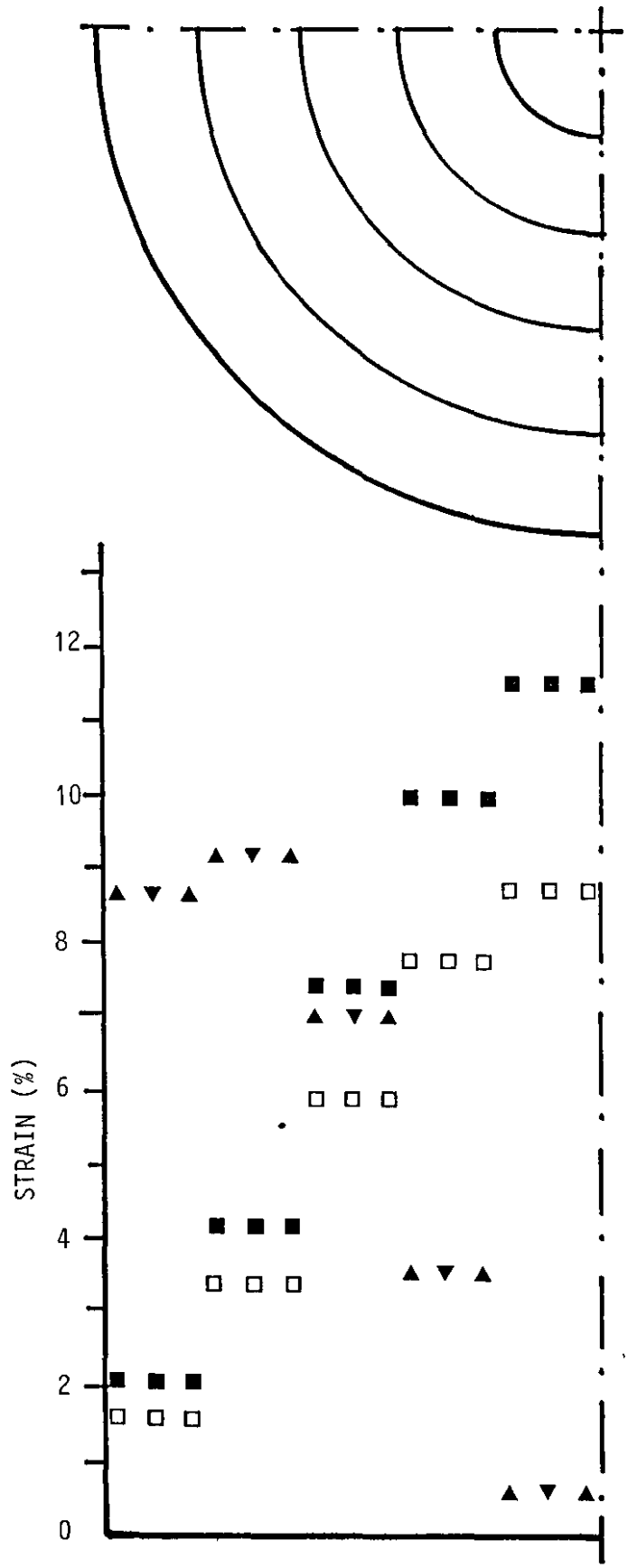

FIGURE 4.5 RADIAL STRAIN DISTRIBUTION FOR IMPULSE OF 12 Ns FOR CIRCULAR PLATES

■ ■ ■ MODEL INCLUDING LATERAL DISPLACEMENTS
▲▼▲ MODEL EXCLUDING LATERAL DISPLACEMENTS
□□□ MEASURED (TEST NO. 1106855)

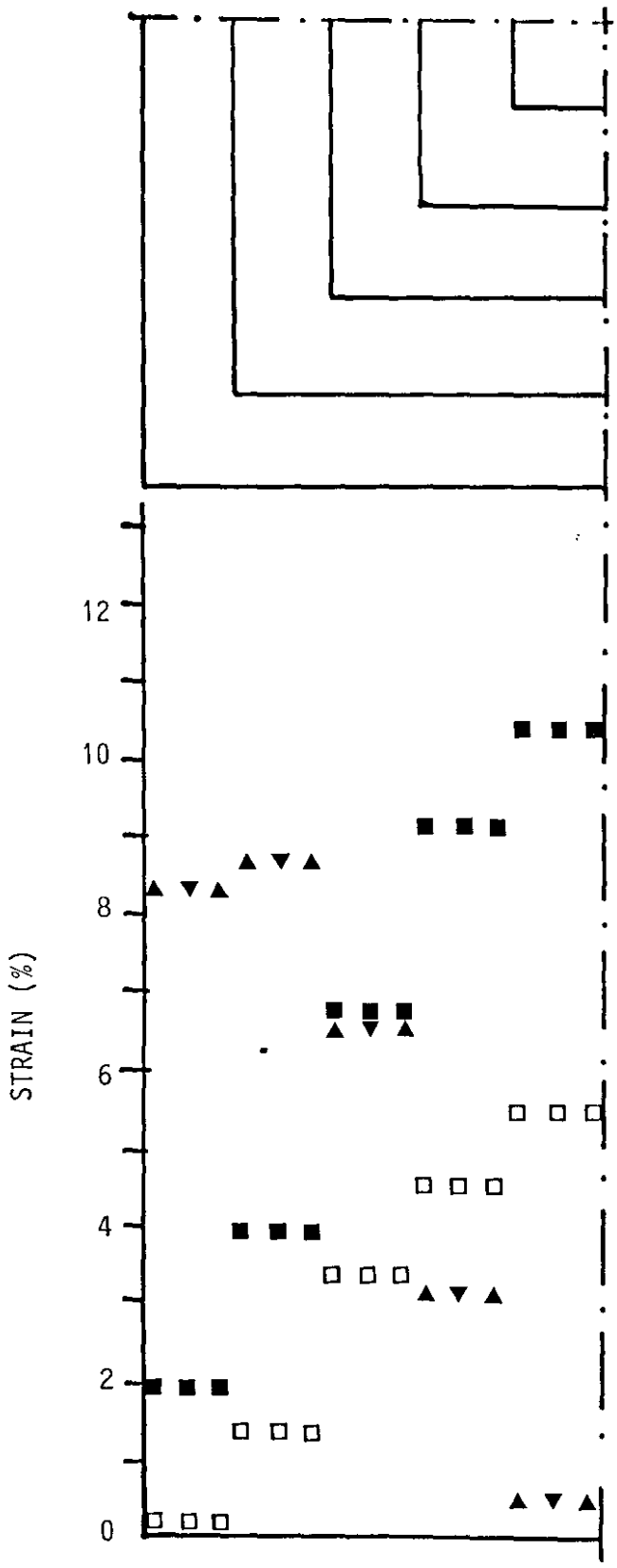

FIGURE 4.6 RADIAL STRAIN DISTRIBUTION FOR IMPULSE OF 12 Ns FOR SQUARE PLATES

■■■ MODEL INCLUDING LATERAL DISPLACEMENTS
▲▼▲ MODEL EXCLUDING LATERAL DISPLACEMENTS
□□□ MEASURED (TEST NO. 0605854)

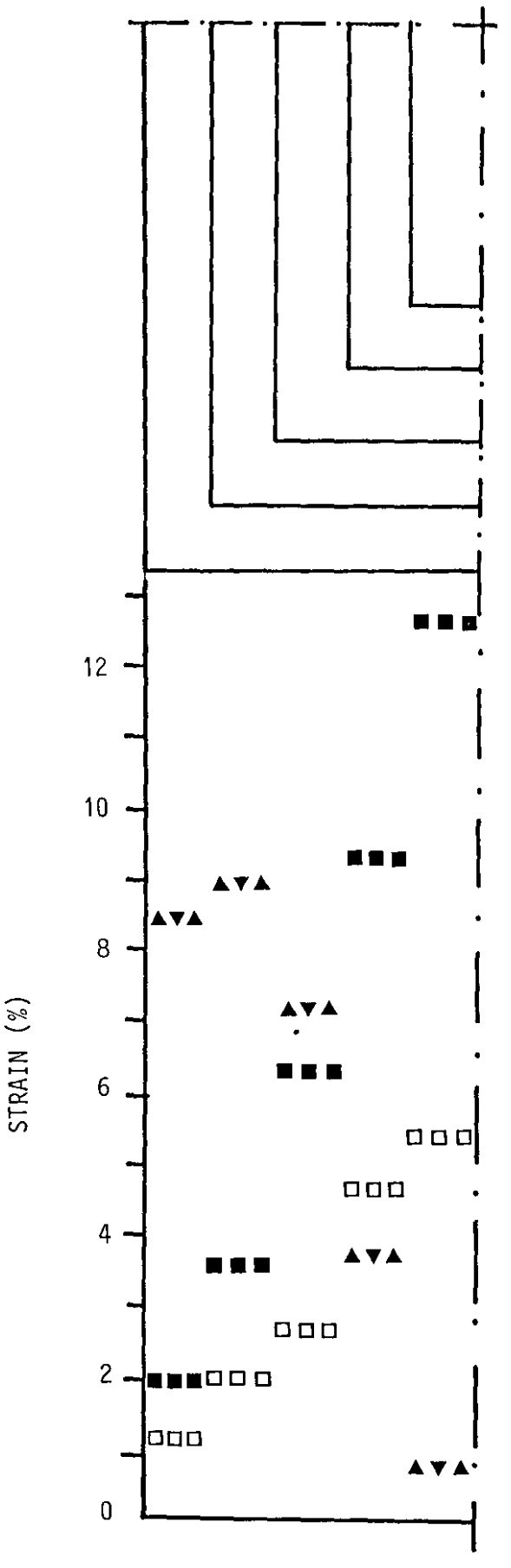

FIGURE 4.7 RADIAL STRAIN DISTRIBUTION FOR IMPULSE OF 12Ns FOR RECTANGULAR PLATES

■■■ MODEL INCLUDING LATERAL DISPLACEMENTS
▲▼▲ MODEL EXCLUDING LATERAL DISPLACEMENTS
□□□ MEASURED (TEST NO. 2201852)

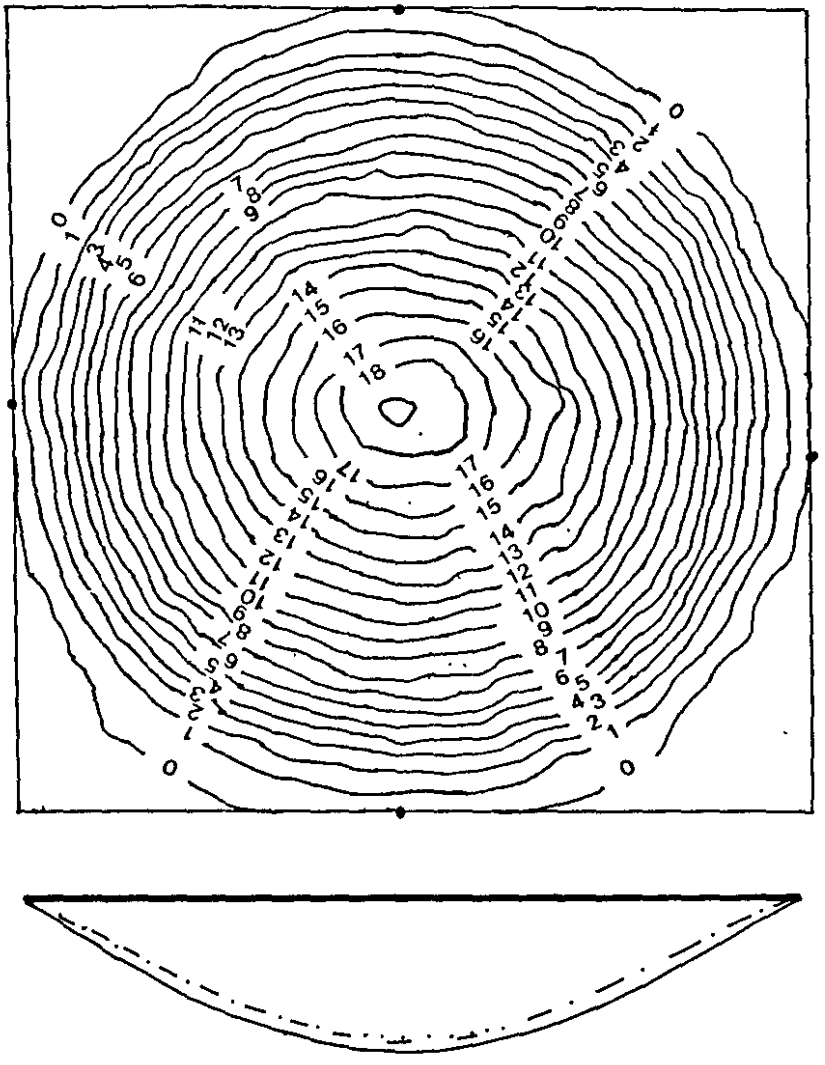

FIGURE 4.8 FINAL MODE PROFILE AND CONTOUR PLOT

——— MODEL INCLUDING LATERAL DISPLACEMENTS
— — — MODEL EXCLUDING LATERAL DISPLACEMENTS
. . . . . MEASURED (TEST NO. 1906854)

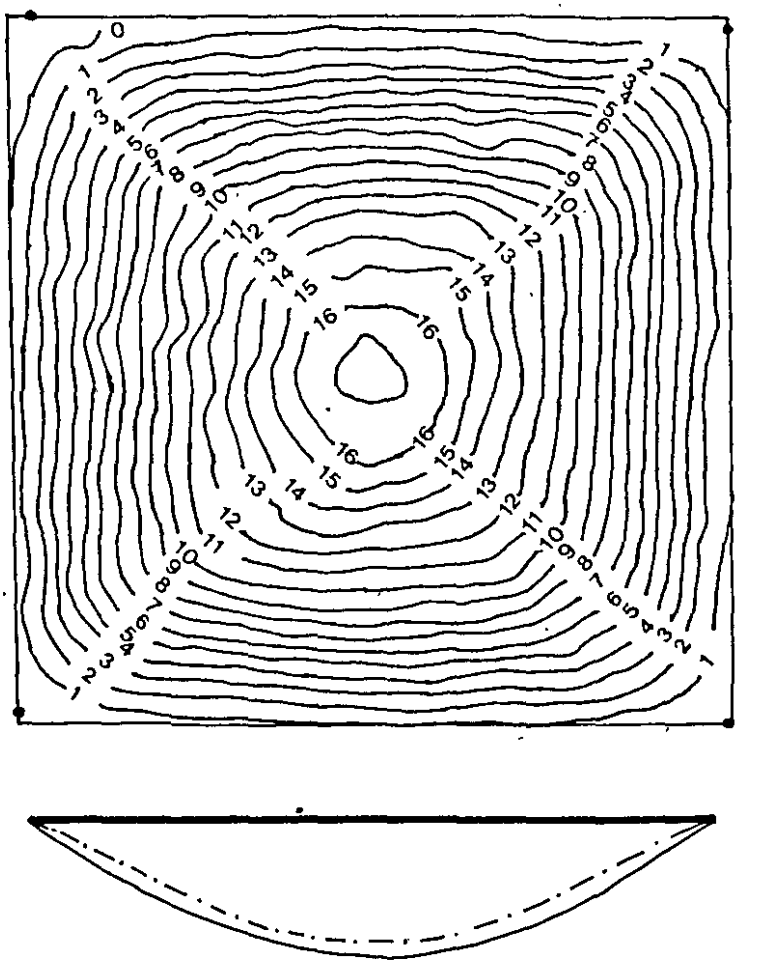

FIGURE 4.9 FINAL MODE PROFILE AND CONTOUR PLOT

——— MODEL INCLUDING LATERAL DISPLACEMENTS
— — — MODEL EXCLUDING LATERAL DISPLACEMENTS
· · · · · · MEASURED (TEST NO. 0705853)

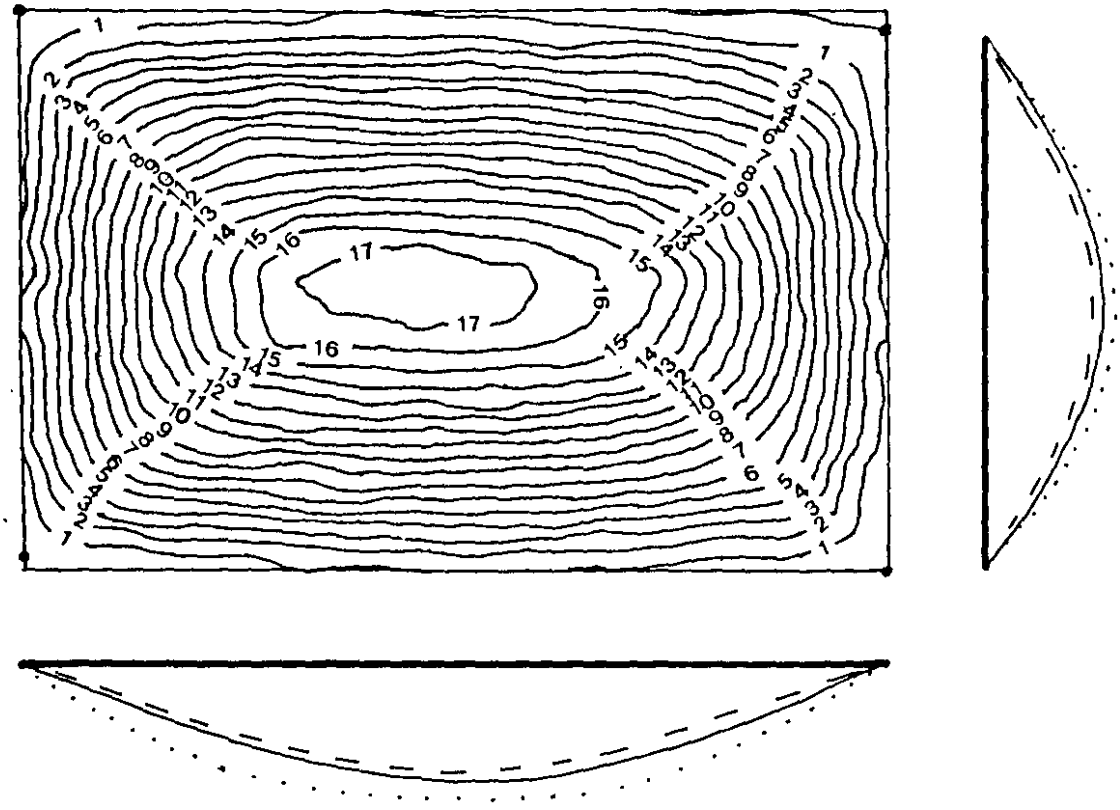

FIGURE 4.10 FINAL MODE PROFILE AND CONTOUR PLOT

——— MODEL INCLUDING LATERAL DISPLACEMENTS
— — — MODEL EXCLUDING LATERAL DISPLACEMENTS
· · · · · · MEASURED (TEST NO. 0102851)

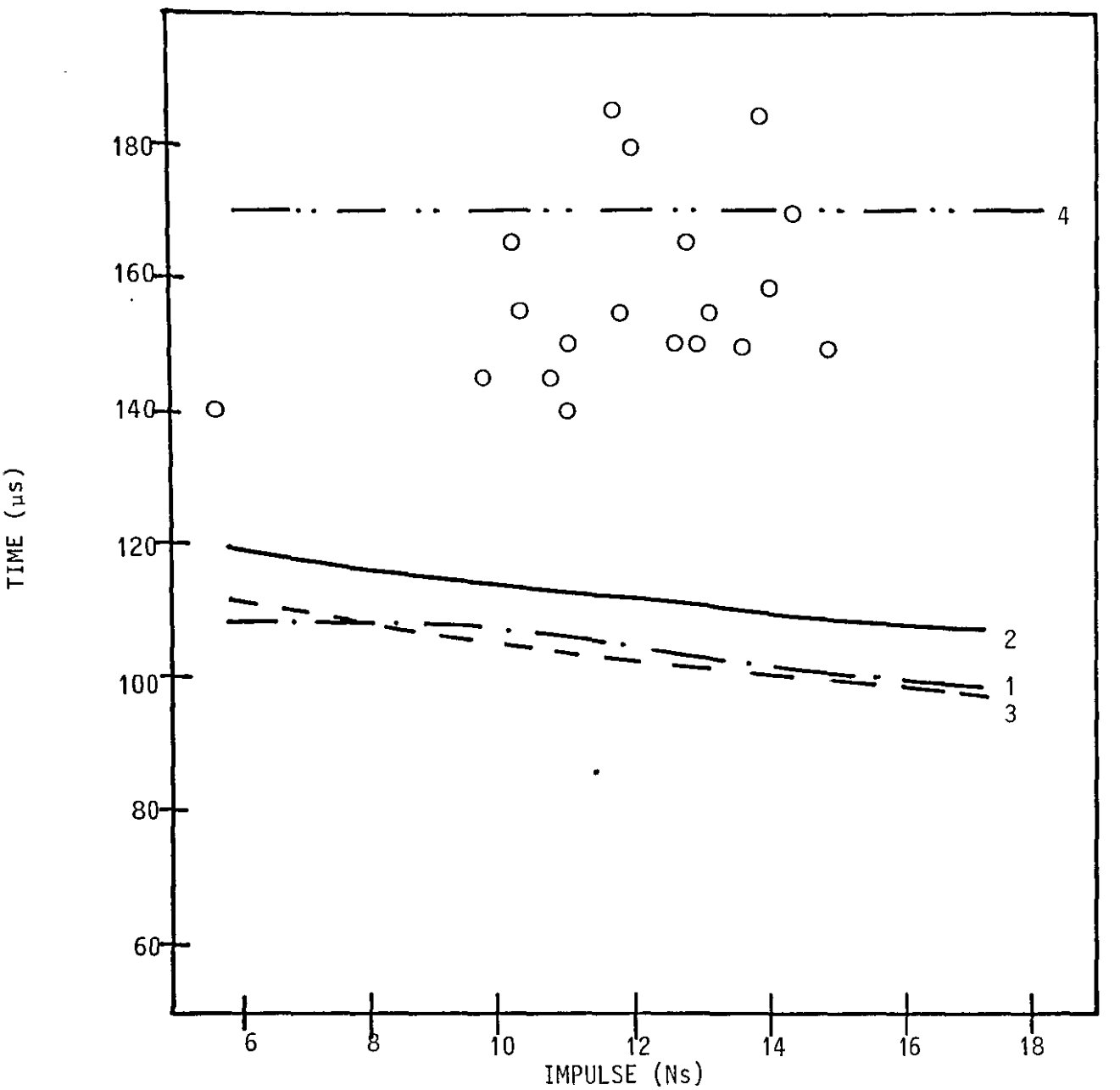

FIGURE 4.11 GRAPH OF TIME TO REACH INITIAL DEFLECTION vs IMPULSE FOR CIRCULAR PLATES
O - Experimental Data; 1 - Model including lateral displacements;
2 - Model excluding lateral displacements; 3 - Symonds & Wierzbicki(66);
4 - Lippman(56)

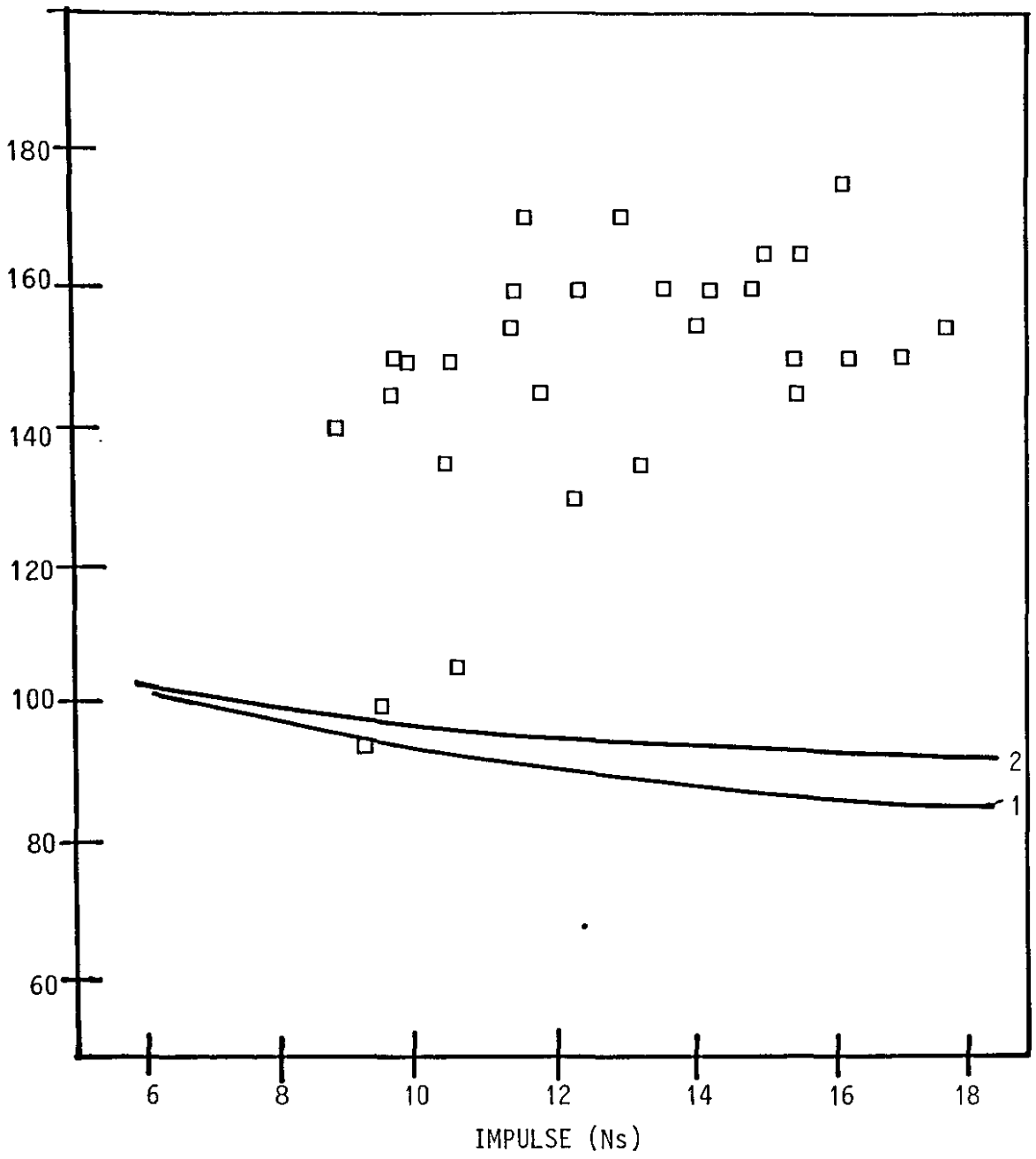

FIGURE 4.12 GRAPH OF TIME TO REACH INITIAL DEFLECTION vs IMPULSE FOR SQUARE PLATES
□ Experimental Data; 1 - Model including Lateral Displacements;
2 - Model excluding Lateral Displacements.

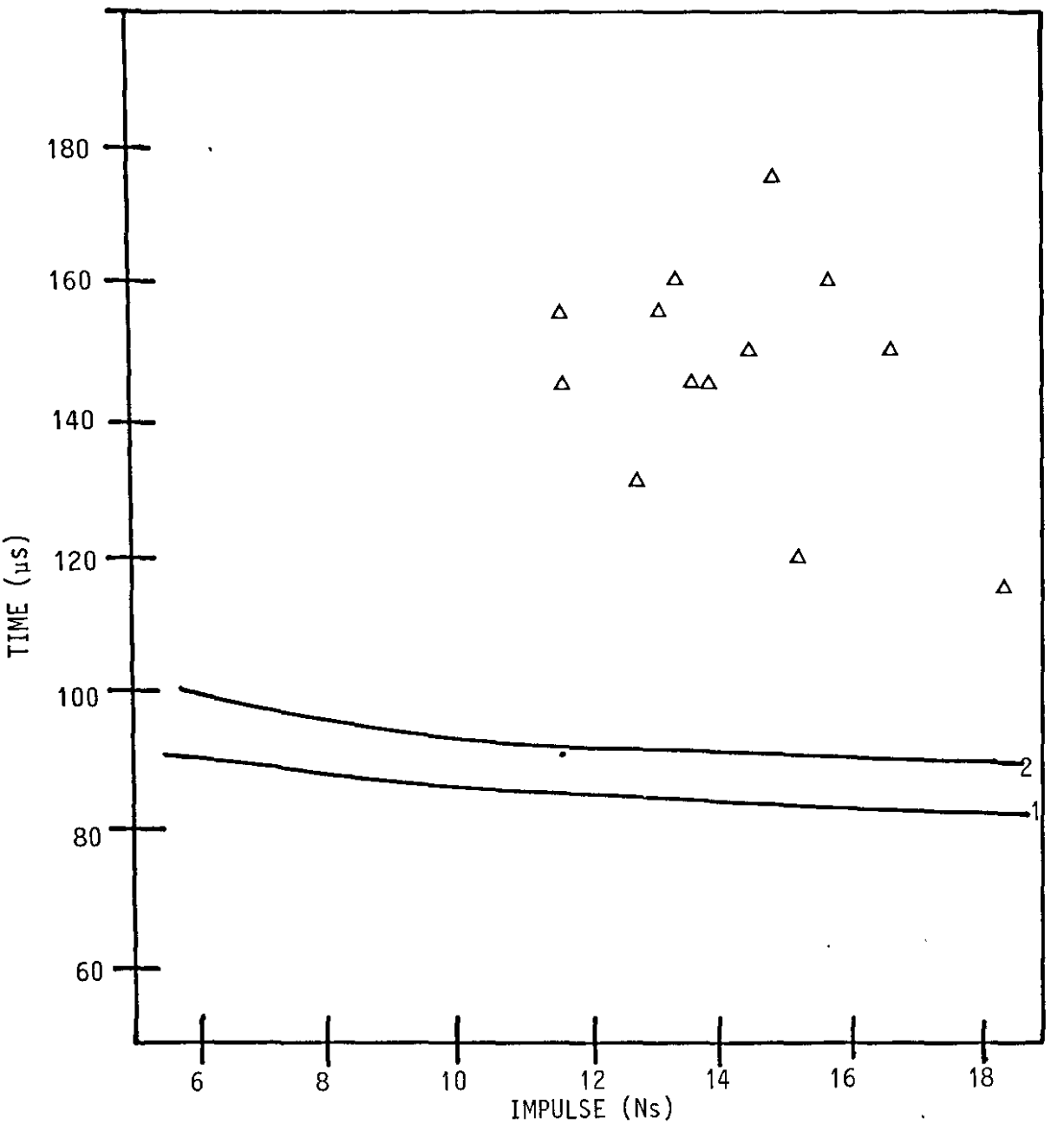

FIGURE 4.13 GRAPH OF TIME TO REACH INITIAL DEFLECTION vs IMPULSE FOR RECTANGULAR PLATES

△ Experimental Data; 1 - Model including Lateral Displacements; 2 - Model excluding Lateral Displacements

4.2 COMPARISON OF PRESENT EXPERIMENTAL DATA WITH PREVIOUS RESEARCHERS

In an attempt to compare present experimental results with other experiments, which have different target dimensions, use is made of a dimensionless damage number defined by Johnson [15] as

$$\alpha = \rho v^2 / \sigma_d \qquad (4.1)$$

which is used as a guide for assessing the behaviour of metals in impact situations. Here ρ is the material density, v the impact velocity and σ_d the damage stress. Table 4.1 shows the regime of damage as a function of damage number and also for comparison shows the results of some circular plate experiments. It can be seen that α predicts an order of magnitude deformation and in doing so, does not consider the method of impact, the interpretation of σ_d, the target geometry and boundary conditions or the target dimensions.

Since here we wish to compare results of deformed plates of similar geometries, boundary conditions and loading, it seems reasonable to introduce factors which would allow all other variables to be normalised into dimensionless groups.

Johnson's damage number can be written in terms of the impulse as

$$\alpha_0 = \frac{I^2}{A_0^2 t^2 \rho \sigma_d} = \frac{I_0^2}{t^2 \rho \sigma_d} \qquad (4.2)$$

where I is the total impulse, A_0 is that area of the plate over which the impulse is imparted, I_0 is the impulse per area of impulse, and t is the plate thickness. Fig. 4.14 shows a plot of deflection-thickness ratio versus α_0 for circular plates of varying dimensions and material properties. This indicates the order of magnitude reliability of Johnson's damage number, but

as can be seen, the variations for similar loading conditions are a factor of up to 2,5. For dissimilar loading conditions, the variation has a factor of up to 8,5.

In the case of quadrangular plates, we introduce a geometry number defined as

$$\beta = \frac{L}{B} \tag{4.3}$$

where L and B are the plate length and breadth respectively. A geometrical damage number is then written as

$$\phi = \left[\beta\alpha_o \left(\frac{A_o}{A}\right)^2\right]^{\frac{1}{2}} \tag{4.4}$$

where A is the area of the plate.

A relationship between the distance from the plate centre to the nearest boundary and the plate thickness is introduced as the aspect ratio λ , where

$$\lambda = R/t \text{ for circular plates} \tag{4.5a}$$

$$\lambda = \frac{B/t}{\sqrt{\beta}} \text{ for quadrangular plates} \tag{4.5b}$$

The loading area per total plate area must also be considered and this is accounted for by a loading parameter assumed to be

$$\zeta = 1 + \ell n\,(R/R_o) \tag{4.6}$$

for circular plates only and where R_o is the radius of the loaded area. Equation (4.6) implies that when $R_o \to R$, then $\zeta \to 1$ and the plate is uniformly loaded over the full area, and when R_o is very small, the loading tends to a point loaded situation and is more concentrated, resulting in a larger mid-point deflection. The effect of partial loading on quadrangular plates has not been included.

Combining equations (4.4), (4.5), and (4.6) results in a modified damage number which incorporates dimensions and loading given by

$$\phi = \psi \lambda \xi \qquad (4.7)$$

For circular plates then

$$\phi_c = \frac{I\ (1 + \ell n\ R/R_c)}{\pi R t^2 (\rho \sigma_c)^{\frac{1}{2}}} \qquad (4.8a)$$

and for quadrangular plates

$$\phi_q = \frac{I}{2 t^2 (BL\ \rho \sigma_c)^{\frac{1}{2}}} \qquad (4.8b)$$

Table 4.2 summarizes all the dimensionless parameters, and Table 4.3 summarizes the experimental data.

The geometry and material density variables in Equation (4.8) are easily obtainable. The variables I and σ_d are measured experimentally - I from impulse tests and for convenience σ_d is given the value of σ_c, the static yield stress.

Figures 4.15a and 4.16a show dimensionless plots of deflection-thickness ratio versus ϕ for the experimental results on circular and quadrangular plates respectively. Also shown are dimensionless plots of theoretical predictions described in Chapter 2. Least-squares correlation analysis of the circular plate experimental data yields a correlation coefficient of 0.973 and these experimental results are almost all within one deflection-thickness of the least squares line, as shown in Fig. 4.15b.

For the quadrangular plates (Fig.4.16b), the experimental results are also all mostly within one deflection-thickness-ratio of the least squares correlation which in this case has a correlation coefficient of 0.980.

All readings thus far reported were for deformations in

which no tearing of the plate was observed. However, a few experiments were performed in which a small part, (approximately one-tenth), of the boundary perimeter, tearing was observed. This partial tearing of the plate was observed at the clamped boundaries at impulses of 17,7 Ns and 19,0 Ns for the square and rectangular plates. This translates to ϕ values of 51 and 56 respectively. For the circular plates tearing occurred at an impulse of 15,6 Ns which translates to a ϕ value of 26. These tearing ϕ values may serve as a guideline for design of plates subjected to impulsive loading by means of symmetrically positioned sheet explosive.

Insufficient data on impulse parameters does not permit an attempt to be made to perform a similar detailed analysis for the other forms of impulsive loading, ie underwater blast pressure, air blast pressure and inertial frame loading. However, it is noted that Ghosh *et al* [27] has used Johnsons damage number in their analysis of the comparison between their experimental results and some theoretical predictions.

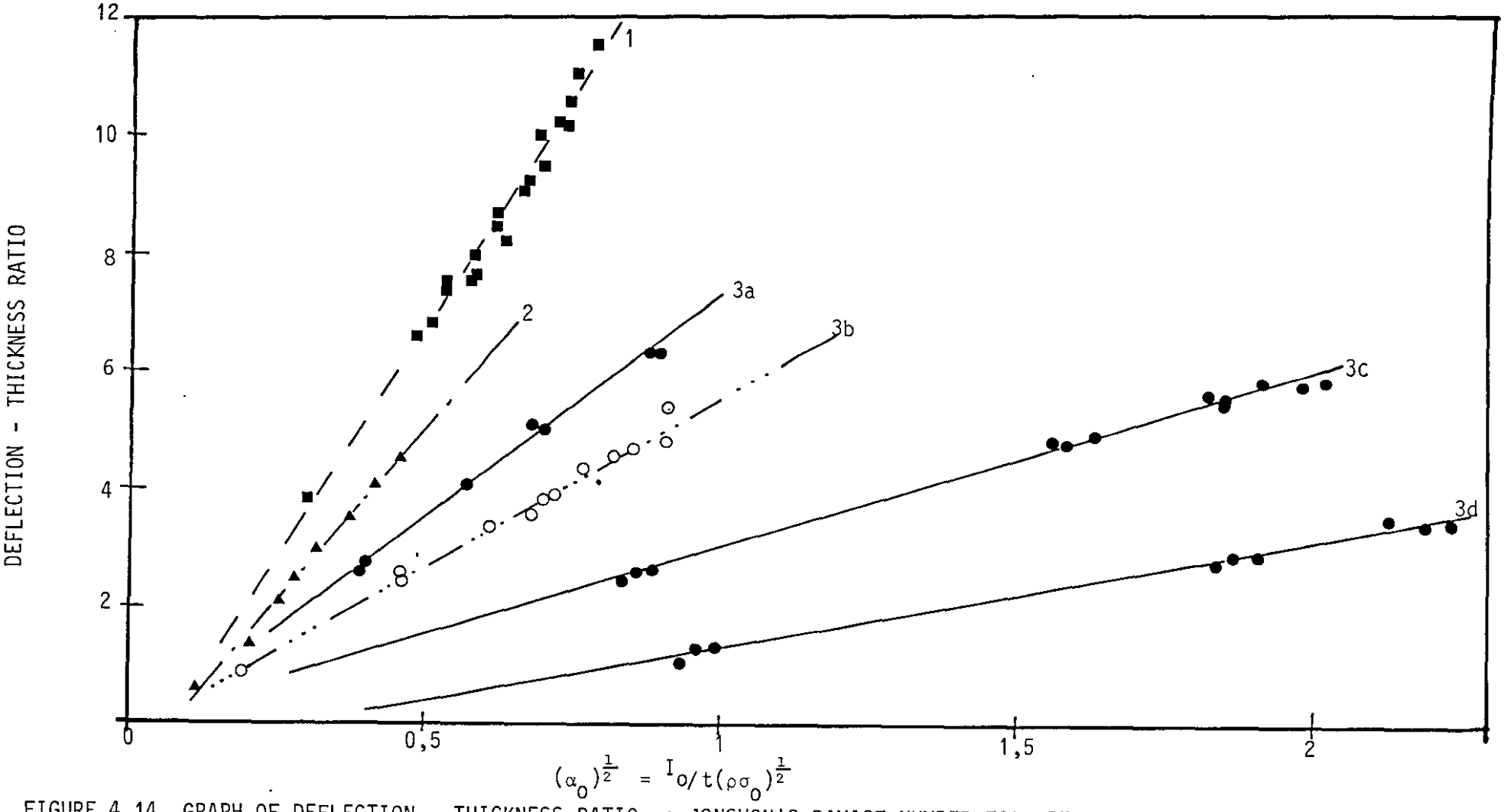

FIGURE 4.14 GRAPH OF DEFLECTION - THICKNESS RATIO vs JONSHON'S DAMAGE NUMBER FOR DIFFERENT PLATE GEOMETRIES AND LOADING CONDITIONS. (The lines represent the least squares fit to the respective data)

1. Present Experiments; R = 50mm, t = 1,6mm; mild steel uniformly loaded;
2. Wierzbicki & Florence(18); R = 50mm, t = 6,3mm; mild steel uniformly loaded;
3. Bodner & Symonds(26); R = 32mm; a,c,d,- t = 1,90mm; mild steel: b - t =2,3mm; titanium
   a,b - uniformly loaded: c - loaded $R_o/R = \frac{1}{2}$: d - loaded $R_o/R = \frac{1}{3}$

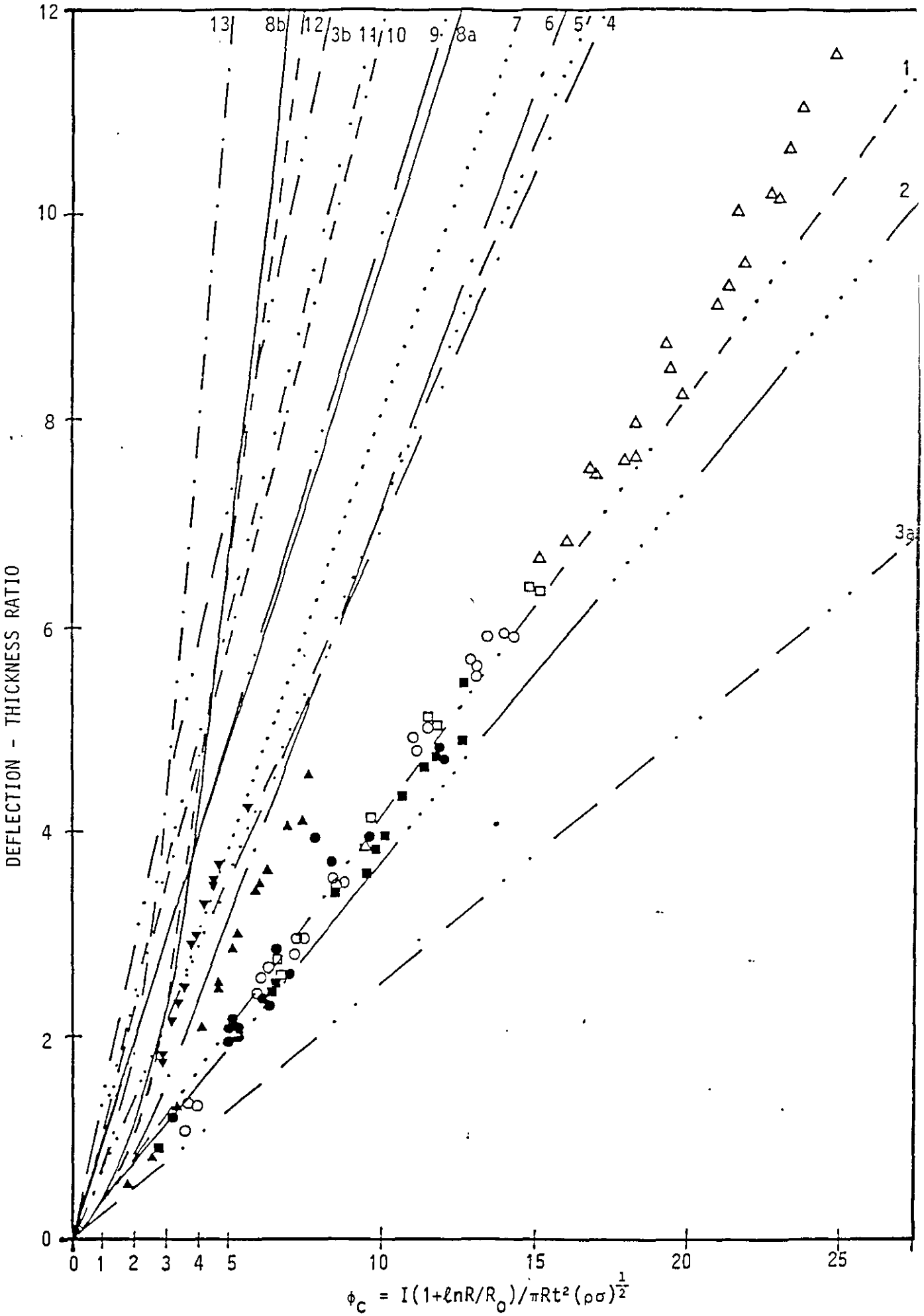

FIGURE 4.15a GRAPH OF DEFLECTION-THICKNESS RATIO vs DIMENSIONLESS No. ϕ_c

Experimental Data

		Material	Loading	Radius	Thickness
△	Nurick	A	D	50	1,6
	Bodner &				
■	Symonds	B	D	32	2,3
□		A	D	32	1,9
●		B	E	22	2,3
○		A	E	32	1,9
	Wierzbicki				
▲	& Florence	A	D	50	6,3
▼		C	D	50	6,3

Notes
A - steel; B - Titanium; C - Aluminum
D - uniform loading; E - partial loading

Predictions

1 - Lippman[56]; 2 - Perrone & Bhadra[68]; 3 - Noble & Oxley[54], a - Circular Profile, b - Conical Profile; 4 - Calladine[71]; 5 - Duffey[92]; 6 - Guedes Soares[57]; 7 - Westine & Baker[69]; 8 - Wierzbicki & Florence[18], a - large deflections, b - small deflections; 9 - Hudson[33]; 10 - Batra & Dubey[55]; 11 - Ghosh & Weber[27]; 12 - Wang & Hopkins[39]; 13 - Wang[40]

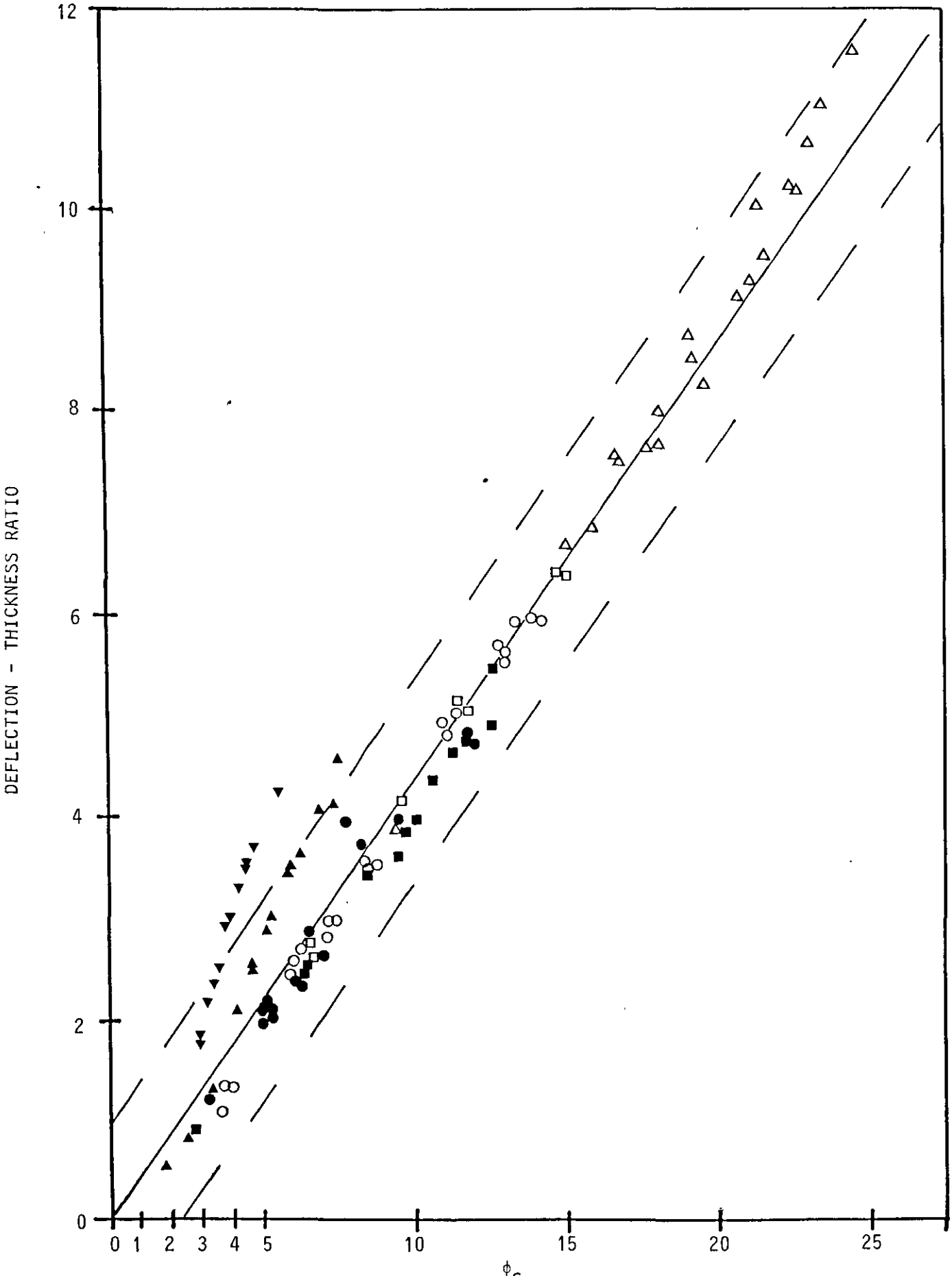

FIGURE 4.15b GRAPH OF DEFLECTION - THICKNESS RATIO vs DIMENSIONLESS NO ϕ_c , SHOWING LEAST SQUARE CORRELATION (——) BOUNDED BY±1 DEFLECTION THICKNESS RATIO (- - —)

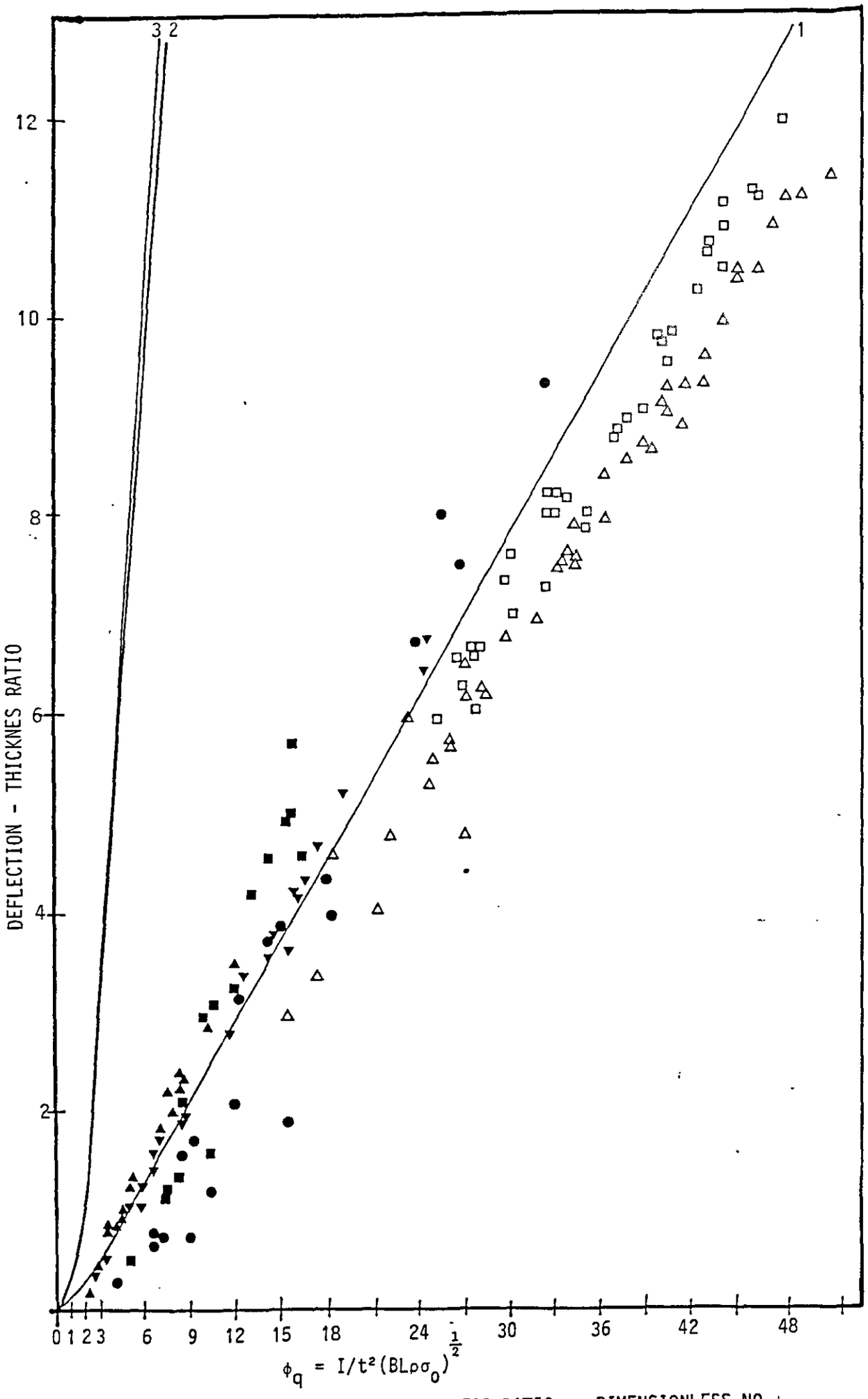

FIGURE 4.16a GRAPH OF DEFLECTION - THICKNESS RATIO vs DIMENSIONLESS NO ϕ_q

Experimental Data

	Material	β= L/B	Thickness
□ Nurick	A	1.0	1.6
△	A	1.62	1.6
● Jones & Baeder[23]	A	4.0	2.69
■	B	2.0	2.69
		1.33	2.69
		1.0	2.69
▼ Jones, Uran & Tekin[22]	A	1.69	1.63
▲	B		2.49
			4.39

Note

A - steel; B - Aluminum

All uniformly loaded

Predictions _

1. Baker[70]
2. Jones et al[22,23] β=1.6
3. Jones et al[22,23] β=1.0

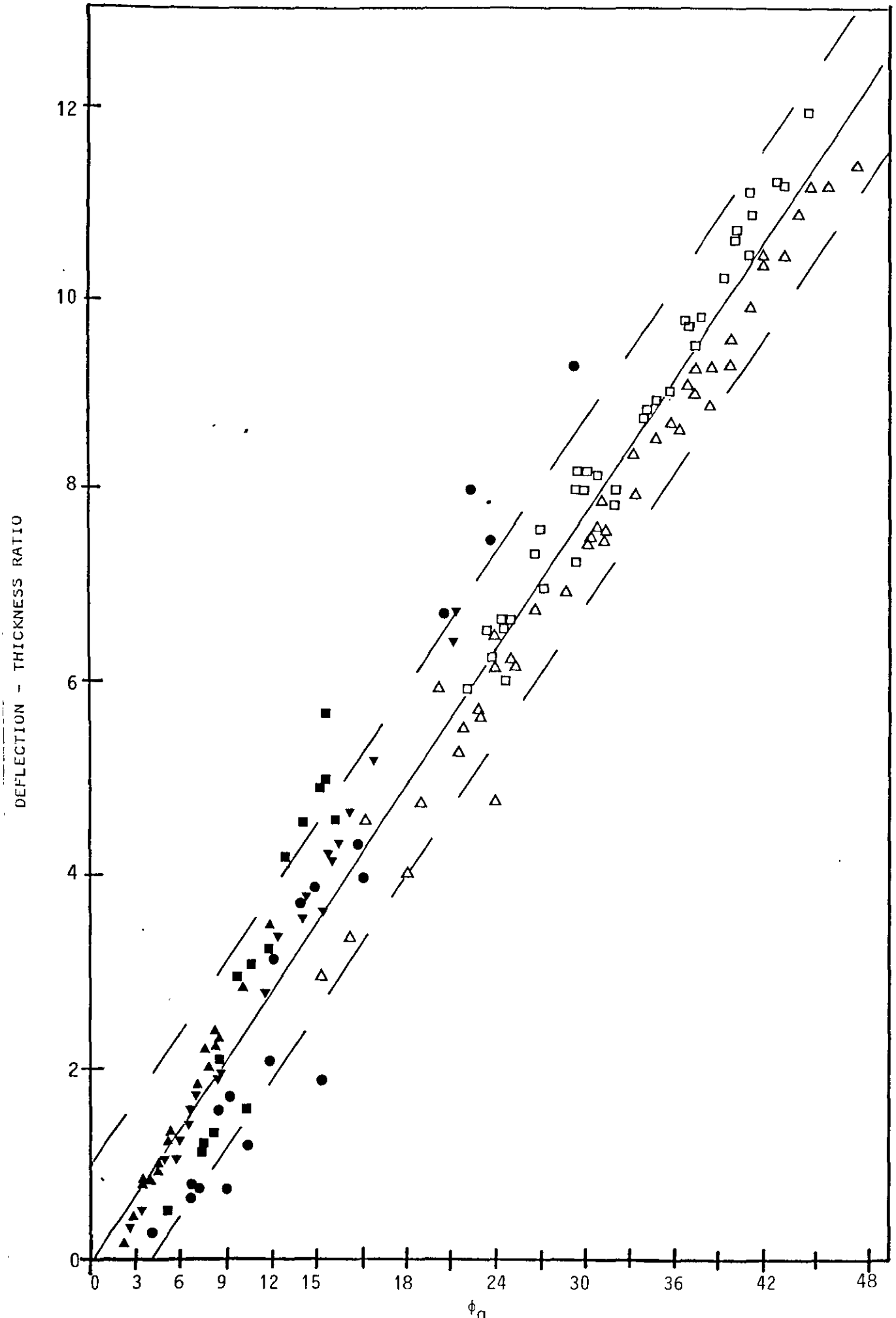

FIGURE 4.16b GRAPH OF DEFLECTION - THICKNESS RATIO vs DIMENSIONLESS NO. ϕ_q, SHOWING LEAST SQUARES CORRELATION (——) BOUNDED BY ± 1 DEFLECTION THICKNESS RATIO (- - -)

TABLE 4.1 REGIME OF DAMAGE (FROM JOHNSON[15]) AND SOME RELATED EXAMPLES

Damage No. α	$\alpha^{1/4}$	Regime	Plate Example t mm	I Ns	$\frac{R}{t}$	$\frac{\delta}{t}$	α	Ref
$1x10^{-5}$	0,0032	quasi-static	2,95	0,2	25	0,1	$6,6x10^{-6}$	75
		elastic	1,17	0,1	64	0,5	$1x10^{-5}$	75
			1,17	0,15	64	0,7	$2,4x10^{-5}$	75
$1x10^{-3}$		plastic behaviour	0,61	0,28	98	11,5	0,004	29
(0,001)	0,0316	starts	6,22	35	16	0,6	0,013	18
$1x10^{-1}$		moderate plastic	0,61	1,36	98	46	0,09	29
(0,1)	0,316	behaviour	1,6	5,7	31	3,8	0,10	x
		(slow bullet speeds)	1,9	3,1	32	2,6	0,16	26
			6,2	138	16	4,6	0,20	18
			1,6	14	31	11,1	0,60	x
			1,9	7	32	6,4	0,77	26
$1x10^{1}$		extensive plastic						
(10)	3,162	deformation						
		ordinary bullet speeds						
$1x10^{3}$	31,622	hypervelocity impact						

x - Present Experiments.

TABLE 4.2 Dimensionless Parameters

Johnsons Damage Number (eqn. 4.1)	α	$\frac{\rho v^2}{\sigma_d}$ or $\frac{I^2}{A^2 t^2 \rho \sigma_d}$	
		Circular Geometry	Quadrangular Geometry
Geometry No. (eqn.4.3)	β	-	$\frac{L}{B}$
	$\mu = \alpha\beta$	$\frac{I^2}{A^2 t^2 \rho \sigma_d}$	$\frac{I^2}{B^2 L t^2 \rho \sigma_d}$
Geometrical Damage No. (eqn. 4.4)	$\phi = (\surd)^{\frac{1}{2}}$	$\frac{I}{At(\rho\sigma_d)^{\frac{1}{2}}}$	$\frac{I}{Bt(BL\rho\sigma_d)^{\frac{1}{2}}}$
Aspect No. (eqn. 4.5)	λ	$\frac{R}{t}$	$\frac{B}{t}$
Loading Paramater (eqn. 4.6)	ξ	$1 + \ell n(R/R_o)$	-
(eqns. 4.8)	$\phi = \psi\lambda\xi$	$\frac{I}{\pi R t^2 (\rho\sigma_d)^{\frac{1}{2}}}$	$\frac{I}{t^2 (BL\rho\sigma_d)^{\frac{1}{2}}}$
	$\phi_L = \psi\lambda\xi$	$\frac{I(1+\ell n\frac{R}{R_o})}{\pi R t^2 (\rho\sigma_d)^{\frac{1}{2}}}$	

TABLE 4.3 SUMMARY OF COMPARATIVE EXPERIMENTAL DATA

A. CIRCULAR PLATES

Sheet Explosive Blast	Diameter mm	Specimen Type	Static Yield Stress MPa	Plate Thickness mm	Deflection Thickness Ratio	Response Time μs
Florence & Werzbicki						
1966 [17]	100	Aluminium	290	6,3	1,6 - 7	
1970 [18]		Mild Steel	283	6,3	0,4 - 4	
Duffey & Key						
1967 [19]	150	Aluminium	280	1,6	4 - 9	
1968 [20]				3,2	1,5 - 1,7	
		Mild Steel	540	1,6	3 - 4	
Bodner & Symonds						
1979 [26]	64	Titanium	255	2,3	0,9 - 6	65-75
		Mild Steel	223	1,9	0,5 - 7	100-120
Nurick						
Present Work	100	Mild Steel	282	1,6	4 - 12	140-190
Inertial Forming Machine						
Ghosh et al	120	Lead	40,3	0,61	44	
1976 [27]		Aluminium	162	0,31	42	
1979 [30]						
1984 [29]						

TABLE 4.3 (continued)

B NON-CIRCULAR PLATES

Sheet Explosive Blast	Diameter mm	Specimen Type	Static Yield Stress MPa	Plate Thickness mm	Deflection Thickness Ratio	Response Time μs
Jones, Uran & Tekin 1970 [22]	129 x 76	Mild Steel	248	1,6	3,5 - 7,0	
			233	2,5	1 - 4,5	
			254	4,4	0,3 - 1,7	
		Aluminium	284	3,1	1,8 - 3,5	
			281	4,8	0,8 - 2,4	
			286	6,2	0,2 - 1,4	
Jones & Baeder 1972 [23]	128 x 32	Mild Steel	251	2,7	0,3 - 1,2	
		Aluminium	279	2,7	0,5 - 1,2	
	128 x 64	Mild Steel	251	2,7	0,8 - 4	
		Aluminium	279	2,7	1,2 - 3	
	128 x 96	Mild Steel	251	2,7	0,7 - 7,5	
		Aluminium	279	2,7	2,0 - 4,5	
	128 x 128	Mild Steel	251	2,7	1,6 - 9,5	
		Aluminium	279	2,7	3,0 - 6,0	
Nurick Present Work	113 x 70	Mild Steel	282	1,6	3 - 12	
	89 x 89	Mild Steel	296	1,6	6 - 12	90-180

TABLE 4.4 RESUME OF PREDICTED RESULTS FOR CIRCULAR PLATES

IMPULSE (Ns)		PREDICTED DEFLECTION (mm)	PREDICTED TIME (μs)	MODE SHAPE AT NODE POINTS					STRAIN - BETWEEN NODES				
				ϕ_0	ϕ_1	ϕ_2	ϕ_3	ϕ_4	$\bar{\phi}_0$	$\bar{\phi}_1$	$\bar{\phi}_2$	$\bar{\phi}_3$	$\bar{\phi}_4$
6	I	8.4	109	1	0.934	0.768	0.532	0.263	0.002	0.010	0.020	0.026	0.024
	II	9.1	118	1	0.950	0.805	0.578	0.301	0.026	0.021	0.018	0.009	0.005
8	I	11.0	109	1	0.934	0.767	0.530	0.261	0.003	0.017	0.034	0.044	0.041
	II	11.7	115	1	0.951	0.808	0.583	0.304	0.056	0.048	0.034	0.019	0.009
10	I	13.5	109	1	0.033	0.767	0.531	0.262	0.004	0.025	0.050	0.066	0.063
	II	14.3	113	1	0.952	0.811	0.588	0.307	0.083	0.072	0.052	0.029	0.014
12	I	15.9	106	1	0.934	0.768	0.532	0.263	0.006	0.035	0.070	0.092	0.087
	II	16.9	112	1	0.953	0.875	0.593	0.311	0.115	0.100	0.074	0.042	0.021
14	I	18.2	103	1	0.934	0.769	0.534	0.263	0.007	0.045	0.092	0.122	0.115
	II	19.5	111	1	0.954	0.817	0.595	0.311	0.151	0.133	0.100	0.058	0.029
14.6	I	119.0	103	1	0.934	0.770	0.535	0.264	0.008	0.049	0.100	0.133	0.126
	II	20.3	110	1	0.958	0.822	0.605	0.321	0.163	0.143	0.103	0.064	0.032

NOTE - I - lateral deflection excluded
II - lateral deflection included

TABLE 4.5 RESUME OF PREDICTED RESULTS FOR SQUARE PLATES

IMPULSE (Ns)		PREDICTED DEFLECTION (mm)	PREDICTED TIME (μs)	MODE SHAPE AT NODE POINTS					STRAIN - BETWEEN NODES				
				ϕ_0	ϕ_1	ϕ_2	ϕ_3	ϕ_4	$\bar{\phi}_0$	$\bar{\phi}_1$	$\bar{\phi}_2$	$\bar{\phi}_3$	$\bar{\phi}_4$
10	I	11.6	94	1	0.936	0.774	0.538	0.265	0.004	0.022	0.048	0.063	0.060
	II	12.3	97	1	0.952	0.810	0.587	0.306	0.076	0.066	0.048	0.027	0.014
12	I	13.5	91	1	0.936	0.774	0.538	0.265	0.005	0.030	0.064	0.086	0.081
	II	14.5	96	1	0.953	0.814	0.592	0.310	0.105	0.092	0.068	0.039	0.020
14	I	15.7	88	1	0.936	0.774	0.538	0.265	0.006	0.041	0.087	0.116	0.109
	II	16.7	95	1	0.954	0.817	0.597	0.314	0.138	0.121	0.091	0.054	0.028
16	I	17.7	88	1	0.936	0.774	0.538	0.265	0.008	0.052	0.110	0.147	0.139
	II	18.9	95	1	0.955	0.822	0.603	0.319	0.175	0.155	0.118	0.071	0.038
17.5	I	19.3	87	1	0.936	0.774	0.538	0.265	0.010	0.062	0.131	0.175	0.165
	II	20.6	94	1	0.957	0.827	0.613	0.327	0.206	0.183	0.141	0.086	0.046

NOTE - I - lateral deflection excluded
II - lateral deflection included

TABLE 4.6 RESUME OF PREDICTED RESULTS FOR RECTANGULAR PLATES

IMPULSE (Ns)		PREDICTED DEFLECTION (mm)	PREDICTED TIME (μs)	MODE SHAPE AT NODE POINTS					STRAIN - BETWEEN NODES				
				ϕ_0	ϕ_1	ϕ_2	ϕ_3	ϕ_4	$\bar{\phi}_0$	$\bar{\phi}_1$	$\bar{\phi}_2$	$\bar{\phi}_3$	$\bar{\phi}_4$
6	I	6.0	90	1	0.924	0.753	0.579	0.256	0.002	0.011	0.020	0.025	0.024
	II	6.4	92	1	0.940	0.783	0.558	0.289	0.036	0.023	0.014	0.007	0.003
8	I	7.8	88	1	0.924	0.753	0.579	0.256	0.004	0.018	0.034	0.043	0.041
	II	8.3	93	1	0.940	0.785	0.561	0.292	0.063	0.045	0.030	0.017	0.009
10	I	9.6	97	1	0.924	0.753	0.579	0.256	0.005	0.028	0.052	0.065	0.062
	II	10.1	92	1	0.940	0.788	0.565	0.295	0.092	0.068	0.045	0.026	0.014
12	I	11.3	86	1	0.924	0.753	0.579	0.256	0.008	0.038	0.071	0.090	0.085
	II	11.9	91	1	0.940	0.790	0.570	0.300	0.127	0.094	0.064	0.037	0.020
14	I	13.0	84	1	0.924	0.753	0.579	0.256	0.010	0.050	0.094	0.119	0.113
	II	13.7	90	1	0.942	0.795	0.575	0.305	0.168	0.125	0.085	0.051	0.027
16	I	14.6	83	1	0.924	0.753	0.579	0.256	0.013	0.064	0.119	0.150	0.143
	II	15.5	90	1	0.945	0.800	0.580	0.310	0.213	0.160	0.112	0.067	0.038
17.5	I	15.9	82	1	0.924	0.753	0.579	0.256	0.015	0.075	0.141	0.178	0.169
	II	16.9	89	1	0.946	0.804	0.586	0.310	0.250	0.189	0.134	0.082	0.047

NOTE - I - lateral deflection excluded
II - lateral deflection included

CHAPTER 5 - DISCUSSION AND CONCLUSION

5.1 OVERVIEW

This thesis presents two approaches for predicting the deflection of circular and quadrangular plates subjected to impulsive loading.

The first, a mode approximation technique presents an extension of previous work. This extension has three major components,

(i) the use of membrane mode analysis in which the mode shape is computed,

(ii) the inclusion of lateral displacements, and

(iii) this analysis predicts a solution which gives results supported by the experimental evidence in the range 4 - 12 plate thicknesses. Almost all previous predictions over estimate or underestimate the predictions in the range of 7 - 12 plate thicknesses. This is possibly due, in part, to the fact that previous experiments were limited to a maximum of approximately 8 plate thicknesses, the range in which some theoretical predictions showed comparable results with the experiments.

The second approach uses the experimental results in a dimensionless form, the analysis of which results in an empirical solution.

Each of these approaches will now be discussed.

5.2 THEORETICAL SOLUTION

The central permanent deflection predicted for the circular plate, as shown in Fig. 4.1, compares favourably with the experimental results, particularly at the higher deflection-thickness ratios, where the membrane effect is predominant. By comparison, the predictions of Lippman [56], Symonds and Wierzbicki[66] and Perrone and Bhadra [68], who tend to underestimate the deflection-thickness

ratio, and Duffey[19] and Guedes Soares[57], who overestimate the deflection-thickness ratio, are less accurate. These over- and underestimates are results of predictions which assume a mode shape which remained fixed throughout the motion.

The predicted deflections for the square plate shown in Fig. 4.2 also compare favourable with the experimental data. No other large deflection membrane mode approximation results are known to the author for quadrangular plates. However, Westine[70] presents a prediction, using energy equilibrium and a fixed mode shape, which overestimates the deflection, particularly at the higher deflection-thickness ratios.

Predictions for the rectangular plates show a slightly different trend from the experimental results, although the correlation is reasonably good. Whereas for the axisymmetric cases, (circular and square), the predictions are larger than the experimental results, for the rectangular plates the opposite is true. This is attributed to the choice of shape of the contours. For the axisymmetric cases the mid-point is coincident with $\phi_{..}$, whereas in the rectangular case the mid-point lies at the centre of the line $\phi_{..}$.

In all three cases the predictions which included lateral displacements show slightly larger transverse deflections than those which exclude lateral displacements. This may be attributed to the fact that, by introducing the assumption that the displacement, velocity and acceleration fields act at all times perpendicular to the plate surface, assumes that the element between nodes is also rotated, leading to larger displacements.

The mode shapes, shown in Figs. 4.8 - 4.10 again show the favourable comparison between predicted and experimental results, particularly for the axisymmetric cases.

A dimensionless plot shown in Fig. 4.4, illustrates that for plates of equal area and thickness, and similar material properties, the mid-point deflection of the circular plate exceeds that of the square plate, which in turn exceeds that of the rectangular plates, particularly at higher deflection-thickness ratios. This might be attributed to the distance from the plate mid-point to the nearest boundary. In this case, these distances are R = 50 mm (circular), B = 44.5 mm (square) and B = 35 mm (rectangular). This consideration was taken into account when adjusting Johnson's damage number for plates of varying geometry, thickness and material properties.

Hitherto, the discussion has illustrated that the predicted results compare favourably with the experiments, hence showing the advantage of including in the mode approximation an algorithm for computing the mode shape.

The inclusion of lateral displacements allow the final in-plane radial strain to be computed for each element. The results of this computation are plotted in Figs. 4.5 - 4.7 and show a trend that compares favourably with the experimental readings. Other attempts to predict this strain distribution, for example using the model described in this thesis but excluding the radial displacements, show a distribution which is inverted, ie the strain is small at the centre and large at the outer boundary, which is obviously in disagreement with the experimental evidence.

Figures 4.11 - 4.13 show plots of time to reach initial deflection vs impulse. In all cases the experimental data ranges between 100μs and 180μs.

5.3 EMPIRICAL SOLUTION

In the attempt to compare experimental results presented by different researchers using different plate dimensions and different plate materials, it became obvious that Johnson's damage number was a good guide, as shown in Fig. 4.14. However, this did not provide a suitable means for comparison, and hence an extension to Johnson's damage number was formulated. Figures 4.15 and 4.16 show plots of deflection-thickness ratio vs this new dimensionless number ϕ. Also shown in Figs. 4.15a and 4.16a are plots of predictions which do not consider strain rate effects, and therefore the predictions presented in this thesis and those of Symonds and Wierzbicki[66] are omitted. It will be noted that there are similarities between Fig. 4.15a and Fig. 4.1 and between Fig. 4.16a and Figs 4.2 and 4.3.

However, the important issue here is illustrated in Figs. 4.15b and 4.16b in which the experimental data results are bounded on either side of the least squares fit by a one deflection thickness ratio confidence limit. It can be seen that in both cases most of the data points lie within these bounds.

Figures 5.1 shows both the least squares fit and bounds of Figs. 4.15b and 4.16b, from which guidelines for a design code may be considered. The least squares analysis yields from the circular plate experimental data

$$\left[\delta/t\right]_c = 0.425\phi_c + 0.277 \qquad (5.1)$$

where the number of data points was 109 with a correlation coefficient of 0.974.

From the quadrangular plate experimental data, the analysis results are

$$\left[\delta/t\right]_q = 0.236\phi_q + 0.001 \qquad (5.2)$$

using 156 data points with a correlation coefficient of 0.984 and recalling that

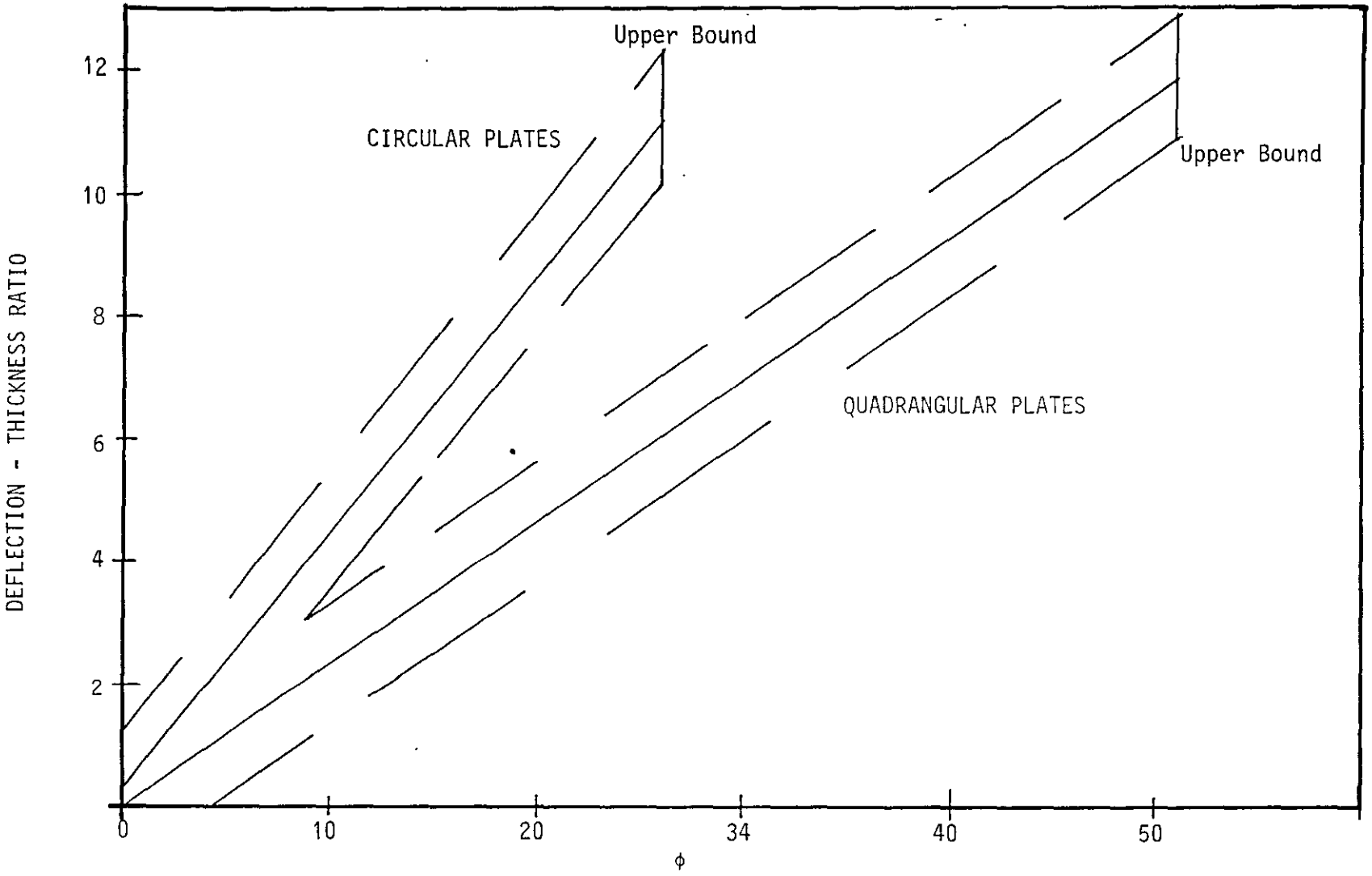

FIGURE 5.1 GRAPH OF DEFLECTION - THICKNESS RATIO vs $\phi_{c,q}$

$$\phi_c = I(1 + \varepsilon n\ (R/R_o)) / \pi R t^2 (\rho \sigma_o) \qquad (5.3a)$$

$$\phi_s = I / t^2 (BL \rho \sigma_o) \qquad (5.3b)$$

Hence it may now be possible to determine the deflection-thickness ratio of a circular or quadrangular plate subjected to an impulsive load, by using eqns. (5.1, 5.2), with the proviso that there is an upper limit to ϕ. Although this has not been investigated in detail, it is appropriate to recall that tearing occurred along the clamped boundary at values of $\phi_c = 26$ and $\phi_s = 51$ respectively. The maximum non-tearing deflection-thickness ratios recorded were 11,60 and 11,97 for circular and quadrangular plates respectively corresponding to values of $\phi_c = 26{,}6$ and $\phi_s = 50{,}7$. Hence these maximum non-shear deflection-thickness measurement values are close to the tearing conditions and could be considered as the ϕ upper bounds as shown in Fig. 5.1.

There appears to be some justification of eqns. (5.1) and (5.2). Consider two plates, one circular the other quadrangular, of equal area, thickness and material properties, subjected to an impulse over the entire plate area: then from eqns. (5.3)

$$\phi_c / \phi_s = 1 / (\pi)^{1/2} = 0{,}564 \qquad (5.4)$$

and substituting into eqn. (5.1)

$$[\delta / t] = 0{,}240\ \phi_s + 0{,}277 \qquad (5.5)$$

A comparison of eqns. (5.2) and (5.5) show similar gradients.

5.4 IN CLOSING

The instantaneous mode algorithms presented in this thesis, for rigid viscoplastic impulsively loaded fully clamped circular, square and rectangular plates, have been shown to provide deflection results which compare favourably with the experiments. In addition, the inclusion of the lateral displacement in the model results in the predicted lateral strain distribution to be in fair agreement with the measured distribution.

The measured contours give confidence that the series of contours assumed in the model are reasonably accurate, and also that the experimental method used to simulate uniform loading is satisfactory.

The experimental technique has been shown to be reproducible and consistent providing deflection-time histories while simultaneously measuring the impulse.

An analysis of all experimental results provides a useful design guideline for predicting maximum central deflections of impulsively loaded plates. An indication of when tearing might occur is also included.

REFERENCES

1 TAYLOR, G.I. 1950. The Distortion Under Pressure of a Diaphragm which is Clamped along its Edge and Stressed beyond its Elastic Limit. Underwater Explosion Research. Vol. 3. The Damage Process pp 107-121-.. Office of Naval Research (Originally Written 1942).

2 TRAVIS, F W and JOHNSON, W. 1961. Experiments in the Dynamic Deformation of Clamped Circular Sheets of Various Metals Subject to an Underwater Explosive Charge. Sheet Metal Industries, Vol. 39, pp 456-474.

3 JOHNSON, W., POYNTON, A., SINGH, H., and TRAVIS, F.W. 1966. Experiments in the Underwater Explosive Stretch Forming of Clamped Circular Blanks. Int. J. Mech. Sc., Vol. 8, pp 237-270.

4 JOHNSON, W., KORMI, K. and TRAVIS, F.W. 1966. An Investigation into the Explosive Deep Drawing of Circular Blanks using the Plug Cushion Technique. Int. J. Mech. Sci., Vol. 6, pp 293-328.

5 JOHNSON, W., KORMI, K. and TRAVIS, F.W. 1964. The Explosive Drawing of Square and Flat-bottomed Circular Cups and Bubble Pulsation Phenomena. Advances in Machine Tool Design Res., pp. 293-328.

6 MINSHALL, S. 1955. Properties of Elastic and Plastic Waves Determined by Pin Contactors and Crystals. J. Appl. Phys. Vol. 26 pp 463-469.

7 FINNIE, T.M. 1962. Explosive Forming of Circular Diaphragms. Sheet Metal Industries. Vol. 39 pp 391-398.

8 WILLIAMS, T. 1962. Some Metallurgical Aspects of Metal Forming. Sheet Metal Industries. Vol. 39 pp 487-494.

9 BOYD, D.E. 1966. Dynamic Deformation of Circular Membranes, ASCE Vol. 92 EM3 pp 1-15.

10 COLE, R.H. 1948. Underwater Explosions. Princeton University Press.

11 BEDNARSKI, T. 1969. The Dynamic Deformation of a Circular Membrane. Int.J.Mech.Sci. Vol. 11 pp 949-959.

12 WITMER, E.A., BALMER, N.A., LEECH, J.W., PIAN, T.N.N., 1963. Large Dynamic Deformations of Beam, Rings, Plates and Shells. AIAA, Vol. 1., pp 1848-1857.

13 HOFFMAN, A.J. 1955. The Plastic Response of Circular Plates to Air Blast. Masters Thesis, University of Delaware.

14 HUMPHREYS, J.S., 1965. Plastic Deformation of Impulsively loaded Straight Clamped Beams. J.Appl.Mech. Vol 32 pp 7-10.

15 JOHNSON, W. 1972. Impact Strength of Materials. Edward Arnold.

16 FLORENCE, A.L., FIRTH, R.D. 1965. Rigid-Plastic Beams Under Uniformly Distributed Impulses. J.Appl.Mech. Vol 32 pp 481-488.

17 FLORENCE, A.L. 1966. Circular Plates Under a Uniformly Distributed Impulse. Int.J.Solids Structures Vol.2. pp 37-47.

18 WIERZBICKI, T., FLORENCE, A.L. 1970. A Theoretical and Experimental Investigation of Impulsively Loaded Clamped Circular Viscoplastic Plates. Int.J. Solids Structures. Vol. 6, pp 555-568.

19 DUFFEY, T.A. 1967. The Large Deflection Dynamic Response of Clamped Circular Plates Subjects to Explosive Loading. Sandia Laboratories Research Report No. SC-RR-67-532.

20 DUFFEY, T.A., KEY, S.W. 1968. Experimental - Theoretical Correlation of Impulsively Loaded Clamped Circular Plates. Research Report. Sandia Laboratories SC-RR-68-210.

21 JONES, N., GRIFFIN, R.N., VAN DUZER, R.E. 1971. An Experimental Study into the Dynamic Plastic Behaviour of Wide Beams and Rectangular Plates. Int.J.Mech.Sci. Vol. 13, pp 721-735.

22 JONES, N., URAN, T., TEKIN, S.A. 1970. The Dynamic Plastic Behaviour of Fully Clamped Rectangular Plates. Int.J.Solids Structures. Vol. 6, pp 1499-1512.

23 JONES, N., BAEDER, R.A., 1972. An Experimental Study of the Dynamic Plastic Behaviour of Rectangular Plates. Symposium on Plastic Analysis of Structures. Rumania.

24 SYMONDS, P.S., JONES, N. 1972. Impulsively Loading of Fully Clamped Beams with Finite Plastic Deflections and Strain-Rate Sensitivity. Int.J.Mech.Sci. Vol. 14 pp 49-69.

25 BODNER, S.R., SYMONDS, P.S., 1979. Experiments on Dynamic Plastic Loading of Frames. Int.J.Solids Structures. Vol. 15, pp 1-13.

26 BODNER, S.R., SYMONDS, P.S., 1979. Experiments on Viscoplastic Response of Circular Plates to Impulsive Loading. J.Mech.Phys.Solids. Vol.27, pp 91-113

27 GHOSH, S.K., WEBER, H. 1976. Experimental - Theoretical Correlation of Impulsively Loaded Axisymmetric Rigid-plastic Membrane. Mech.Res. Comm., Vol. 3, pp 423-428.

28 GHOSH, S.K., BALENDRA, R., TRAVIS, F.W. 1978. Inertial Forming of Circular and Annular Diaphragms. Advances in Machine Tool Design Res., pp. 845-854.

29 GHOSH, S.K., REID, S.R., JOHNSON, W. 1984. The Large Deflection Impulsive Loading of Clamped Circular Membranes. Structural Impact and Cashworthiness Conf. London. pp 471-481.

30 GHOSH, S.K. and TRAVIS, F.W. 1979. A Unique Experimental High Rate Forming Machine. Int.J.Mech. Eng. Educ., Vol. 7, pp 69-74.

31 BODNER, S.R. 1982. Private Communications.

32 JONES, N. 1968. Impulsive Loading of a Simply Supported Circular Rigid Plastic Plate. Trans. ASME. J: App.Mech. pp 59-65.

33 HUDSON, G.E. 1951. A Theory of the Dynamic Plastic Deformation of a Thin Diaphragm. J.Appl.Phys., Vol. 22, pp 1-11.

34 RICHARDSON, J.M., KIRKWOOD, J.G. 1950. Theory of The Plastic Deformation of Thin Plates by Underwater Explosions. Underwater Explosion Research, Office of Naval Research, Vol. 3, The Damage Process pp. 305-421.

35 FREDERICK, D. 1959. A Simplified Analysis of Circular Membranes Subjected to an Impulsive Loading Producing Large Plastic Deformations. Proc. 4th Annual Conf. on Solid Mechanics. University of Texas. pp 18-35.

36 GRIFFITH, J., VANZANT, H. 1961. Large Deformation of Circular Membranes Under Static and Dynamic Loading. 1st Intl. Cong. on Experimental Mechanics. Paper NO. 702.

37 HOPKINS, H.G., PRAGER, W. 1954. On the Dynamics of Plastic Circular Plates. ZAMP (J. of App.Math and Phs.) Vol. 5, No. 4 pp 317-330.

38 FLORENCE, A.L. 1966. Clamped Circular Rigid-Plastic Plates Under Central Blast Loading. Int. J. of Solids and Structures. Vol. 2, pp 319-335.

39 WANG, A.J. and HOPKINS, H.G. 1954. The Plastic Deformation of Built-in Circular Plates Under Impulsive Load. J. Mech. Phys. Solids, Vol. 3, pp 22-37.

40 WANG, A.J. 1955. The Permanent Deflection of a Plastic Plate Under Bast Loading. J. Appl. Mech., Vol. 22, pp 375-376.

41 PERZYNA, P. 1958. Dynamic Load Carrying Capacity of a Circular Plate. Arch.Mech.Stos. Vol. 10, No. 5, pp 635-647.

42 SANKARANARAYANAN, R. 1966. On the Impact Pressure Loading of a Plastic Spherical Cap. J. of Appl. Mech. Vol. 33, NO. 3. Trans. ASME Vol. 88, Series E, pp 704-706.

43 SYMONDS, P.S. 1953. Dynamic Load Characteristics in Plastic Bending of Beams. J. of Appl. Mech. Vol. 20. Trans ASME Vol. 75, No. 4, pp 475-481.

44 HOPKINS, H.G. 1957. On the Plastic Theory of Plates. Proc., Royal Society, Ldn, Series A. Vol. 241, pp 153-179.

45 SHAPIRO, G.S., 1959. On a Rigid-Plastic Annular Plate Under Impulsive Loading. J. of Appl. Mathematics and Mechanics. (Pnk. Mat. i Mek) Vol. 23 pp 234 - 241

46 FLORENCE, A.L. 1965. Annular Plate Under a Transverse Line Impulse. American Institute of Aeronautics and Astronautics Journal. Vol. 3, No. 9, pp 1726-1732.

47 BOYD, D.E. 1966. Dynamic Deformation of Circular Membranes. AXE, Vol. 92, EM3, pp 1-15.

48 MUNDAY, G., NEWITT, D.M. 1963. The Deformation of Transversely Loaded Disks Under Dynamics Loads. Phil. Trans. of the Royal Soc. Ldn. No. 1065, Vol. 256, pp 1-30.

49 MARTIN, J.B., SYMONDS, P.S. 1966. Mode Approximations for Impulsively Loaded Rigid-Plastic Structures. Proc. ASCE. Vol. 92, No. EM5, pp 43-66.

50 COOPER, R.M., SHIFRIN, G.A. 1954. An Experiment on Circular Plates in the Plastic Range. Proc. of the 2nd U.S. National Cong. of Appl. Mech. pp 527-534.

51 HAYTHORNTHWAITE, R.M., ONAT, E.T. 1955. The Load Carrying Capacity of Initially Flat Circular Steel Plates Under Reversed Loading. J. of the Aer.Sci. Vol. 22, No. 12, pp 867-869.

52 HOPKINS, H.G., PRAGER, W. 1953. The Load Carrying Capacity of Circular Plates. J. of the Mech. and Phys. of Solids. Vol. 2, No. 1, pp 1-13.

53 ONAT, E.T., HAYTHORNTHWAITE, R.M. 1956. The Load Carrying Capacity of Circular Plates at Large Deflection. J. of Appl. Mech. Vol. 23, Trans. ASME, Vol. 78, pp 49-55.

54 NOBLE, CF., OXLEY, P.L.B. 1965. Estimating the Charge Size in Explosive Forming of Sheet Metal. Advances in Machine Tool Design Research. pp 329-337.

55 BATRA, R.C., DUBEY, R.N. 1971. Impulsively Loaded Circular Plates. Int. J. Solids Structures. Vol.7 pp 965-978.

56 LIPPMAN, H. 1974. Kinetics of the Axisymmetric Rigid Plastic Membrane Supplied to Initial Impact. Int. J. Mech. Sci., Vol. 16, pp 297-303 and pp 945-947.

57 GUEDES SOARES, C. 1981. A Mode Solution for the Finite Deflections of a Circular Plate Loaded Impulsively. Rozprawy Inzynierskie Eng. Trans., Vol. 29, pp 99-114.

58 LEE, E.H., SYMONDS, P.S. 1952. Large Plastic Deformations of Beams Under Transverse Impact. J. Appl. Mech. Vol. 19, pp 308-

59 MARTIN, J.B. 1964. Impulsive Loading Theorems of Rigid-Plastic Continua. J.Eng. Mech. Div, ASCE. Vol. 90, pp 27-

60 SYMONDS, P.S., CHON, C.T. 1974. Approximation Techniques for Impulsive Loading Structures of Time Dependent Plastic Behaviour with Finite Deflections. Mechanical Properties of Materials at High Strain Rates. (J. Harding Ed) Inst. of Physics, pp 299-

61 CHON, C.T., SYMONDS, P.S. 1977. Large Dynamic Plastic Deflections of Plates by mode method. Proc. ASCE J. Eng. Mech. Div., Vol. 103 (EM1), pp 169-187.

62 SYMONDS, P.S., CHON, C.T. 1979. Finite Viscoplastic Deflection of an Impulsively Loaded Plate by the Mode Approximation Technique. J. Mech. Phys. Solids, Vol. 27, pp 115-133.

63 JONES, N. 1971. A Theoretical Study of the Dynamic Plastic Behaviour of Beams and Plates with Finite Deflections. Int. J. Sol. Struct. Vol. 7, pp 1007-1029.

64 WIERZBICKI, T. 1970. A Method of Approximation in the Large Deflection Analysis of Impulsively Loaded Rigid-Plastic Structures. Act. Tech. Acad. Sci. Hung. Vol. 68, pp 403-

65 KALISZKY, S. 1973. Large Deformations of Rigid-Viscoplastic STructures Under Impulsive and Pressure Loading. J. Struct. Mech. Vol. 1, pp 295-317.

66 SYMONDS, P.S., WIERZBICKI, T. 1979. Membrane Mode Solution for Impulsively Loaded Circular Plates. J. Appl. Mech., Vol. 46, pp 58-64.

67 PERRONE, N., BHADRA, P. 1979. A Simplified Method to Account for Plastic Rate Sensitivity with Large Deformations. J. Appl. Mech., Vol. 46, pp 811-816.

68 PERRONE, N., BHADRA, P. 1984. Simplified Large Deflection Mode Solutions for Impulsively Loaded Viscoplastic Circular Membranes. J. Appl. Mech., Vol. 51, pp 505-509.

69 WESTINE, P.S., BAKER, W.E. 1974. Energy Solutions for Predicting Deformation in Blast Loaded Structures. Proc. 16th Explosive Safety Seminar, Hollywood Beach, Florida, U.S.A., pp 849-878.

70 BAKER, W.E. 1975. Approximate Techniques For Plastic Deformation of Structures Under Impulsive Loading. Shock and Vibration Digest. Vol. 7, No. 7, pp 107-117.

71 CALLADINE, C. 1984. Private Discussions

72 JOHNSON, W. 1967. Experiments and Efficiency Considerations in High Rate Forming. Australasian Inst. of Metals. Vol. 12 No. 2 pp 139-154.

73 GAMBY, D., LAMPI, L.H. 1984. An Approximate Numerical Method for Circular Membranes under Lateral Pressure. J. of Strain Analysis, Vol. 19, pp 261-267.

74 MANJOINE, M.J. 1944. Influence of Rate of Strain and Temperature on Yield Stress of Mild Steel. J.Appl.Mech. pp 211 - 218.

75 NURICK, G.N., HAMILTON, R.S. and PENNINGTON, D. 1986. A Simple Method to Predit the Intitial and Subsequent Deflections of a Clamped Circular Plate Subjected to Repeated Impacts. Proc. of Soc. of Experimental Mechanics Spring Conf. on Experimental Mechanics, New Orleans, USA.

FURTHER READING.

1 SYMONDS, P.S. 1967. Survey of Methods of Analysis for Plastic Deformation of Structures Under Dynamic Loading. Division of Engineering, Brown University, Providence, Rhode Island.

2 JONES, N. 1975. A Literature Review of the Dynamic Plastic Response of Structures. The Shock and Vibration Digest. Vol. 13. No. 10, pp 3-16.

3 JONES, N. 1978. Recent Progress in the Dynamic Plastic Behaviour of Structures. Part 1. The Shock and Vibration Digest. Vol. 10, No. 9, pp 21-33.

4 JONES, N. 1978. Recent Progress in the Dynamic Plastic Behaviour of Structures. Part II. The Shock and Vibration Digest. Vol.10, No. 10, pp 13-19.

5 JONES, N. 1981. Recent Progress in the Dynamic Plastic Behaviour of Structures. Part III. The Shock and Vibration Digest. Vol. 13, No. 10, pp 3-16.

PAPERS PUBLISHED

1. NURICK, G.N. and MARTIN, J.B. 1984. "The Measurements of the Response to Clamped Circular Plates to Impulsive Loading". Mechanical Properties at High Rates of Strain. (Ed. J. Harding) Publ. by Inst. of Physics, pp 495-502.

2. NURICK, G.N. 1985. "A New Technique to Measure the Deflection-Time History of a Material Subjected to High Strain Rates". Int. J. Impact Engng. 3(1) pp 17-26.

3. NURICK, G.N., PEARCE, H.T. and MARTIN, J.B. 1986. "The Deformation of Thin Plates Subjected to Impulsive Loading". Inelastic Behaviour of Plates and Shells. (Ed. L. Bevilacqua). Springer Verlag, pp

4. NURICK, G.N. 1986. "The Measurement of the Deformation Response of a Structure Subjected to an Explosive Load Using a Light Interference Technique". Proc. 1986 SEM Spring Conf. on Experimental Mechanics. Published by the Society for Experimental mechanics. pp 105-114.

5. NURICK, G.N. 1986 "Using Photo-Voltaic Diodes to Measure the Deformation Response of a Structure Subjected to an Explosive Load". Proc. 17th Int. Cong. on High Speed Photography and Photonics. Published for SPIE - The Int. Soc. for Optical Engineering. pp 215-226.

6. NURICK, G.N., PEARCE, H.T. and MARTIN, J.B. 1987. "Predictions of Transverse Deflections and In-Plane Strains in Impulsively Loaded Thin Plates". Int. J. of Mech. Sci. Vol. 29. No. 6, pp 435-442.

A.1 - Resume of Approximate Methods for Predicting Deformation of Thin Plates Subjected to Uniform Impulsive Loading.

	Mid-Point Deflected Prediction	Dimensionless Form (See Chapter 4) Deflection-Thickness Ratio	Comments (Refer to footnote)
A. Circular Plates			4a:
Hudson [33] 1951	$\frac{0.318I}{tR(\rho\sigma_o)^{1/2}}$	$t\phi$	1a: 2a: 3a:
Wang and Hopkins[39] 1954	$\frac{0.028I^2}{t^3R^2\rho\sigma_o}$	$0.277\phi^2$	1b: 2a: 3a:
Wang [40] 1955	$\frac{0.051\ I^2}{t^3R^2\rho\sigma_o}$	$0.505\phi^2$	1c: 2a: 3a:
Noble and Oxley[54] 1955	$R\left[\left[\frac{0.101I^2}{r^2R^4\rho\sigma_o} + 1\right]^2 - 1\right]^{1/2}$	$\lambda\left[\left[\frac{\phi^2}{\lambda^2} + 1\right]^2 - 1\right]^{1/2}$	1a: 2a: 3b - Conical Profile:
	$\frac{0.080I}{tR(\rho\sigma_o)}$	0.252ϕ	1a: 2a: 3b - Circular Profile:
Duffey[19] 1967	$\frac{0.242I(1 - \nu+\nu^2)^{1/4}}{tR(\rho\sigma_o)^{1/2}}$	$0.761\phi(1 - \nu + \nu^2)^{1/4}$	1a: 2a: 3b - Various Profiles:
Johnson[72] 1967	$R(e^{\epsilon_o} - 1)^{1/2}$ $\frac{2}{3}\epsilon_o\left[2 + \frac{P}{\sigma_o}\epsilon_o\right] = \frac{0.101I^2}{t^2R^4\rho\sigma_o}$	$\frac{2}{3}\epsilon_o\left[2 + \frac{P}{\sigma_o}\epsilon_o\right] = \left[\frac{\phi}{\lambda}\right]^2$	1a: 2a: 3a:
Wierzbicki and Florence[18] 1970	$\frac{0.027\ I^2}{t^2R^2\rho\sigma_o}$	$0.267\phi^2$	1a: 2a: 3a: Small Deflections (bending)
	$\frac{0.055\ I}{(t^3R\rho\sigma_o)^{1/2}}$	$0.173\phi\lambda^2$	1a: 2a: 3a: Large Deflections (bending and membrane)

Batra and Dubey[55] 1972	$\frac{0.382\ I}{tR(\theta\sigma_o)^{1/2}}$	1.201ϕ	1a: 2a - not in this form: 3a
Westine and Baker [70] 1974	$\left[\frac{0.082I^4}{t^2R^4\rho\sigma} + 0.101t^4\right]^{1/4} - 0.637t$	$(0.811\phi^4 + 0.101)^{1/4} - 0.637$	1a: 2b: 3b:
Lipman[56] 1974	$\frac{0.132I}{tR(\rho\sigma_o)^{1/2}}$	0.415ϕ	1a: 2a: 3b - sinusoidal
Ghosh and Weber [27] 1976	$\frac{0.392I}{tR(\rho\sigma_o)^{1/2}}$	1.233ϕ	1a: 2a - not in this form: 3b:
Symonds and Wierzbicki [66] 1979	$\frac{0.212I}{tR(\rho\sigma_o)^{1/2}}$		1a: 2c: 3b - fixed mode:
Guedes Soares[57] 1981	$\left[\frac{0.068I^2}{t^2R^2\rho\sigma_o} + 1^2\right]^{1/2} - t$	$(0.673\phi^2 + 1)^{1/2} - 1$	1a: 2a: 3b:
Calladine [71] 1984	$\frac{0.225I}{tR(\rho\sigma_o)^{1/2}}$	0.708ϕ	1a: 2a: 3b - circular:
Perrone and Bhadra [68] 1984	$\frac{0.117I}{tR(\rho\sigma_o)^{1/2}}$	0.368ϕ	1a: 2c: 3a:
Experimental Evidence	$\frac{0.135I}{Rt(\rho\sigma_o)^{1/2}}$	0.425ϕ	1a: -: -:

B. QUADRANGULAR PLATES

			4b:
Jones et al[22] 1970	$\frac{0.331^2}{t^3 L^2 \rho\sigma_o}\left[\left(3+\frac{\beta^2}{2}\right)^{1/2}-\frac{\beta}{L}\right]^2$	$0.333\frac{\phi^2}{\beta}\left[\left(3+\frac{1^2}{\beta^2}\right)^{1/2}-\frac{1}{\beta}\right]^2$	1a: 2a: 3a:
Baker [70] 1975	$\left[\frac{0.077I^2}{r^2 L^2 \rho\sigma_o}+0.177t^2\right]^{1/2}-0.421t$	$\left[\frac{0.077\phi^2}{\beta}+0.177\right]^{1/2}-0.421$	1a: 2b: 3a: $5-\beta = 1$
	$\left[\frac{0.121I^2}{r^2 L^2 \rho\sigma_o}+0.189t^2\right]^{1/2}-0.435t$	$\left[\frac{0.121\phi^2}{\beta}+0.189\right]^{1/2}-0.435$	1a: 2b: 3a: $5-\beta = 1.616$
Experimental	$\frac{0.235I}{t(BL\rho\sigma_o)^{1/2}}$	0.235ϕ	1a: -: -:

NOTES:

1. Boundary Condition
   (a) Clamped
   (b) Built-in
   (c) Simply Supported.

2. Strain Rate Effects Considered
   (a) No
   (b) Yes
   (c) $\sigma = \sigma_o\left[1+\left(\dot{\epsilon}/\epsilon_o\right)^{1/n}\right]$

3. Assumed Deformed Shape
   (a) No
   (b) Yes

4. Dimensionless Form
   (a) Circular $\phi = \frac{0.318I}{Rt^2(\rho\sigma_o)^{1/2}}$; $\lambda = \frac{R}{t}$
   (b) Quadrangular $\phi = \frac{I}{t^2(BL\rho\sigma_o)^{1/2}}$; $\beta = \frac{L}{B}$; $\lambda = \frac{\beta}{t}$

5. Ratio as used for experiments in this thesis.

6. Notation
   I = Total Impulse; ρ = material density; ν = Poissons Ratio; R = plate radius;
   B = Plate Breadth; L = plate length; t = plate thickness; σ_o = static yield stress;
   σ = dynamic yield stress.

APPENDIX A.2

Eqn (3.2) in full form is written as

$$\dot{\epsilon}_i = \frac{(\phi_i u_o - \phi_{i+1} u_o)(\phi_i \dot{u}_o - \phi_{i+1} \dot{u}_o) + [L + \phi_{i+1} u_o \, Tan(\frac{\theta_{i-1}+\theta_{i+1}}{2}) - \phi_i u_o \, Tan(\frac{\theta_{i-1}+\theta_i}{2}) * [\phi_{i+1} \, u_o \, Tan\frac{\theta_i+\theta_{i+1}}{2}) - \theta_i u_o Tan\frac{\theta_{i-1}+\theta_i}{2})]}{L^2}$$

$$= \frac{u_o \dot{u}_o (\theta_i - \theta_{i+1})^2 + [L + u_o \theta_{i+1} C_{i+1} - u_o \theta_i \; C_i] \; [\theta_{i+1} \; C_{i+1} - \theta_i \; C_i] \; \dot{u}_o}{L^2}$$

$$= \frac{u_o^t \dot{u}_o^t (\theta_i^t - \theta_{i+1}^t)^2 + [L + (\theta_{i+1}^t C_{i+1}^t - \theta_i^t C_i^t) u_o^t] [\theta_{i+1}^t C_{i+1}^t - \theta_i^t C_i^t] \dot{u}_o^t}{L^2}$$

$$= \frac{u_o^t \dot{u}_o^t (\theta_i^t - \theta_{i+1}^t)^2 + [L + (\theta_{i+1}^t C_{i+1}^t - \theta_i^t C_i^t) \dot{u}_o^t \Delta t] [\theta_{i+1}^t C_{i+1}^t - \theta_i^t C_i^t] \dot{u}_o^t}{L^2} \qquad (A.2.1)$$

Substituting eqn (A.2.1) into eqn (3.21) and hence into eqns (3.24) and (3.25) yields:

$$\lambda m_i \phi_i u_o + \sigma_o h \left[1 + \frac{u_o^t \dot{u}_o^t (\phi_i^t - \phi_{i+1}^t)^2 + [L + (\phi_{i+1}^t C_{i+1}^t - \phi_i^t C_i^t) \dot{u}_o^t \Delta t] [\phi_{i+1}^t C_{i+1}^t - \phi_i^t C_i^t] \dot{u}_o^t}{L^2 \; \dot{\epsilon}_o} \right]^{1/n} \frac{u_o (\phi_i - \phi_{i+1})}{[u_o^2 (\phi_i - \phi_{i+1})^2 + L^2]^{1/2}}$$

$$- \sigma_o h \left[1 + \frac{u_o^t \dot{u}_o^t (\phi_{i+1}^t - \phi_{i+2}^t)^2 + [L + (\phi_{i+2}^t C_{i+2}^t - \phi_{i+1}^t C_{i+1}^t) \dot{u}_o^t \Delta] [\phi_{i+2}^t C_{i+2}^t - \phi_{i+1}^t C_{i+1}^t] u_o^t}{L^2 \; \dot{\epsilon}_o} \right]^{1/n} \frac{u_o (\phi_{i+1} - \phi_{i+2})}{[u_o^2 (\phi_{i+1} - \phi_{i+2})^2 + L^2]^{1/2}} = 0 \qquad (A.2.2)$$

and

$$\lambda m_o \dot{u}_o - 2\sigma_o h \left[1 + \frac{u_o^t \dot{u}_o^t (1 - \phi_{i+1})^2 + [L + (\phi_{i+1}^t C_{i+1}^t - 1.0) \dot{u}_o^t \Delta t] [\phi_{i+1}^t C_{i+1}^t - 1.0] \dot{u}^t}{L^2 \; \dot{\epsilon}_o} \right]^{1/n} \frac{u_o (1 - \phi_{i+1})}{[u_o^2 (1 - \phi_{i+1})^2 + L^2]^{1/2}} = 0 \qquad (A.2.3)$$

```
100.            PROGRAM PLATE
110.
120.      C*****     A PRGRAM FOR THE DYNAMIC ANALYSIS OF
130.      C          RIGID VISCO PLASTIC PLATES
140.      C*****
150.
160.            IMPLICIT DOUBLE PRECISION*8(A-H,O-Z)
170.            INCLUDE R.VISCO,LIST
110.I           COMMON/VIS/ NPOIN,DIAM,ELENG,THICK,ENEXP,EPSOD,
120.I          &            YIELD,DENCT,TOL,JTYPE,NTIME,DT,DST,
130.I          &            EMPUL,NITER,NNODS,ITWON,SLAMDA,WIDTH,CENTR
170.I           PARAMETER PI = 3.141592654
175.I           PARAMETER NDIM = 20
180.            INCLUDE R.VIBRA,LIST
220.I           COMMON/VIB/ AMASS(20),AJACOB(20,20),BJACOB(20,20),
230.I          &            AB(20,40),RAD(20),FUNC(20),FNEW(20)
190.            COMMON/ONE/ XT(21), UT, VT
200.            DIMENSION PHIT(21),PHIDT(21),ERATE(11)
210.
220.
230.      C*****     READ THE USER DEFINED INPUT
240.
250.            CALL INPUT
260.
270.      C*****     COMPUTE THE NECESSARY PARAMETERS FROM THE INPUT
280.      C          SUCH AS THE ELEMENT LENGTH AND NODAL MASS
290.
300.            CALL SETVAR
310.
320.      C*****             PRINT THE INPUT FOR CHECKING BY USER
330.
340.            CALL DATAPR
350.
360.      C*****             AN INITIAL DISPLACEMENT IS REQUIRED TO COMPUTE
370.      C                  THE MULTIPLIER AND MODE SHAPES AT TIME ZERO
380.      C
390.      C     KFLAG = 0
400.      C
410.            PHIT(NNODS) = 0.
420.            PHIDT(NNODS) = 0.
430.            IF(JTYPE .EQ. 1) THEN
440.               AGEOM = PI*DIAM*DIAM/4.DO
450.            ELSE IF(JTYPE . EQ. 2) THEN
460.               AGEOM = DIAM*DIAM
470.            ELSE
480.               AGEOM = DIAM*DIAM + DIAM*CENTR
490.            ENDIF
500.            VINIT = EMPUL/(AGEOM*THICK*DENCT)
510.      C
520.      C*****     ASSUME A CONICAL STARTING MODE
530.      C
540.            PHIT(1) = SLAMDA
550.            DO 30 IPOIN = 2,NPOIN
560.            PHIT(IPOIN) = (NPOIN - IPOIN + 1.DO)/NPOIN
570.         30 CONTINUE
580.      C
590.      C          GENERALIZED MOMENTUM BALANCE
600.      C
610.            SUMU = 0.
620.            SUML = 0.
630.            SUMU = SUMU + AMASS(1)
640.            SUML = SUML + AMASS(1)
650.      C
660.      DO 40 IPOIN = 2,NPOIN
670.            SUMU = SUMU + AMASS(IPOIN)*PHIT(IPOIN)
```

```
      SUML = SUML + AMASS(IPOIN)*PHIT(IPOIN)*PHIT(IPOIN)
   40 CONTINUE
C
      VINIT = VINIT*SUMU/SUML
      PRINT*,'    INITIAL VELOCITY = ', VINIT
      DINIT = VINIT*DST
C
C
C
C
C*****     SOLVE THE EQUILIBRIUM EQUATIONS FOR TIME ZERO
C          TO OBTAIN THE MULTIPLIER AND THUS THE ACCELERATION
C          AT TIME ZERO

      T = DST
      WRITE(6,150) T,DINIT,VINIT
C
C
      NPC = NPOIN + 1
      DO 44 KM = 1,NPO
      XT(KM) = 0.DO
   44 CONTINUE
      UT = 0.DO
      VT = 0.DO

      CALL SOLVE(DINIT,VINIT,PHIT,PHIDT)

      RAMDA = PHIDT(1)
      DISPL = DINIT
      VELOC = VINIT
      ACCEL = -RAMDA * VELOC
      ACCIT = ACCEL
      VELIT = VELOC
      DISIT = DISPL
C*****     LOOP FOR NTIME TIME INCREMENTS OR UNTIL THE
C          VELOCITY HAS BECOME ZERO

      DO 70 JTIME = 1,NTIME
C
C
      DO 45 JN = 2,NPOIN
      XT(JN) = PHIT(JN)
   45 CONTINUE
      XT(1) = 1.DO
      UT = DISPL
      VT = VELOC

C*****     INNTER LOOP FOR THE IMPLICIT TIME INTEGRATION

      CO 50 ITER = 1,NITER

C*****     STEP ALONG IN TIME BY AN AMOUNT DT
C          THIS IS AN IMPLICIT SCHEME FO RWHICH AN ITERATION IS
C          REQUIRED, DURING WHICH THE EQUILIBRIUM EQUATIONS
C          ARE SOLVED

      UVELO = VELOC + 0.5*DT*(ACCEL + ACCIT)
      UDISP = DISPL + 0.5*DT*(VELOC + VELIT)
C

C*****     A CHECK IS MADE FOR THE CONVERGENCE OF THE SCHEME
      CALL SOLVE(UDISP,UVELO,PHIT,PHIDT)
```

```
2     1300.
2     1310.            DIF = (UDISP - DISIT)/UDISP
2     1320.            IF(DABS(DIF) .LE. TCL) GOTO 60
2     1330.
2     1340.      C*****     SOLVE AND OBTAIN THE ACCELERATION IN THE
2     1350.      C          NEXT ITERATION
2     1360.
2     1370.
2     1380.            RAMDA = PHIDT(1)
2     1390.            ACCIT = -RAMDA*UVELO
2     1400.            VELIT = UVELO
2     1410.            DISIT = UDISP
2     1420.         50 CONTINUE
2     1430.      C          COMPUTE STRAIN RATE FOR EACH TIMESTEP
2     1440.      C
1     1450.         60 AST = UDISP*UVELO*((1.DO - PHIDT(2))**2.)
1     1460.            CAST = DT*VT*(XT(2)*CTFUN(2) - XT(1)*CTFUN(1))
1     1470.            CBST = PHIDT(2)*CTFUN(2) - 1.DO*CTFUN(1)
1     1480.            EST = ELENG*ELENG
1     1490.            ERATE(1) = (AST + (ELENG + CAST)*CBST*UVELO)/EST
1     1500.      C
1     1510.            DO 55 I = 2,NPOIN
2     1520.            J = I + 1
2     1530.            AST = UDISP*UVELO*((PHIDT(I) - PHIDT(J))**2.)
2     1540.            CAST = DT*VT*(XT(J)*CTFUN(J) - XT(I)*CTFUN(I))
2     1550.            CBST = PHIDT(J)*CTFUN(J) - PHIDT(I)*CTFUN(I)
2     1560.            ERATE(I) = (AST + (ELENG + CAST)*CBST*UVELO)/EST
2     1570.         55 CONTINUE
2     1580.      C
1     1590.            WRITE(17,100) DT,(ERATE(IJ),IJ = 1,NPOIN)
1     1600.        100 FORMAT(8E10.4)
1     1610.      C
1     1620.      C
1     1630.            IF (UVELO .LE. 0.1D0) GOTO 125
1     1640.            DTEND = UVELO*DT/(VELOC - UVELO)
1     1650.            IF(DTEND .LT. DT) THEN
2     1660.               DT = DTEND
2     1670.      C        KFLAG = 1
2     1680.            ENDIF
2     1690.
1     1700.            VELOC = UVELO
1     1710.            DISPL = UDISP
1     1720.            ACCEL = -PHIDT(1)*UVELO
1     1730.      C
1     1740.            T = T + DT
1     1750.            WRITE(6,150) T,DISPL,VELOC
1     1760.
1     1770.         70 CONTINUE
      1780.        125 CONTINUE
      1790.            VELOC = UVELO
      1800.            DISPL = UDISP
      1810.            PRINT*,' PHIDT = ',(PHIDT(IC),IC=1,NPOIN)
      1820.            T = T + DT
      1830.            WRITE(6,150) T,DISPL,VELOC
      1840.
      1850.        150 FORMAT(/5X,' TIME = ',E12.6,/15X,'DISPL = ',E12.6,
      1860.           &/15X,'VELOC = ',E12.6)
      1870.
      1880.            STOP
      1890.            END

END FTN 439 IBANK 320 DBANK 3440 COMMON
```

```
@FTN,S R.INPUT
FTN 11R1A     10/22/86-09:25(0,)
       100.            SUBROUTINE INPUT
       110.
       120.      C*****     READ THE USER DATA FROM FILE 5 IE. ATTACH DATA
       130.
       140.            IMPLICIT DOUBLE PRECISION*8(A-H,O-Z)
       150.            INCLUDE R.VISCO,LIST
       110.I           COMMON/VIS/ NPOIN,DIAM,ELENG,THICK,ENEXP,EPSOD,
       120.I        &              YIELD,DENCT,TOL,JTYPE,NTIME,DT,DST,
       130.I        &              EMPUL,NITER,NNODS,ITWON,SLAMDA,WIDTH,CENTR
       170.I           PARAMETER PI = 3.141592654
       175.I           PARAMETER NDIM = 20
       160.            INCLUDE R.VIRBRA,LIST
       220.I           COMMON/VIB/ AMASS(20),AJACOB(20,20),BJACOB(20,20),
       230.I        &              AB(20,40),RAD(20),FUNC(20),FNEW(20)
       161.            CHARACTER TITLE*72
       162.            CHARACTER KWORD*6
       163.            CHARACTER SHAPE*4
       170.
       180.            READ(5,100) KWORD
       190.            IF(KWORD.EQ.'*START') THEN
1      200.               READ(5,101) TITLE
1      210.            ELSE
1      220.               PRINT*,'>>>> THE TITLE CARD IS MISSING'
1      230.            ENDIF
1      231.      C
       232.            WRITE(6,105) TITLE
       233.      105 FORMAT(1H1,5HO,10X,A72)
       240.
       250.      C*****     LOOP OVER THE REMAINING CARDS
       260.
       270.            DO 10 ILOOP = 1,8
       280.
1      290.            READ(5,100) KWORD
1      300.
1      310.            IF(KWORD.EQ.'*NODES') THEN
2      320.               READ(5,100) NPOIN, SLAMDA
2      330.               GOTO 10
2      340.            ELSE IF(KWORD.EQ.'*DIMEN') THEN
2      350.               READ(5,110) DIAM, THICK
2      360.               GOTO 10
2      370.            ELSE IF(KWORD.EQ.'*MATER') THEN
2      380.               READ(5,110) ENEXP, EPSOD, YIELD, DENCT
2      390.               GOTO 10
2      400.            ELSE IF(KWORD.EQ.'*TIMES') THEN
2      410.               READ(5,110) DT, NTIME, DST
2      420.               GOTO 10
2      430.            ELSE IF(KWORD.DQ.'*TOLER') THEN
2      440.               READ(5,110) NITER, TOL
2      450.               GOTO 10
2      460.            ELSE IF(KWORD.EQ.'*SHAPE') THEN
2      470.               READ(5,111) SHAPE
2      480.                  IF(SHAPE.EQ.'CIRC') THEN
3      490.                     JTYPE = 1
3      500.                  ELSE IF(SHAPE.EQ.'SQUA') THEN
3      510.                     JTYPE = 2
3      520.                  ELSE IF(SHAPE.EQ.'RECT') THEN
3      530.                     JTYPE = 3
3      535.                     READ(5,110) WIDTH
```

```
3       540.                  ENDIF
2       550.               GOTO 10
2       560.            ELSE IF(KWORD.EQ.'*IMPUL') THEN
2       570.               READ(5,110) EMPUL
2       580.               GOTO 10
2       590.            ELSE IF(KWORD.EQ.'*FINIS') THEN
2       600.               GOTO 20
2       610.            ENDIF
2       620.
1       630.          10 CONTINUE
        635          100 FORMAT(A6)
        636.         101 FORMAT(A72)
        637.         110 FORMAT( )
        638.         111 FORMAT(A4)
        640.
        650.          20 RETURN
        660.             END

END FTN 140 IBANK 200 DBANK 3394 COMMON


@FTN,S R.DATAPR
FTN 11R1A    10/22/86-09:25(0,)
        100.             SUBROUTINE DATAPR
        110.             IMPLICIT DOUBLE PRECISION*8(A-H,O-Z)
        120.             INCLUDE R.VISCO
        130.             INCLUDE R.VIBRA
        140.       C
        150.             PRINT*'THE INPUT DATA WILL BE PRINTED IN FUTURE'
        160.       C
        170.             RETURN
        180.             END

END FTN 23 IBANK 5 DBANK 3394 COMMON


@FIN,S R.SETVAR
FTN 11R1A    10/22/86-09:25(0,)
        100.             SUBROUTINE SETVAR
        110.
        120.       C*****     SET THE VALUES FOR CERTAIN NECESSARY PARAMETERS
        130.
        140.             IMPLICIT DOUBLE PRECISION*8(A-H,O-Z)
        150.             INCLUDE R.VISCO,LIST
        110.I            COMMON/VIS/ NPOIN,DIAM,ELENG,THICK,ENEXP,EPSOD,
        120.I           &            YIELD,DENCT,TOL,JTYPE,NTIME,DT,DST,
        130.I           &            EMPUL,NITER,NNODS,ITWON,SLAMBDA,WIDTH,CENTR
        170.I            PARAMETER PI = 3.141592654
        175.I            PARAMETER NDIM = 20
        155.             INCLUDE R.VIBRA,LIST
        160.
        220.I            COMMON/VIB/ AMASS(20),AJACOB(20,20),BJACOB(20,20),
        230.I           &            AB(20,40),RAD(20),FUNC(20),FNEW(20)
        165.             NNODS = NPOIN + 1
        166.             ITWON = 2*NPOIN
        170.             R = 0.5*DIAM
        180.             CENTR = WIDTH - DIAM
        190.             ELENG = R/NPOIN
        200.
        210.             DO 10 IPOIN = 1,NPOIN
1       220.             RAD(IPOIN) = R*(2.*IPOIN - 1) / (2.*NPOIN)
1       230.          10 CONTINUE
```

```
1       240.
        250.            IF(JTYPE.EQ.1) THEN
1       260.               ACONS = PI*DENCT*THICK
1       270.            ELSE
1       280.               ACONS = 4.*DENCT*THICK
1       290.            ENDIF
1       300.
        310.            AMASS(1) = ACONS*RAD(1)*RAD(1)
        312.            IF(JTYPE .EQ. 3) THEN
1       314.               AMASS(1) = AMASS(1) + 2.*CENTRE*RAD(1)*DENCT*THICK
1       316.            ENDIF
1       320.
        330.            DO 20 JPOIN = 2,NPOIN
1       340.            J = JPOIN - 1
1       350.            AMASS(JPOIN) = ACONS*(RAD(JPOIN)*RAD(JPOIN) - RAD(J)*RAD(J))
1       352.            IF(JTYPE .EQ. 3) THEN
2       353.               AMADD = 2.*CENTRE*(RAD(JPOIN) - RAD(J))*DENCT*THICK
2       354.               AMASS(JPOINT) = AMASS(JPOIN) + AMADD
2       355.            ENDIF
1       360.         20 CONTINUE
1       370.
        380.            RETURN
        390.            END

END FTN 145 IBANK 42 DBANK 3394 COMMON


@FTN,S R.SOLVE
FTN 11R1A    10/22/86-09:25(0,)
        100.            SUBROUTINE SOLVE(D,V,X,XD)
        200.
        300.      C*****     SOLVE THE SYSTEM OF NONLINEAR EQUILIBRIUM EQUATIONS
        400.      C          USING A NEWTON-RAPHSON ITERATION DURING EACH OF
        500.      C          THE ITERATION OF THE IMPLICIT SCHEME FOR EACH STEP
        600.
        700.            IMPLICIT DOUBLE PRECISION*8(A-H,O-Z)
        800.            INCLUDE R.VISCO,LIST
        110.I           COMMON/VIS/ NPOIN,DIAM,ELENG,THICK,ENEXP,EPSOD,
        120.I          &            YIELD,DENCT,TOL,JTYPE,NTIME,DT,DST,
        130.I          &            EMPUL,NITER,NNODS,ITWON,SLAMDA,WIDTH,CENTR
        170.I           PARAMETER PI = 3.141592654
        175.I           PARAMETER NDIM = 20
        900.            INCLUDE R.VIBRA,LIST
        220.I           COMMON/VIB/ AMASS(20),AJACOB(20,20),BJACOB(20,20),
        230.I          &            AB(20,40),RAD(20),FUNC(20),FNEW(20)
       1000.            DIMENSION X(1),XD(1)
       1200.
       1300.
       1400.      C*****     ZERO THE JACOBIAN MATRIX
       1500.
       1600.            DO 10 I = 1,NPOIN
1      1700.            DO 15 J = 1,NPOIN
2      1800.            AJACOB(I,J) = 0.DO
2      1900.         15 CONTINUE
1      2000.         10 CONTINUE
1      2100.
1      2200.      C*****     LOOP FOR NITER ITERATIONS OF THE NEWTON METHOD
1      2300.
       2400.            DO 99 ITER = 1,NITER
       2500.
       2600.
       2700.      C*****     BEGIN TO ASSEMBLE THE JACOBIAN BY COMPUTING THE
```

```
      2800.      C          FIRST COLUMN (UNKNOWN IS LAMDA)
      2900.
1     2910.            AJACOB(1,1) = AMASS(1)*V
1     3000.            DO 25 J = 2,NPOIN
2     3100.            AJACOB(J,1) = AMASS(J)*X(J)*V
2     3200.         25 CONTINUE
2     3300.
2     3400.      C*****     CREATE COLUMNS 2 THROUGH NPOIN - 1 OF AJACOB
2     3500.
1     3600.            M = NPOIN - 1
1     3700.
1     3800.            DO 30 J = 2,M
2     3900.            I = J - 1
2     4000.            K = J + 1
2     4100.            IF(J.EQ.2) THEN
3     4200.               CALL DERIVK(AJACOB(I,J),1.D0,X(J),D,V,I,RAD)
3     4250.               CALL DERIVJ(AJACOB(J,J),X(1),1.D0,X(J),X(K),D,V,J,
3     4251.           &RAD,AMASS)
3     4300.            ELSE
3     4400.               CALL DERIVK(AJACOB(I,J),X(I),X(J),D,V,I,RAD)
3     4700.            CALL DERIVJ(AJACOB(J,J),X(1),X(I),X(J),X(K),D,V,J,RAD,AMASS).
3     4710.            ENDIF
2     4800.            CALL DERIVI(AJACOB(K,J),X(J),X(K),D,V,K,RAD)
2     4900.      C
2     5000.         30 CONTINUE
2     5100.      C
1     5200.            CALL DERIVK(AJACOB(M,NPOIN),X(M),X(NPOIN),D,V,M,RAD)
1     5300.            CALL DERIVJ(AJACOB(NPOIN,NPOIN),X(1),X(NPOIN),0.D0,D,V,
1     5310.           &NPOIN,RAD,AMASS)
1     5320.      C
1     5330.      C
1     5400.      C
1     5500.      C*****     THE JACOBIAN MUST BE INVERTED
1     5501.      C          AFTER IT HAS BEEN AUGMENTED BY THE IDENTITY
1     5502.      C          MATRIX ON ITS RIGHT HAND SIDE
1     5503.      C
1     5504.            DO 60 IAB = 1,NPOIN
2     5505.            DO 55 JAB = 1,ITWON
3     5506.            AB(IAB,JAB) = 0.D0
3     5507.         55 CONTINUE
2     5508.         60 CONTINUE
2     5509.      C
2     5510.      C
1     5511.            DO 65 JAB = 1,NPOIN
2     5512.            AB(JAB,1) = AJACOB(JAB,1)
2     5513.         65 CONTINUE
2     5514.      C
2     5515.      C
1     5516.            DO 70 J = 2,M
2     5517.            I = J - 1
2     5518.            K = J + 1
2     5519.            AB(I,J) = AJACOB(I,J)
2     5520.            AB(J,J) = AJACOB(J,J)
2     5521.            AB(K,J) = AJACOB(K,J)
2     5522.         70 CONTINUE
1     5523.            AB(M,POIN) = AJACOB(M,POIN)
1     5524.            AB(NPOIN,NPOIN) = AJACOB(NPOIN,NPOIN)
1     5525.      C
1     5526.      C
1     5527.            DO 75 IPOIN = 1,NPOIN
2     5528.            JPOIN = IPOIN + NPOIN
2     5529.            AB(IPOIN,JPOIN) = 1.D0
```

```
2     5530.          75 CONTINUE
2     5531.      C
2     5532.      C
2     5600.      C
1     5700.            CALL INVERT(AB,BJACOB,NPOIN,ITWON,NDIM)
1     5800.      C
1     5900.      C*****     MULTIPLY BJACOB BY THE FUNCTION EVALUATED AT X
1     6000.      C
1     6100.            CALL FEVAL(X,FUNC,D,V,AMASS,RAD)
1     6200.            CALL MULTPY(BJACOB,FUNC,FNEW)
1     6300.      C
1     6400.      C*****     COMPUTE THE NEW APPROXIMATION POINT
1     6500.      C
1     6600.            DO 40 IPOIN = 1,NPOIN
2     6700.            XD(IPOIN) = X(IPOIN) - FNEW(IPOIN)
2     6800.          40 CONTINUE
2     6900.      C
2     7000.      C*****     A CHECK FOR CONVERGENCE OF THE SOLUTION
2     7100.      C
1     7200.            DO 50 JPOIN = 1,NPOIN
2     7300.            IF (DABS(((XD(JPOIN) - X(JPOIN))/XD(JPOIN))).GT.TOL) THEN
3     7400.                GOTO 95
3     7500.            ENDIF
2     7600.          50 CONTINUE
2     7700.      C
1     7800.            GOTO 100
1     7900.      C
1     7910.          95 CONTINUE
1     7920.             DO 97 JP = 1,NPOIN
2     7930.             X(JP) = XD(JP)
2     7940.          97 CONTINUE
1     8000.          99 CONTINUE
1     8100.      C
1     8200.      C
      8300.        100 CONTINUE
      8400.      C
      8500.            DO 150 JP = 1,NPOIN
1     8600.      X(JP) = XD(JP)
1     8700.        150 CONTINUE
1     8800.      C
1     8900.      C
      9000.            RETURN
      9100.            END

END FTN 518 IBANK 146 DBANK 3394 COMMON


@FTN,S R.FUNCS
FTN 11R1A    10/22/86-09:25(0,)
       100.            FUNCTION A1(Y,Z,D,V,J)
       110.            IMPLICIT DOUBLE PRECISION*8(A-H,O-Z)
       120.            INCLUDE R.VISCO
       125.            COMMON/ONE/ XT(21), UT, VT
       130.      C
       132.            K = J + 1
       140.            P = 1.DO/ENEXP
       141.            CB = XT(K)*CTFUN(K) - XT(J)*CTFUN(J)
       142.            CC = Z*CTFUN(K) - Y*CTFUN(J)
       143.            PNEW = (ELENG + DT*VT*CB)*CC*V
       160.            P2 = (Y-Z)*(Y-Z)
       165.            PA = (D*V*P2 + PNEW)/(EPSOD*ELENG*ELENG)
       170.      C
```

```
180.            A1 = 1.D0 + (PA**P)
190.            RETURN
200.            END
210.      C
220.      C
230.            FUNCTION A3(Y,Z,D,V,J)
240.            IMPLICIT DOUBLE PRECISION*8(A-H,O-Z)
250.            INCLUDE R.VISCO
251.            COMMON/ONE/ XT(21), UT, VT
253.            K = J + 1
254.            CB = ELENG + DT*VT*(XT(K)*CTFUN(K) - XT(J)*CTFUN(J))
255.            CC = Z*CTFUN(K) - Y*CTFUN(J)
260.            P = 1.DO/ENEXP
270.            P1 = 1.DO - P
280.            P2 = 2.*D*V*(Y - Z)
281.            P3 = EPSOD*ELENG*ELENG
282.            P4 = 0.5*P2*(Y-Z)
283.            P5 = (P4 + CB*CC*V)/P3
284.            P6 = P/(P5**P1)
290.            A3 = P6*(P2 - V*CB*CTFUN(J))/P3
300.            RETURN
310.            END
320.      C
330.      C
340.            FUNCTION C1(X,Y,D)
350.            IMPLICIT DOUBLE PRECISION*8(A-H,O-Z)
360.            INCLUDE R.VISCO
370.      C
380.            P = ELENG*ELENG
390.            P2 = D*D*(X-Y)*(X-Y)
400.            C1 = DSQRT(P + P2)
410.            RETURN
420.            END
430.      C
440.      C
450.            FUNCTION C3(X,Y,D)
460.            IMPLICIT DOUBLE PRECISION*8(A-H,O-Z)
470.            INCLUDE R.VISCO
480.      C
490.            P = ELENG*ELENG
500.            P3 =    D*D*(X-Y)
510.            P4 = DSQRT(P+P3*(X-Y))
520.            C3 = P3/P4
```

```
      RETURN
      END
C
C
C
C
C
C
      FUNCTION CTFUN(J)
      IMPLICIT DOUBLE PRECISION*8(A-H,O-Z)
      INCLUDE R.VISCO
      COMMON/ONE/ XT(21), UT, VT
C
      IF (J .EQ. 1) THEN
           CTFUN = 0.DO
           GOTO 99
      ENDIF
C
      I = J - 1
      K = J + 1
      BI = ((XT(I) - XT(J))**2.)*UT*UT
      BJ = ((XT(J) - XT(K))**2.)*UT*UT
      ELSQ = ELENG*ELENG
      ELI = DSQRT(ELSQ + BI)
      ELJ = DSQRT(ELSQ + BJ)
C
      G1 = XT(I) - XT(J)
      G2 = XT(J) - XT(K)
      G3 = ELI + ELENG
      G4 = ELJ + ELENG
C
      ANUM = UT*(G1*G4 + G2*G3)
      ADEN = G3*G4 - UT*UT*G1*G2
C
      CTFUN = ANUM/ADEN
   99 RETURN
      END
C
C
C
C
C
C
      FUNCTION A4(Y,Z,D,V,J)
      IMPLICIT DOUBLE PRECISION*8(A-H,O-Z)
      INCLUDE R.VISCO
      COMMON/ONE/ XT(21), UT, VT
      K = J + 1
      CB = ELENG + DT*VT*(XT(K)*CTFUN(K) - XT(J)*CTFUN(J))
      CC = Z*CTFUN(K) - Y*CTFUN(J)
      P = 1.DO/ENEXP
      P1 = 1.DO - P
      P2 = 2.*D*V*(Y - Z)
      P3 = EPSOD*ELENG*ELENG
      P4 = 0.5*P2*(Y - Z)
      P5 = (P4 + CB*CC*V)/P3
      P6 = P/(P5**P1)
```

```
       970.              A4 = -P6*(P2 - V*CB*CTFUN(K))/P3
       980.              RETURN
       990.              END
      1000.       C

END FTN 538 IBANK 266 DBANK 80 COMMON


@FTN,S R.DERIV
FTN 11R1A    10/22/86-09:25(0,)
       100.              SUBROUTINE DERIVK(A,X,Y,D,V,J,RAD)
       110.              IMPLICIT DOUBLE PRECISION*8(A-H,O-Z)
       120.              INCLUDE R.VISCO
       130.              DIMENSION RAD(1)
       140.              YNAUT = THICK*YIELD
       150.              IF(JTYPE .EQ. 1) THEN
1      160.                 CONST = 2.*PI*RAD(J)
1      170.              ELSE IF (JTYPE .EQ.2) THEN
1      180.                 CONST = 8.*RAD(J)
1      190.              ELSE
1      200.                 CONST = 8.*RAD(J) + 2.*CENTR
1      210.              ENDIF
       220.              CONST = YNAUT*CONST
       230.              S1 = (+A4(X,Y,D,V,J)*D*(X-Y) - D*A1(X,Y,D,V,J))*C1(X,Y,D)
       240.              S2 = -C3(X,Y,D)*A1(X,Y,D,V,J)*D*(X-Y)
       250.       C
       260.              A = -CONST*(S1 - S2)/(C1(X,Y,D)*C1(X,Y,D))
       270.              RETURN
       280.              END
       290.       C
       300.       C




       310.              SUBROUTINE DERIVJ(A,W,X,Y,Z,D,V,J,RAD,AMASS)
       320.              IMPLICIT DOUBLE PRECISION*8(A-H,O-Z)
       330.              INCLUDE R.VISCO
       340.              DIMENSION RAD(1),AMASS(1)
       350.              J1 = J - 1
       360.       C
       370.              YNAUT = THICK*YEILD
       380.              YNAUT1 = THICK*YEILD
       390.              IF(JTYPE .EQ. 1) THEN
1      400.                 CONST = 2.*PI*RAD(J)
1      405.                 CONST1 = 2.*PI*RAD(J1)
1      410.              ELSE IF(JTYPE .EQ. 2) THEN
1      420.                 CONST = 8.*RAD(J)
1      425.              CONST1 = 8.*RAD(J1)
1      430.              ELSE
1      440.                 CONST = 8.*(RAD(J) + 2.*CENTR
1      445.                 CONST1 = 8.*RAD(J1) + 2.*CENTR
1      450.              ENDIF
       460.              CONSJ = YNAUT*CONST
       470.              CONSJ1 = YNAUT1*CONST1
       480.       C
       490.              Q1 = W*AMASS(J)*V
       500.              S1 = ((A3(Y,Z,D,V,J)*D*(Y-Z)) + D*A1(Y,Z,D,V,J))*C1(Y,Z,D)
       510.              S2 = C3(Y,Z,D)*A1(Y,Z,D,V,J)*D*(Y-Z)
```

```
      520.            S3 = C1(Y,Z,D)
      530.            Q2 = CONSJ*(S1 - S2)/(S3*S3)
      540.            S4 = (+A4(X,Y,D,V,J1)*D*(X-Y) - D*A1(X,Y,D,V,J1))*C1(X,Y,D)
      550.            S5 = -C3(X,Y,D)*A1(X,Y,D,V,J1)*D*(X-Y)
      560.            S6 = C1(X,Y,D)
      570.            Q3 = CONSJ1*(S4-S5)/(S6*S6)
      580.      C
      590.            A = Q1 - Q2 + Q3
      600.      C
      610.            RETURN
      620.            END
      630.      C
      640.      C




      650.            SUBROUTINE DERIVI(A,X,Y,D,V,J,RAD)
      660.            IMPLICIT DOUBLE PRECISION*8(A-H,O-Z)
      670.            INCLUDE R.VISCO
      680.            DIMENSION RAD(1)
      690.      C

      700.            J1 = J - 1
      710.            YNAUT = THICK*YIELD
      711.            IF(JTYPE .EQ. 1) THEN
1     712.               CONST = 2.*PI*RAD(J1)
1     713.            ELSE IF (JTYPE .EQ. 2) THEN
1     714.               CONST = 8.*RAD(J1)
1     715.            ELSE
1     716.               CONST = 8.*RAD(J1) + 2.*CENTR
1     717.            ENDIF
      720.            CONS = YNAUT*CONST
      730.      C
      740.            S1 = (A3(X,Y,D,V,J1)*D*(X-Y) + D*A1(X,Y,D,V,J1))*C1(X,Y,D)
      750.            S2 = C3(X,Y,D)*A1(X,Y,D,V,J1)*D*(X-Y)
      760.            S3 = C1(X,Y,D)
      770.      C
      780.            A = CONS*(S1 - S2)/(S3*S3)
      790.      C
      800.            RETURN
      810.            END


END FTN 622 IBANK 245 DBANK 34 COMMON


@FTN,S R.FEVAL
FTN 11R1A    10/22/86-09:25(0,)
      100.            SUBROUTINE FEVAL(X,FUNC,D,V,AMASS,RAD)
      110.            IMPLICIT DOUBLE PRECISION*8(A-H,O-Z)
      120.            INCLUDE R.VISCO
      140.            DIMENSION X(1),FUNC(1),AMASS(1),RAD(1)
      150.      C
      160.      C
      170.            Q1 = X(1)*AMASS(1)*V
      180.            YNAUT = THICK*YIELD
```

```
      181.              IF(JTYPE .EQ. 1) THEN
1     182.                 CONST = 2.*PI*RAD(1)
1     183.              ELSE IF (JTYPE .EQ. 2) THEN
1     184.                 CONST = 8.*RAD(1)
1     185.              ELSE
1     186.                 CONST = 8.*RAD(1) + 2.*CENTR
1     187.              ENDIF
      190.              CONS = YNAUT*CONST
      200.              Q2 = A1(1.DO,X(2),D,V,1)*D*(1.DO-X(2))
      210.              Q3 = C1(1.DO,X(2),D)
      220.              FUNC(1) = Q1 - CONST*Q2/Q3
      230.       C
      240.       C
      250.       C
      260.              DO 50 IP = 2,NPOIN
1     270.              IP1 = IP - 1
1     280.              YNAUT = THICK*YIELD
1     282.              YNAUT1 = THICK*YIELD
1     283.              IF(JTYPE .EQ. 1) THEN
2     285.                 CONST = 2.*PI*RAD(IP)
2     286.                 CONST1 = 2.*PI*RAD(IP1)
2     287.              ELSE IF (JTYPE .EQ. 2) THEN
2     289.                 CONST = 8.*RAD(IP)
2     290.                 CONST1 = 8.*RAD(IP1)
2     291.              ELSE
2     293.                 CONST = 8.*RAD(IP) + 2.*CENTR
2     294.                 CONST1 = 8.*RAD(IP1) + 2.*CENTR
2     295.              ENDIF
1     300.              CONSI = YNAUT*CONST
1     310.              CONSI1 = YNAUT1*CONST1
1     320.       C
1     330.              K = IP + 1
1     340.              Q1 = X(1)*AMASS(IP)*V*X(IP)
1     350.              Q2 = A1(X(IP),X(K),D,V,IP)*D*(X(IP) - X(K))
1     360.              Q3 = C1(X(IP),X(K),D)
1     366.              IF (IP .EQ. 2) THEN
2     367.                 Q4 = A1(1.DO,X(IP),D,V,IP1)*D*(1.DO - X(IP))
2     368.                 Q5 = C1(1.DO,X(IP),D)
2     369.              ELSE
2     370.              Q4 = A1(X(IP1),X(IP),D,V,IP1)*D*(X(IP1) - X(IP))
2     380.              Q5 = C1(X(IP1),X(IP),D)
2     385.              ENDIF
2     390.       C
2     400.       C
1     410.              FUNC(IP) = Q1 - CONSI*Q2/Q3 + CONSI1*Q4/Q5
1     420.       C
1     430.          50 CONTINUE
1     440.       C
      450.              RETURN
      460.              END

END FTN 336 IBANK 104 DBANK 34 COMMON

@FTN,S  R.INVERT
FTN 11R1A     10/22/86-09:25(0,)
      100.              SUBROUTINE INVERT(AB,B,N,NP,NDIM)
      110.       C
      120.       C
      130.       C*****     THIS ROUTINE SOLVES A SET OF LINEAR EQUATIONS
      140.       C          THUS INVERTING A MTARIX IF THE AUGMENTED RHS
      150.       C          IS JUST THE IDENTITY MATRIX
      160.       C
```

```
      C
            IMPLICIT DOUBLE PRECISION*8(A-H,O-Z)
            DIMENSION AB(NDIM,1), B(NDIM,1)
      C
      C*****     BEGIN THE REDUCTION
      C
            NM1 = N - 1
            DO 35 I = 1,NM1
      C
      C
      C*****     FIND THE ROW NUMBER OF THE PIVOT ROW
      C          INTERCHANGE ROWS SO PIVOT IS ON DIAGONAL
      C
            IPVT = I
            IP1 = I + 1
            DO 10 J = IP1,N
               IF(DABS(AB(IPVT,I)) .LT. DABS(AB(J,I)))  IPVT = J
         10 CONTINUE
      C
      C*****     CHECK FOR A NEAR SINGULAR MATRIX
      C
            IF(DABS(AB(IPVT,I)) .LT. 1.0D-6) THEN
               PRINT*,  SOLUTION NOT FEASIBLE - NEAR ZERO PIVOT'
               RETURN
            END IF
      C
      C
            IF (IPVT .NE. I) THEN
               DO 20 JCOL = 1,NP
                  SAVE = AB(I,JCOL)
                  AB(I,JCOL) = AB(IPVT,JCOL)
                  AB(IPVT,JCOL) = SAVE
         20 CONTINUE
            END IF
      C
      C
      C*****     CHECK FOR ZEROS, OTHERWISE REDUCE ELEMENTS
      C          BELOW THE DIAGONAL TO ZERO
      C
            DO 32 JROW = IP1,N
               IF (AB(JROW,I) .NE. 0.D0) THEN
                 RATIO = AB(JROW,I)/AB(I,I)
                 AB(JROW,I) = RATIO
                 DO 30 KCOL = IP1,NP
                    AB(JROW,KCOL) = AB(JROW,KCOL) - RATIO*AB(I,KCOL)
         30         CONTINUE

               ENDIF
         32 CONTINUE
      C
         35 CONTINUE
      C
      C
      C*****     CHECK AB(N,N) FOR SIZE
      C
            IF (DABS(AB,N,N)) .LT. 1.0D-6) THEN
               PRINT*,    SOLUTION NOT FEASIBLE - NEAR ZERO PIVOT'
               RETURN
            END IF
      C
      C
      C*****     NOW THE BACK SUBSTITUTION
```

```
1      790.      C
       800.            NP1 = N + 1
       810.            DO 50 KCOL = NP1,NP
1      820.               AB(N,KCOL) = AB(N,KCOL)/AB(N,N)
1      830.               DO 45 J = 2,N
2      840.                 NVBL = NP1 - J
2      850.                 L = NVBL + 1
2      860.                 VALUE = AB(NVBL,KCOL)
2      870.                 DO 40 K = L,N
3      880.                  VALUE = VALUE - AB(NVBL,K)*AB(K,KCOL)
3      890.            40   CONTINUE
2      900.                 AB(NVBL,KCOL) = VALUE/AB(NVBL,NVBL)
2      910.            45   CONTINUE
1      920.            50 CONTINUE
1      930.      C
1      940.      C
1      950.      C*****     RETURN THE MATRIX B AS THE INVERSE, EQUAL TO
1      960.      C          THE AUGMENTED PART OF THE MATRIX AB
1      970.      C
       980.            DO 70 IPOIN = 1,N
1      990.            DO 65 JPOIN = 1,N
2     1000.            JIP = JPOIN + N
2     1010.            B(IPOIN,JPOIN) = AB(IPOIN,JIP)
2     1020.         65 CONTINUE
1     1030.         70 CONTINUE
1     1040.      C
1     1050.      C
1     1060.      C
      1070.            RETURN
      1080.            END


END FTN 416 IBANK 64 DBANK


@FTN,S R.MULTPY
FTN 11R1A    10/22/86-09:25(0,)
       100.            SUBROUTINE MULTPY(BJACOB,FUNC,FNEW)
       110.            IMPLICIT DOUBLE PRECISION*8(A-H,O-Z)
       120.            INCLUDE R.VISCO
       130.            DIMENSION BJACOB(NDIM,1,FUNC(1),FNEW(1)
       140.      C
       150.      C
       160.            DO 20 I = 1,NPOIN
1      170.            FNEW(I) = 0.
1      180.            DO 15 J = 1,NPOIN
2      190.            FNEW(I) = FNEW(I) + BJACOB(I,J)*FUNC(J)
2      200.         15 CONTINUE
1      210.         20 CONTINUE
1      220.      C
1      230.      C
       240.            RETURN
       250.            END


END FTN 80 IBANK 27 DBANK 34 COMMON
```